Effect of Particle Shape, Silica Coating and Laser Irradiation on Thermal Conductivity of Some Metal Oxide Based Nanofluids

Thesis submitted

by

Bhupender Pal

(**Regd. No. 901109007**)

In fulfillment of the requirement for

the degree of

Doctor of Philosophy

Under the supervision of

Dr. Bonamali Pal

(Professor and Head)

School of Chemistry and Biochemistry

Thapar University, Patiala-*147 004*

Punjab (India)

November 2015

Dedicated to

My

Parents

&

Teachers

Certificate

This is to certify that the thesis entitled "***Effect of Particle Shape, Silica Coating and Laser Irradiation on Thermal Conductivity of Some Metal Oxide Based Nanofluids***" being submitted by Mr. Bhupender Pal in fulfillment of the requirement for the award of the Degree of Doctor of Philosophy in the School of Chemistry and Biochemistry, Thapar University, Patiala, is a record of candidate's own independent and original research work carried out by him under my supervision and guidance. The material embodied in this thesis has not been submitted in part or full to any other University or Institute for the award of any degree.

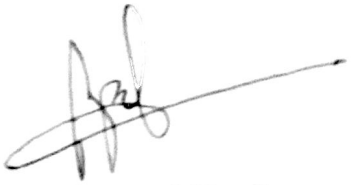

(Supervisor and Head)

Dr. Bonamali Pal

Professor and Head

School of Chemistry and Biochemistry

Thapar University, Patiala- 147004

Punjab (India)

Candidate's Declaration

I, hereby declare that the work presented in the thesis entitled "***Effect of Particle Shape, Silica Coating and Laser Irradiation on Thermal Conductivity of Some Metal Oxide Based Nanofluids***" in fulfillment of the requirement for the award of the Degree of Doctor of Philosophy, School of Chemistry and Biochemistry, Thapar University, Patiala, is an authentic record of my own work carried out under the supervision of Dr. Bonamali Pal, Professor and Head, School of Chemistry and Biochemistry, Thapar University, Patiala, India. The matter embodied in this thesis has not been submitted in part or full to any other university or institute for the award of any degree in India or Abroad.

Bhupender Pal

(Supervisor)

Dr. Bonamali Pal

Professor and Head

School of Chemistry and Biochemistry

Thapar University, Patiala- 147004

Punjab (India)

Acknowledgements

I wholeheartedly thank the Almighty for giving me the strength to remain on the path to success.

A statement of thanks is not evident to inculcate my deep sense of gratitude and obligation to all those who helped me in one way or another in completion of thesis. I would like to take this opportunity to thank many people who have helped and encouraged me throughout this research.

First and foremost, I am extremely grateful to my research supervisor, Dr. Bonamali Pal, Professor and Head, School of Chemistry and Biochemistry, for his valuable supervision, scholarly inputs and consistent encouragement throughout the research work. He always made it a point to be available to clarify my doubts despite his busy schedules and I consider it as a great opportunity to do my doctoral programme under his guidance and to learn from his research expertise. His guidance was of paramount importance in providing a well rounded understanding of my research for long-term career goals.

I gratefully acknowledge the funding for the years of research through a grant from the University Grants Commission, Government of India.

I am also thankful to my doctoral committee members Dr. Ranjana Prakash, Dr. Amjad Ali and Dr. S.S. Mallick for their encouragement, constructive criticism and inspirations.

Many thanks to all the faculty members of School of Chemistry and Biochemistry, Thapar University, Patiala for providing necessary guidance during my research work. I am also thankful to Mr. Chandar Thakur, School of Chemistry and Biochemistry for the constant official help and cooperation.

I would also like to thanks Dr. B.K. Chudasama and Ms. Chandani (School of Physics and Material Science, Thapar University, Patiala) for Zeta potential and conductance analysis. I would like to extend my thanks to SAI labs, Thapar University, Patiala, SAIF IIT Bombay.

Special thanks to my senior labmates Mr. Rohit Singh, Mrs. Rupinder Kaur, Mr. Inderpreet Singh Grover, Mrs. Nidhi Gupta and Miss Alka Sharma who have extended their support in a very special way. I gained a lot from them, through their personal and scholarly interactions, their suggestions at various points in my research programme.

I am also thankful to my batch mates and friends Mrs. Anila, Mrs. Jaspreet Kaur, Miss Tanushree Basu, Mrs. Shweta Sareen, Miss Prinka, Mr. Rayees Ahmad Rather, Mr. Akul Sen Gupta, Mr. Yuvraj Singh, Mr. Rayees Ahmad, Mr. Abir Jameel and Mr. Roopchand Prajapat for always standing by my side and sharing a great relationship as compassionate friends. I will forever cherish the warmth shown by them, whose smiling faces always inspired me.

I feel a deep sense of gratitude for my parents (*father, Ved Ram and Mother, Dolma Devi*) and sisters (*Shakuntla Devi and Kanta Devi*) who have always showered unconditional love on me, encouraged and supported me in every aspect. They formed a part of my vision and taught me the good things that really matter in life. My special thanks to my dearest and nearest cousin brother Mr. Mukesh Kumar for his moral support during my course of work.

Besides this, I am thankful to the persons who knowingly and unknowingly helped me during the successful completion of this work.

Bhupender Pal

Table of contents

List of Figures

Chapter 4

Chapter 5

List of Tables

List of Abbreviations

TC	Thermal conductivity
NPs	Nanoparticles
NFs	Nanofluids
Vol.%	Volume percentage
H_2O	Water
0D	One dimensional
1D	Two dimensional
2D	Three dimensional
LASER	Light amplification by stimulated emission of radiation
EG	Ethylene glycol
DIW	De-ionized water
EMT	Effective medium theory
T	Temperature
IEP	Isoelectric point
SDS	Sodium dodecylsulfate
SDBS	Sodium dodecyl benzene sulfonate
CTAB	Cetyltrimethylammonium bromide
HCTAB	Hexadecyltrimethylammonium bromide
PVP	Polyvinylpyrrolidone
DTAB	Dodecyl trimethylammonium bromide
TEOS	Tetraethyl orthosilicate
mL	Milliliter
µL	Micro-liter

mol	Mole
mmol	Millimole
mM	Milli molar
nm	Nanometer
ASTM	American Society for Testing and Materials
IEEE	Institute of Electrical and Electronics Engineers
DLS	Dynamic light scattering
XRD	X-ray diffraction
UV	Ultraviolet
Vis	Visible
HR-TEM	High resolution transmission electron microscopy
TEM	Transmission electron microscopy
SEM	Scanning electron microscopy
EDX/EDS	Energy Dispersive X-ray (EDX) Spectroscopy
JCPDS	Joint committee on powder diffraction standards
BET	Brunauer-Emmett-Teller
TGA	Thermogravimetric Analysis
FTIR	Fourier-Transform Infrared Spectroscopy
L	Length
W	Width
TiO_2 P25	Commercially available P25-TiO_2
mV	Millivolts
TNR	Titania Nanorods
TNT	Titania Nanotubes
PZC	Point of zero charge
NS	Nanospheres
NW	Nanowires
NR	Nanorods
NT	Nanotubes
ANP	Anisotropic nanoparticles
NC	Nanocomposites

VF	Volume fraction
VS	Viscosity
a.u.	Arbitrary unit
hcp	Hexagonal close packing
fcc	Face centred cubic
m	meter
g	gram
mg	Milligram

ρ_{nf}	density of nanofluids
ρ_p	density of particles
ϕ	volume fraction
ρ_w	density of water
k_{eff}	effective thermal conductivity
k_f	thermal conductivity of fluid
k_p	thermal conductivity of particles
k_0	thermal conductivity of base fluid
Pr	Prandtl number
Re	Reynolds number
d_p	particle diameter
R_b	interfacial resistance
γ	gamma
E_g	band gap
Å	angstrom
α	alpha
A	absorbance
°	degree
λ	wavelength
β	beta
%	percentage
μ	micro
θ	Theta
h	hour
υ	frequency
ζ	zeta
V	Volt
s	second

Abstract

This thesis represents an effect of particle shape, silica coating and laser irradiation on thermal conductivity of some metal oxide nanoparticles in basefluids. Heat conduction of the metal oxide nanoparticles varied as a function of geometric morphology and surface area of elongated nanoparticles. Dispersion stability of the nanoparticles in basefluids is a major problem in nanofluids; therefore, nanoparticles have been coated with a thin layer of SiO_2 for improved dispersion stability and thermal conductivity. Metal oxide (TiO_2, CuO and WO_3) nanoparticles in basefluids have also been irradiated by UV-Vis light LASER irradiation and investigated their effect on thermal conductivity. The whole work is divided into five chapters which are described below.

Chapter 1: **Introduction and Literature**: The first chapter provides brief introduction about thermal conductivity, nanofluids, metal oxide's size and shape, core/shell structure and importance of silica coating and LASER irradiation. Literature review, research gap, objectives, experimental section and characterization techniques are also incorporated in this chapter.

Chapter 2: Section A: Shape dependent thermal conductivity of TiO_2-ethylene glycol and de-ionized water based suspension: This section demonstrates the importance of various shapes and crystal phases of TiO_2 nanostructures such as TiO_2 P-25 (70:30 anatase and rutile), as-prepared nanorods (pure anatase) and sodium titanate nanotubes (orthorhombic $Na_2Ti_2O_5.H_2O$ crystal) on the thermal conductivity of ethylene glycol and de-ionized water. It was observed that TiO_2 nanorods (L×W = 81-134 nm × 8-13 nm and surface area = 79 m^2g^{-1}) always showed higher thermal conductivity than porous nanotubes (L×W = 85-115 nm × 9-12 nm and surface area = 176 m^2g^{-1}) and commercial TiO_2 P-25 (30-55 nm surface area = 56 m^2g^{-1}),) which was explained by their differences in crystallinity, crystal phases, compactness, surface exposed atoms, surface area and much greater mean free path of longitudinal phonon vibrations along its lateral dimensions. The subsequent effect of sonication time from 5-10 h results into the breakdown of TiO_2 nanorods cluster (42 to 28 nm) with the instantaneous increase in negative zeta potential values from -31 to -45 mV, respectively, which seems to be an additional cause for the enhancement in its thermal conductivity.

Section B: SiO_2@TiO_2 nanocomposites for enhanced thermal conductivity and dispersion stability in de-ionized water: This section presents the synthesis of bare and SiO_2 coated TiO_2 nanoparticles and investigate their effect on thermal conductivity of de-ionized water; as prepared nanoparticles were characterized by powder X-ray diffraction, Fourier transform infrared spectroscopy and transmission electron microscopy etc. These nanoparticles were dispersed in de-ionized water at various volume fractions (0.01%) and their thermophysical (density, thermal conductivity, refractive index etc) properties were studied. The experimental results showed that a thin layer of SiO_2 coating (3-6 nm) over TiO_2 nanostructures exhibit superior dispersion (0.5 vol%) stability as evident by steady zeta potential (-30 ↔ -36 mV), no significant change in particle-size (95↔133 nm) distribution, density (1.001↔0.998 g/cm^3) and refractive index (1.336↔1.333) etc. Thin Si-OH layer over surface imparts superior hydrophilicity, larger surface area for effective solute-solvent (SiO_2@TiO_2-H_2O) interaction for improved colloidal stability. Thereby, thermal conductivity is found to be quite stable (0.625↔0.614 W/m.K) up to 2-3 months, whereas aqueous suspension of bare TiO_2 particles quickly settles down. Depending on the thickness of SiO_2 layer and volume fraction of SiO_2@TiO_2, a maximum of 8-10% increment of thermal conductivity was achieved at 0.01 vol.%.

Chapter 3: Section A: Anisotropic CuO nanostructures of different size and shape exhibit thermal conductivity superior than typical bulk powder: This work demonstrates the preparation of monoclinic crystalline CuO nanospheres (5-10 nm), nanorods (L × W = 100-140 nm × 30-40 nm) and nanowires (200-210 nm × 2-5 nm) for the study of thermal conductivity when dispersed in de-ionized water and ethylene glycol (0.005-0.1 vol.%). It has been observed that CuO nanorods and nanowires having surface area 53 and 61 m^2/g, respectively, always displayed higher thermal conductivity than CuO nanospheres possessing lower surface area (41 m^2/g) which attributed to the differences in their per-particle surface area, percentage of surface exposed atoms, anisotropic lengthy shape and large phonon-mean-free paths. The experimental results revealed higher thermal conductivity than obtained from theoretical models due to particle shape effect as expected from Hamilton-Crosser equation. It has also been found that density is directly proportional to thermal conductivity and increases with the increase in volume fraction. The decrease in aggregated particle size (130–104 nm) and an increase in zeta potential

value (−32 to −37 mV) of CuO nanospheres cause more stability of CuO dispersion with 3-6 h of sonication.

Section B: SiO_2@CuO nanocomposites for enhanced thermal conductivity and dispersion stability in de-ionized water: This research demonstrates the synthesis of bare and SiO_2 coated CuO nanoparticles and investigate their effect on thermal conductivity of de-ionized water. The samples were characterized by powder X-ray diffraction, Fourier transform infrared spectroscopy and transmission electron microscopy etc. The nanoparticles were dispersed (0.01 vol.%) in de-ionized water and sonicated for half an hour before the measurement of thermophysical properties. The experimental results showed that a thin layer of SiO_2 coating (2-6 nm) over CuO nanoparticles display superior dispersion stability as marked by steady zeta potential (-31 ↔ -40 mV) and density (1.003↔1.002 g/cm^3). Thin Si-OH layer over surface imparts superior hydrophilicity, larger surface area for effective solute-solvent (SiO_2@CuO-H_2O) interaction for improved colloidal stability. Thereby, thermal conductivity is found to be quite stable (0.625↔0.614 W/m.K) up to 2-3 months, whereas aqueous suspension of bare CuO nanoparticles quickly settles down. Depending on the thickness of SiO_2 layer and concentration of SiO_2@CuO, a maximum of 8-10% enhancement in thermal conductivity was achieved.

Chapter 4: Section A: WO_3 nanostructures of different size and shape for improved dispersion stability and thermal conductivity in aqueous suspension: This work presents the preparation of different anisotropic (cubic, spherical and rod shaped) nanoparticles of WO_3 (monoclinic and hexagonal crystal structure) and studied their relative thermal conductivity in de-ionized water and ethylene glycol. Experimental results showed that thermal conductivity increases (7-12%) with the increase in volume fraction (0.01-1%) and density. WO_3 nanorods having surface area 61 m^2g^{-1} showed higher (10-12%) increment in thermal conductivity than WO_3 anisotropic nanoparticles (6-8%) possessing lower surface area 41 m^2g^{-1} which attributes to the differences in their surface exposed atoms, long phonon mean free path and lengthy shape factor etc. The results also showed that choice of stabilizer for better thermal conductivity and dispersion stability depend upon the nature of stabilizers and nanoparticle's interaction with stabilizer. Sodium dodecyl sulfate was found to be best stabilizer for WO_3-de-ionized suspension as compared to other stabilizers (CTAB, Triton-x-100, PVP, PVA and Oleic acid). The dispersion behavior of WO_3-de-ionized water suspension was also investigated under different

pH values (2-12). The point of zero charge (1.5-2) of WO_3-de-ionized water suspension was identified in terms of its colloidal stability.

Section B: A thin layer of SiO_2 coating for highly improved dispersion stability and thermal conductivity of WO_3-H_2O suspension: Long term dispersion stability for an improved thermal conductivity is a challenging issue that needs to be solved for heat transfer applications**.** Hence, this research investigated that a thin layer of SiO_2 coating (2-5 nm) over WO_3 nanostructures (SiO_2@WO_3) of different shapes exhibited superior dispersion (0.01%) stability for longer duration as evident by steady zeta potential (-30 ↔ -60.70 mV), no significant change in particle-size (139↔147 nm) distribution, density (1.001↔0.988 g/cm^3) and refractive index (1.335↔1.332) etc. Thin Si-OH layer over WO_3 surface imparts superior hydrophilicity, larger surface area for effective solute-solvent (SiO_2@WO_3-H_2O) interaction for improved colloidal stability showing no sedimentation and color change of SiO_2@WO_3 dispersion (0.01%) even after 3 days due to repulsive interaction between negatively charged Si-O$^-$ particles. Thereby, thermal conductivity is found to be quite stable (0.631↔0.618 W/m.K) up to 3 days, whereas aqueous suspension of bare WO_3 particles quickly settle down and thermal conductivity rapidly decreased to a value of 0.584 W/m.K. Depending on the thickness of SiO_2 layer and volume fraction of SiO_2@WO_3, a maximum of 8-10% increment of thermal conductivity was achieved where anisotropic WO_3 displayed always higher enhancement in (~5%) thermal conductivity than typical spherical nanoparticles.

Chapter 5 Phase-dependent Thermophysical Properties of α-and γ-Al_2O_3 in Aqueous Suspension: This study demonstrates the thermal conductivity and viscosity of as prepared crystalline α-Al_2O_3 and amorphous γ-Al_2O_3 nanoparticles, having size in the range of 30-50 nm. The α-Al_2O_3 and γ-Al_2O_3 aqueous suspension exhibited ~10% and 6% enhancement in thermal conductivity of de-ionized water, but α-Al_2O_3 showed (~4-6%) higher thermal conductivity than γ-Al_2O_3 aqueous suspension. This is ascribed to better crystallinity of α-Al_2O_3 phase having regular and long order arrangement of atoms which favours rapid transfer of phonon vibration from one atom to another than amorphous γ-Al_2O_3 phase with irregular atomic arrays, and thereby decreases the heat transfer rate. Ultra-sonication helps in the breakdown of large clusters with an increase in the dispersion stability and thermal conductivity as verified by particle size distribution and zeta potential measurements. The viscosity of both (α, γ-Al_2O_3 phase**)** aqueous

suspensions is higher than de-ionized water. Viscosity is inversely proportional to thermal conductivity, which increased with increase in concentration and decrease with increase in temperature. The Al_2O_3 aqueous suspension showed Newtonian characteristics at lower concentration (0.05 vol.%).

Chapter 1

1. INTRODUCTION AND LITERATURE

1.1 Background

1.1.1 Thermal Conductivity

Normally, the liquids have higher thermal conductivity (TC) than that of gases but much less than that of solids. In liquids heat conduction takes place through molecular vibrations, collisions and diffusion. At higher temperature, the molecules vibrate at higher frequency and transfer heat to the molecules of lower frequency [1]. Due to the stronger intermolecular forces between polar liquids they have higher TC than non-polar liquids [2]. In solids, heat is conducted by various heat carriers such as flow of free electrons in case of metals and lattice vibrations (phonon vibrations) in case of semiconductors as shown in figure 1.1 (a-b). In solids, the TC is highly dependent on their structure and atomic arrangement for example carbon nanotubes/diamond has TC of 2000-3000 W/m.K whereas amorphous carbon has TC of ~1.6 W/m.K [3,4]. This is due to long order arrangement of atoms in case of crystalline solids and short order arrangement of atoms in case of amorphous solids. The TC of the crystalline solids is also affected by impurities, crystallite size and phase of the materials, whereas the degree of molecular order is the main factor which affects the heat conduction in case of amorphous solids [5].

***1.1.1.1 Lattice Thermal Conductivity*:** In a solid crystalline lattice, the phonon vibrations arise due to vibrations of atoms within the lattice as shown in figure 1.1 (b). Due to the closeness of atoms, the vibrations of atoms are strongly attached to the nearby atoms. The acoustic waves moving through the lattice are equivalent to the oscillating motion of these attached atoms, therefore, with the change in temperature the energy transmitted through the lattice by these phonon waves [6] as shown in figure 1.1 (b). The alteration in the direction of the phonon wave can occurred due to very strong order interactions between the atoms which lead to decease in TC, this process is called phonon scattering [7]. The phonon scattering are divided into two categories, one is elastic phonon scattering and another one is inelastic phonon scattering. In case of elastic phonon scattering, the momentum of phonon is conserved but in case of inelastic phonon scattering the momentum of phonon is not conserved. The TC is also decreased by

inelastic scattering because it creates resistance to thermal transport. In a crystal structure phonon scattering takes place due to collisions of phonons with each other or with defects (such as grain boundaries and impurities).

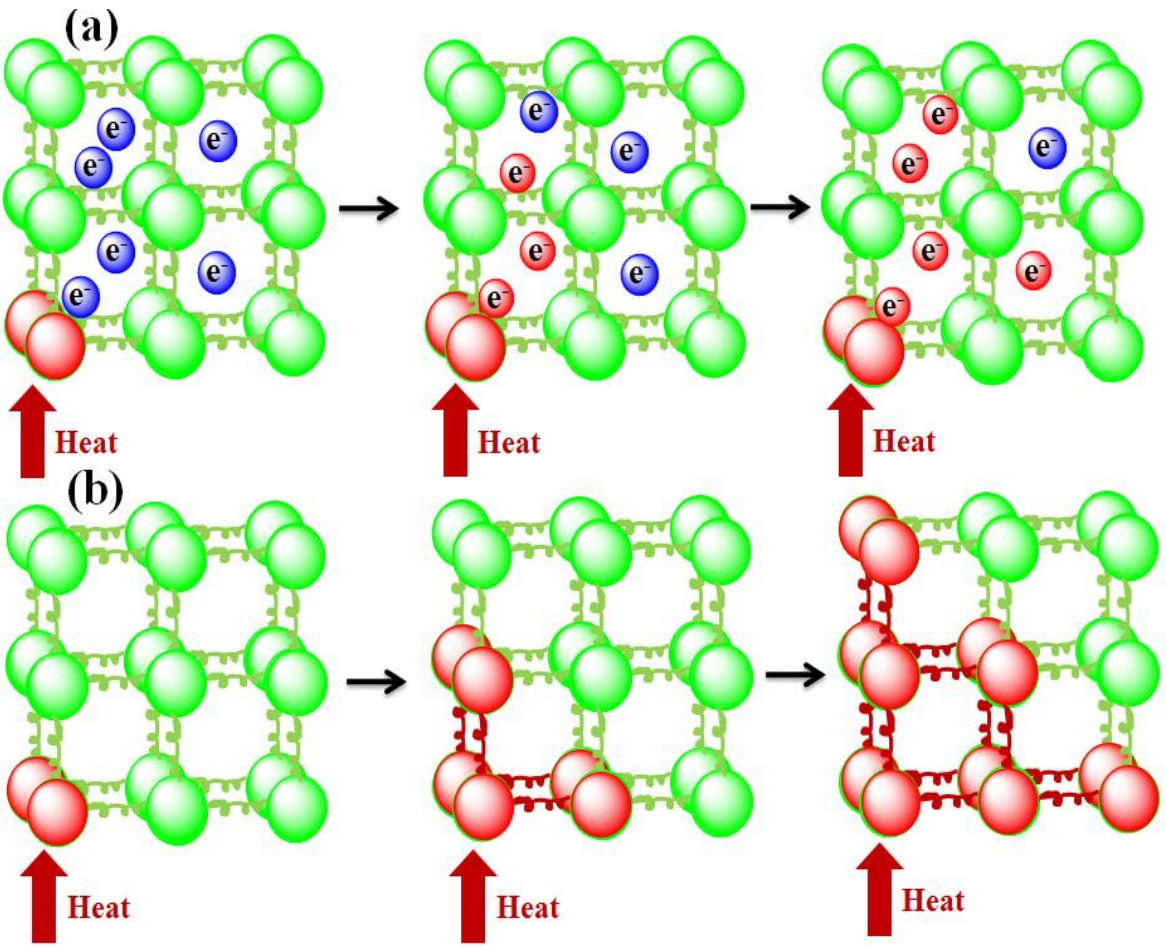

Figure 1.1: Schematic representation of heat conduction by **(a)** free electrons in case of metals and **(b)** phonon vibrations (lattice vibrations) in case of semiconductors.

1.1.2 Inspiration of Improving Thermal Conductivity of Fluids

Ethylene glycol, water and oils (conventional heat transfer fluids) have numerous industrial applications, such as energy supply/storage, transportation, air-conditioning, aerospace, nuclear power plant and electronics cooling etc [8-12]. Cooling now becomes the primary issue of all these industries due to the low TC of these conventional heat transfer fluids [13]. Currently, the

thermal management has major concern of component design and become one of the top technical confront due to decreasing size of the equipments and their increasing power [14]. The search for new heat transfer fluids with higher TC and more efficient cooling capacity is an emergency now because of increasing demand for machines and devices to operate effectively. The conduction of these fluids can be increased by dispersing solid particles in it [15] because solids have higher TC than liquids [16] as shown in table 1. Thus, the addition of millimeter or micrometer sized particles into these fluids have been studied, however, it has been difficult to use these fluids in heat transfer applications due to sedimentation, erosion and clogging of particles in fluid channels [17-19]. Consequently, thermal management system is in the need for superior cooling techniques and innovative heat transfer fluids with better heat transfer efficiency than conventional heat transfer fluids. This problem can be overcome by nanotechnology by producing nanometer sized nonmetallic, metallic or metalloids particles which have unique mechanical, optical, electrical, magnetic, and thermal properties. The dispersion of these nanoparticles (NPs) in any heat transfer fluids is known as nanofluids (NFs), the term is coined by Choi [20] in 1995.

1.1.3 Nanofluids

Nanofluids have been consider as future heat transfer fluids when Eastman et al. in 1996 [21] reported 60% enhancement in effective TC after dispersing 5 vol.% of CuO in distilled water. After that many research groups [22-24] have reported improved heat transfer properties with only a small addition of particles, even less than 1 vol.%. Nanofluids have many applications as shown in figure 1.2. The solids (metal, metal oxides and nonmetals) and liquids which can be used in NFs are listed in the table 1; the choice of materials is based on applications part.

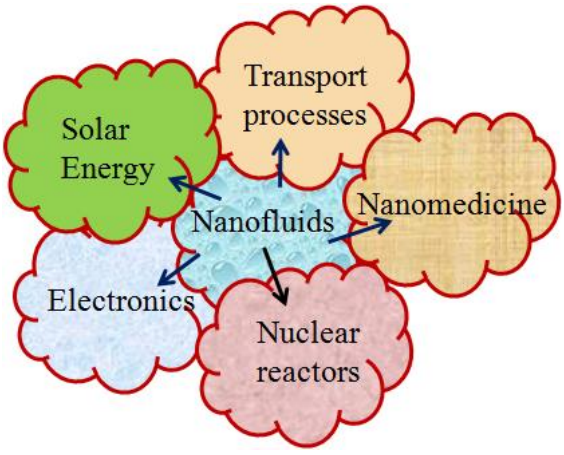

Figure 1.2: Applications of Nanofluids.

Table 1.1: Thermal conductivity of some liquids and solids used in nanofluids.

Materials		Thermal Conductivity (W/m.K)
Liquids (base fluids)	H_2O	0.613
	Ethylene glycol	0.253
	Engine oil	0.145
Solids (Metallic)	Ag	428
	Cu	401
	Au	318
	Al	237
	Fe	83.5
Nonmetallic	Si	148
	SiC	270
	Al_2O_3	40
	CuO	76.5
	CNTs	2000-3000

1.1.3.1 Why metal oxide nanoparticles and significance of their size and shape

Metal oxides NPs display interesting electronic, magnetic and thermal properties. The TC of heat transfer fluids can be enhanced by dispersing appropriate metal oxide NPs (TiO_2, Al_2O_3, CuO and SiO_2 etc) in it as reported in many research articles [25-27], metal oxides NPs are also easy to

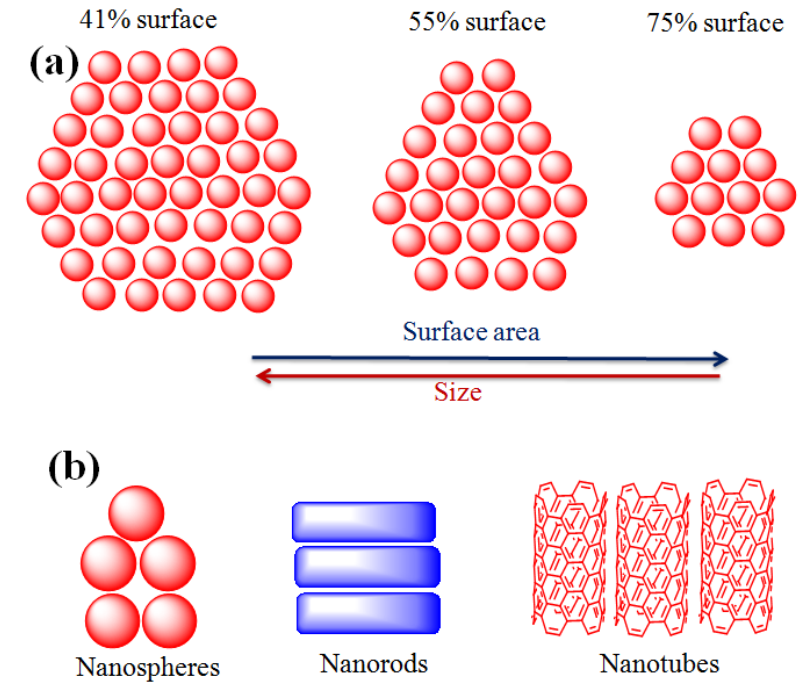

Scheme 1.3: Schematic representation showing change in surface area with the change in (a) size and (b) shape of particles.

synthesize as compare to metals and chemically stable in various solvents. The NPs have higher surface-area-to-volume ratio and surface active atoms (figure 1.3a) which not only improve the heat transfer efficiency but also increased the dispersion stability. As heat transfer takes place generally through the surface atoms [28], anisotropic NPs having more surface exposed atoms can further modify the material's [29,30] properties significantly for better heat conduction capacity. The properties of NPs can be altered significantly by changing their size and shape and make them an ideal candidate for many applications, such as optoelectronic, energy storages, sensing, catalysis, biomedicine and magnetic resonance imaging [31,32]. It is feasible to synthesize not only symmetrical shape NPs but also a variety of other shapes (such as cube, prism, hexagon, octahedron, disk, wire, rod, tube, etc) can be synthesized (figure 1.3b) due to advances in new synthesis techniques [33]. The shape of NPs can be classified according to their dimensionality, such as 0D, 1D and 2D (spheres, nanorods and prisms etc) as shown in figure 1.3b. The shape of the NPs can be controlled by regulating a number of kinetic and thermodynamic parameters [34].

1.1.4 Core/Shell structure and importance of silica coating: The coating of core particles have so many benefits such as ability to increase functionality, stability, surface modification, dispersibility, decrease in utilization of precious materials, controlled release of the core and so on. In core/shell type NPs, the inner material is called core and the outer thin layer is called shell. The core/shell materials can be categorized based on their

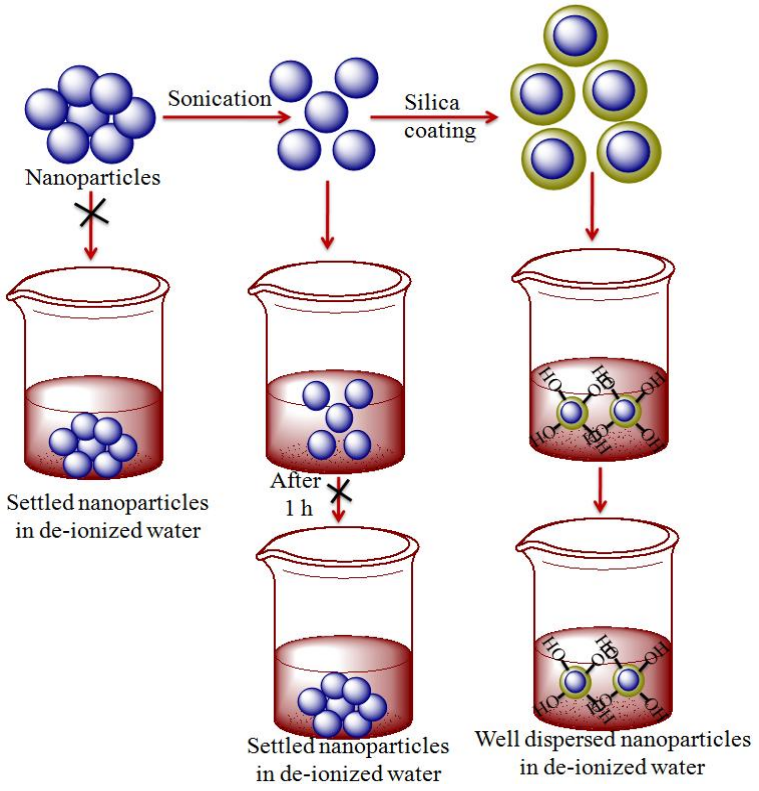

Figure 1.4: Schematic representation showed importance of silica coated nanoparticles as compare to bare nanoparticles when dispersed in de-ionized water.

interactions with each other such as organic/organic, organic/inorganic, inorganic/organic and inorganic/inorganic materials [35]. In core/shell NPs, the choice of shell and core materials is depend on their use in various applications. The SiO_2 as a shell has so many benefits such as high stability in aqueous solution (figure 1.4), chemical inertness, optical transparency and easy processability as compare to other organic and inorganic materials [36]. Silica is also thermally stable and can be used for higher temperature based applications. The primary parameters which favor the significant stability of SiO_2 sols are lower van der Waals interactions than those involving other NPs and tightly attachment of positively charged molecules to polymeric silicate layer at water-silica interfaces under basic conditions [37]. Thus, silicate layer play a role of both steric and electrostatic protection on different cores and act as dispersing agent [38]. These advantages make SiO_2 an ideal and low-cost material to modify surface properties.

1.1.5 LASER irradiation of nanoparticles: Since the size of the suspended particles in NFs critically affects the effective TC, particle fragmentation processes that can reduce the particle size can be employed to enhance the TC of NFs. Among such processes, the light amplification by stimulated emission of radiation (LASER) ablation-based processes offer efficient means to decrease the particle size (figure 1.5). It has been reported that high power laser pulse irradiation onto liquid suspensions can result in substantial decrease in size of the constituent NPs [39-41]. According to earlier studies, the laser irradiation not only suitable for altering particle size but also alter the shape and size distribution effectively (figure 1.5). Therefore, the laser fragmentation is expected to alter the thermal transport properties of NFs significantly.

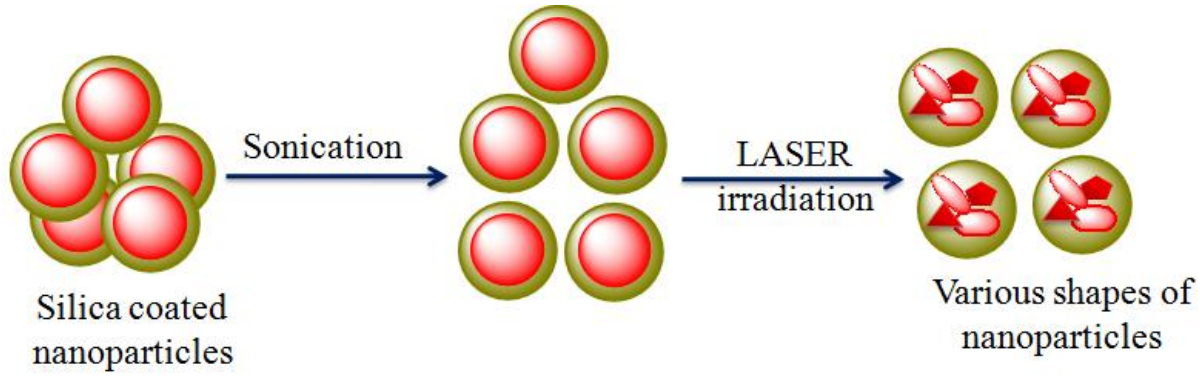

Figure 1.5: Schematic representation of formation of various unconventional shapes by LASER irradiation.

1.2 Literature review

1.2.1 Thermal Conductivity of Nanofluids

The TC of NFs has drawn increasing consideration since Choi [20] first postulated that the TC can be improved by adding conductive (metals) solid particles in conventional heat transfer fluid. Eastman et al [42] reported 60% and 40% enhancement in TC for CuO-H_2O and Al_2O_3-H_2O based NFs by loading of 5% NPs in it. Consequently, many research groups have presented data for various NFs (CuO, TiO_2, Al_2O_3, Cu, Ag, Au etc), some of them showed that TC have good agreement with the conventional models, while other showed anomalous higher TC than predicted models. Experimental studies have shown that the effective TC of NFs is influenced by the volume fraction, size and shape, temperature, pH, additives and dispersion method of NPs.

1.2.2 Various factors affecting TC of nanofluids:

1.2.2.1 Influence of particle size: An enhancement in TC with reduction in particle size was reported by few research groups, whereas other reported a decrease in TC with reduction in particle size [43]. For TiO_2 (3%) ethylene glycol (EG) based NFs, the TC enhancement for the 10 nm sample was approximately double than 70 nm sample (16 %). The TC enhancement for 36 nm Al_2O_3-H_2O based NF was 8% higher than 47 nm Al_2O_3-H_2O based NF as reported by Li and Peterson [44]. An enhancement in TC with the reduction in particle size (150 to 45 nm) for water based Al_2O_3 NFs was also reported [45]. An EG based ZnO (10, 30 and 60 nm) and (10, 34 and 70 nm) TiO_2 NFs showed linear increment in TC enhancement ratio with reduction in particle size [46]. A significant increase in the effective TC was observed for ZnO-H_2O based NFs when the particles were fragmented in various small sizes with high power laser irradiations [47]. An enhancement in TC with increase in NPs size was also accounted for aqueous SiO_2 suspension [48].

1.2.2.2 Effect of Volume Fraction: The volume fraction of NPs exhibit linear relationship with TC of NFs, but some reports showed non-linear relationship especially at low volume fraction (< 1%) [49,50]. Paraffin liquid, monoethylene glycol and transformer oil based CuO NFs (diameter 30 and 40 nm) displayed very high TC enhancement with the increase in particle concentrations. De-ionized water (DIW) based CuO NFs showed TC enhancements of 18, 28 and 31% at volume fractions of 1, 3 and 5% respectively [51] and EG-CuO based NFs displayed TC increment more

than 20% at a particle concentration of 4 vol.% [52]. Al_2O_3 NPs dispersed in transformer oil and water-EG mixture (40:60) showed high TC enhancement with increase in volume fraction [53]. Ethylene glycol and DIW based TiO_2 (tubes and spheres) NFs showed larger TC enhancement with particle loading, a 14.4% enhancement in TC was observed for EG-TiO_2 based NFs (loading of 1 vol.%) which was greater than theoretically predicated models [54]. Spherical (15 nm) and rod shaped (10 nm × 40 nm diameter by length) TiO_2 NPs (5 vol%) dispersed in H_2O showed 29.7% and 32.8% enhancement in TC which was also beyond the Effective Medium Theory (EMT) predictions [55]. At loading of 1 vol.% of TiO_2 in EG displayed 14% enhancement in TC that was higher than EMT predictions [56]. Though, the Al_2O_3-water based NFs showed good agreement with EMT predictions and suggesting no anomalous enhancement in TC as reported by recent benchmark studies [57].

1.2.2.3 Effect of shape of particles: An enhancement in TC with increase in particle's aspect ratio was reported by most the studies. Currently, it was reported that Al_2O_3 nanorods suspended in poly-alpha-olefin displayed higher enhancement in TC than nanospheres [57]. Rod (diameter = 10 nm, length = 40 nm) and spherical (15 nm) shaped TiO_2 NPs showed 32.8% and 29.7% enhancement in TC at particle loading of 5 vol%, [58]. The Al_2O_3 based NFs with various shapes (bricks, platelets, blades and cylinders) showed higher enhancement in TC for cylindrical shaped dispersion as compare to other shapes [59]. Some research groups [60,61] reported that the aggregates of higher aspect ratio are main factors for quick heat flow over long space. A differential effective medium theory was proposed by Zhou and Gao [62,63] based on Bruggeman's model [64] to calculate the effective TC of non-spherical solid NPs dispersion, they reported that non-spherical NPs showed higher enhancement in effective TC than spherical shaped NPs.

1.2.2.4 Effect of Temperature: Some research groups showed slight influence of temperature on TC of NFs, whereas other reports showed an increase in TC with increasing temperature (T). An Al_2O_3-H_2O and CuO-transformer oil based NFs showed that with the increase in temperature TC also increases [65,66]. The comparative increment in TC was observed more at higher temperature for CuO and Al_2O_3water based NFs [67]. An increase in enhancement of TC with increase in T was observed for ZnO, CuO and Al_2O_3 NPs dispersed in H_2O-EG mixture (40:60) [68]. At particle loading of 0.2 vol.% of Al_2O_3 in DIW, the enhancement in TC was 3.26% at

30°C and 10.76% at 60°C. For CuO NFs, the TC enhancement increased from 6.52 to 23.98% when the T was increased from 30 to 60°C [69,70]. In another report, the effective TC was reported to increase with increase in T (27.5 to 34.7°C) for CuO and Al_2O_3-H_2O based NFs [71]. The comparative TC was found to be decrease with increase in T (15-35°C) for H_2O based TiO_2 NFs [72].

1.2.2.5 Influence of base fluid and nanoparticles materials: The TC ratio decreases with increase in TC of the base fluids was reported by most of the studies. At same NPs concentration, the TC enhancement of EG based NFs was higher than that of H_2O based NFs in case of both $Al_2O_3$and CuO based suspension [73,74]. Some groups reported that the TC of NPs is not a main factor linked to TC of NPs, whereas some reported that the TC enhancement of NFs is higher when the dispersed NPs have higher TC. The metals (Cu, Al) based NFs showed higher enhancement in TC than metal oxides (CuO, Al_2O_3) based NFs when suspended in various base fluids such as EG, transformer oil and DIW [75]. Currently, it was reported that CuO-EG based NFs showed higher TC enhancement than Al_2O_3-EG based NFs at same concentration [76]. It was also found that Fe based NFs displayed 16.5% TC enhancement whereas WO_3 NFs displayed only 13.8% TC enhancement at particle loading of 0.3 vol.% [77]. At 1 volume fraction, TiO_2-DIW suspension displayed more enhancement of TC (14.4%) than Al_2O_3 suspension (4%) although bulk TiO_2 crystal have lower TC than Al_2O_3 crystal.

1.2.2.6 Effect of surface charge/pH: Surface charge of NPs is another important factor which affects the TC of the NFs [78]. At acidic pH, the TC ratio was observed to be increased whereas at basic pH, the TC ratio was decreased for H_2O based Cu and Al_2O_3 NFs. The pH value far from the isoelectric point (IEP) improved the suspension stability and TC of H_2O based SnO_2 NFs [79]. As the pH of H_2O based CuO NFs varied far from the IEP of particles, the particles become more stable and eventually change the TC of the fluid [80]. Electrokinetic properties are responsible for stability of aqueous based NFs; strong repulsive forces and high surface charge density improves the dispersion stability [81,82]. Zeta is zero at IEP of the suspension, therefore, at IEP the charge density becomes equal to surface charge density, which is the initial point of the diffuse layer and the charge density in this layer is zero. The repulsive energy is smaller for small particles therefore large zeta potential is required [83].

1.2.2.7 Effect of additives: In aqueous suspension addition of stabilizers improves the stability of NPs because they increase the hydrophilicity for aqueous suspension and decrease the hydrophilicity for non-aqueous suspension [84]. Cu and Al_2O_3-DIW based NFs demonstrated that an optimal SDBS concentration ascribed to the higher TC of the NFs [85]. In CNTs H_2O suspension, the effect of CTAB concentrations on TC is very low [86]. The surfactants that have been used for stability of NPs in base fluids are sodium dodecylsulfate (SDS) [87], SDBS [88], oleic acid [89], cetyltrimethylammonium bromide (CTAB) [90], dodecyl trimethylammonium bromide (DTAB), hexadecyltrimethylammonium bromide (HCTAB), and polyvinylpyrrolidone (PVP) [91].

1.2.2.8 Effect of sonication and aggregation: In current study, it was reported that different sonication power affects the effective TC of NFs [92]. In both alumina and copper oxide NFs higher power sonicator help in breakdown of large cluster into smaller one and give higher enhancement in TC. It was found that TC decreases with elapsed time after sonication due to particle agglomeration in H_2O based CuO NFs [93]. The effective TC showed higher enhancement immediately after sonication but with the passage of time it again decreases. It was found that assembly of NPs offer additional conduction paths which improved the effective TC of NFs, whereas large aggregates results decrease in TC.

1.3 Research gap

Literature review shows that the TC of the NFs can be altered by particle's size, volume fraction, surface charge and agglomeration [44, 51, 81, 93]. Very little information is available about the effect of shape of metal oxides NPs on the TC of NFs. With the advent of nanomaterials, it is recently demonstrated that many anisotropic and lengthy elongated shapes exhibit improved optical, electronic and thermal properties. Hence, it is expected that heat conduction of the metal oxide NPs will vary as a function of the geometric morphology and surface area of elongated NPs. The lengthy elongated shapes possessed large per-particle surface area and higher surface exposed atoms may exhibit better phonon conduction for higher TC.

Another major problem is the dispersion stability of NPs in the base fluid due to their very strong van der Waals interactions which quickly increase the aggregation of particles and finally settle down. Many attempts were made to overcome this problem by varying pH, using stabilizer or

applying strong force on the clusters of suspended particles. However, it declines the TC gradually due to chemical interaction and charge imbalance resulting into coagulation of NPs with passage of time, another drawback of surfactant addition is high temperature (above 70°C) applications, the bonding between surfactant and NPs can be damaged. Therefore, there is a need to stabilize the NPs for a longer time in order to improve their thermophysical properties for future applications. Out of various stabilizers, silica (SiO_2) being a chemically inert, is found to be the effective coating material for the improvement of dispersion in aqueous media through hydrophilic interactions. Silica is also thermally stable even at very high temperature, transparent and electrical insulator; this could be beneficial for heat transfer systems like cooling for high voltage applications. Thus, coating a thin layer of SiO_2 may lead to improve the surface hydrophilicity, functionality, stability, and dispersibility etc. for the overall improvement in TC, which is not investigated so far.

According to earlier studies, the laser irradiation not only suitable for altering particle size but also alter the shape and size distribution effectively. Therefore, the laser fragmentation is expected to alter the thermal transport properties of NFs significantly.

1.4 OBJECTIVES:

1. Preparation and characterization of different shapes of metal oxides nanoparticles such as CuO, TiO_2, WO_3 and Al_2O_3 and to study their dispersion stability in DI water and EG based fluids.
2. Surface modification of these metal oxide nanoparticles with a thin layer of SiO_2 shell and evaluation of dispersion stability.
3. To study the effect of LASER light irradiation of these metal oxides for dispersion stability.
4. Evaluation of thermal conductivity of stable metal oxide based nanofluids at various temperatures.

1.5 EXPERIMENTAL SECTIONS

1.5.1 Materials and methods

1.5.1.1 Chemicals

Titanium isopropoxide ($Ti\{OCH(CH_3)_2\}_4$), Titanium tetrachloride ($TiCl_4$)**,** Ethanol (C_2H_5OH), Sodium Hydroxide (NaOH), Nitric acid (HNO_3), Methanol (CH_3OH), De-ionized water (H_2O), Ammonium hydroxide (NH_4OH), Teraethyl orthosilicate [$Si(OC_2H_5)_4$], Cupric nitrate trihydrate ($Cu(NO_3)_2 \cdot 3H_2O$), Cupric acetate [$Cu(CH_3COO)_2$], Glacial acetic acid (CH_3COOH), Tungsten hexachloride (WCl_6), Sodium tungstate dehydrate ($Na_2WO_4 \cdot 2H_2O$), Urea [$CO(NH_2)_2$], Sodium Chloride (NaCl), Hydrochloric Acid (HCl), Cetyltrimethylammonium bromide ($(C_{16}H_{33})N(CH_3)_3Br$, Sodium dodecyl sulfate $CH_3(CH_2)_{11}OSO_3Na$, Triton X-100 $C_{14}H_{22}O(C_2H_4O)_n$), Oleic acid $CH_3(CH_2)_7CH{=}CH(CH_2)_7COOH$, Polyvinylpyrrolidone, Polyvinyl alcohol $[CH_2CH(OH)]_n$, Ethylene glycol, Engine oil, Aluminium sulphate hydrate ($Al_2(SO_4)_3.xH_2O$) and Propanol ($CH_3CH_2CH_2OH$).

1.5.1.2 Synthesis of TiO_2 nanoparticles:

TiO_2 nanotubes and nanorods have been synthesized from TiO_2 P-25 (70:30 anatase:rutile) as shown in figure 1.6. Nanotubes were synthesized by hydrothermal method [94] in which 2 g of TiO_2 P-25 was mixed with 50 ml of 10 N NaOH and stirred for half an hour. Then the solution was transferred to Teflon lined autoclave and treated at 130 °C for 20 h in a muffle furnace. The final slurry was washed with 0.1 N HNO_3, methanol and de-ionized water, then dried overnight at 80 °C in an oven. As prepared TiO_2 nanotubes were used for the synthesis of TiO_2 nanorods. A 500 mg of TiO_2 nanotubes were mixed with 40 ml DIW and maintained pH 5-6, then autoclaved at 175 °C for 48 h. The final product was filtered, washed with distilled water and methanol and dried at the 70°C for 3 h.

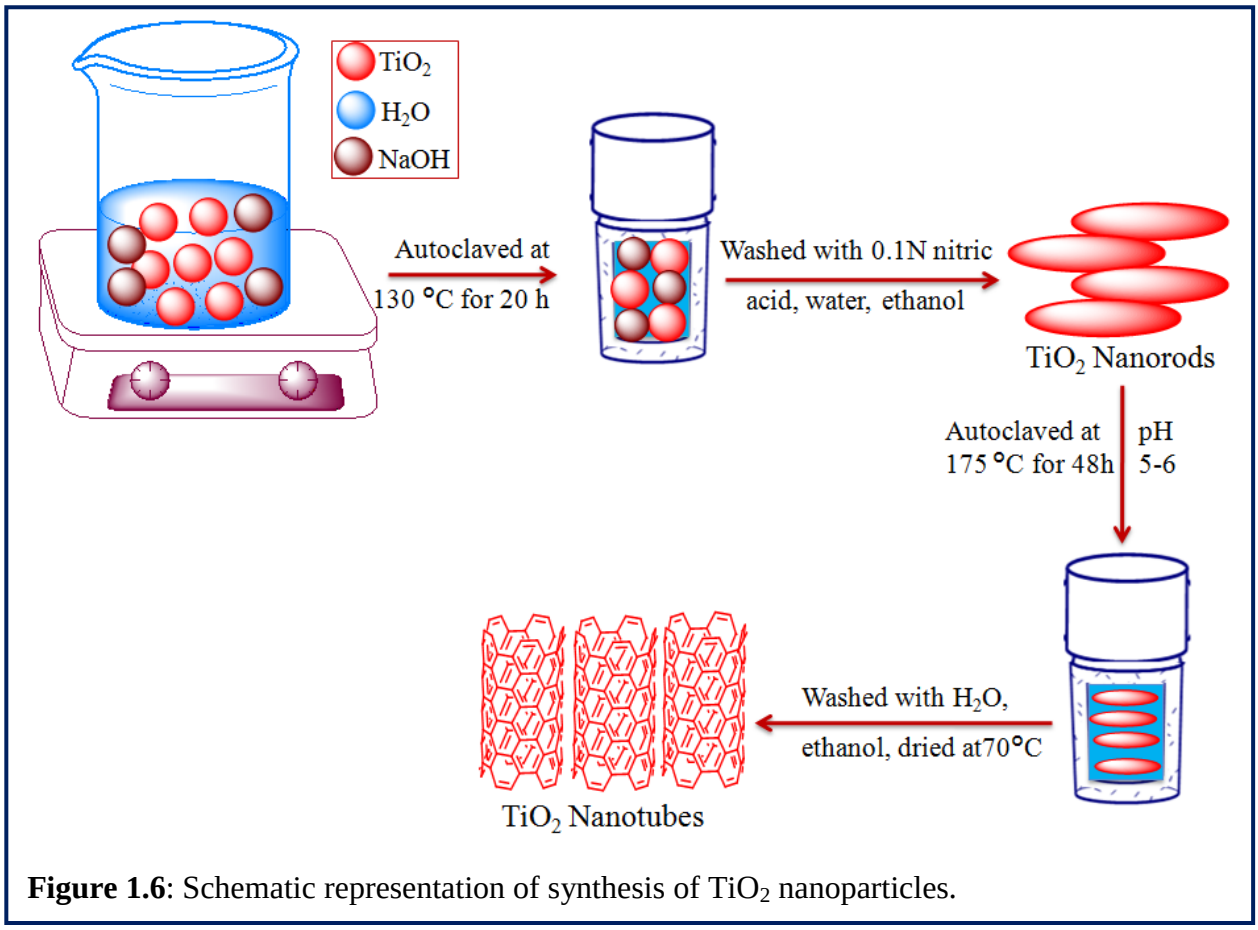

Figure 1.6: Schematic representation of synthesis of TiO_2 nanoparticles.

1.5.1.3 Synthesis of SiO_2@TiO_2 nanocomposites:

Shell/Core (SiO_2@TiO_2) nanocomposites have been synthesized by Stober process [95] as shown in figure 1.9. In a beaker 60 ml of ethanol, 20 ml of de-ionized water, I ml of ammonia solution and 0.5 g of TiO_2 NPs was mixed and sonicated for 1 hour to make homogeneous dispersion. In another break 20 ml of ethanol and various concentrations (80, 100, 120, 140 and 160 µl) of tetraethyl orthosilicate (TEOS) were mixed. After that this solution was added drop wise in breaker A and stirred for 2 h at room temperature and aged for 12 hours. The final product was washed with ethanol several times and dried under vacuum overnight to get the final SiO_2@TiO_2 nanocomposites.

1.5.1.4 Synthesis of CuO nanoparticles:

Nanospheres: A 0.02 M aqueous solution of $Cu(CH_3COO)_2$ was mixed with 1 ml of glacial acetic acid in a round-bottomed flask as shown in figure 1.7. Then the solution was heated to 100°C for 3 h with vigorous stirring. The pH of the above solution was maintained 6-7 by adding 0.1 M of sodium hydroxide in it and black precipitates formed immediately [96]. Then the solution was cool down at room temperature. Finally precipitates were centrifuged and washed with distilled water and absolute ethanol 3-4 times. ***Nanorods***: A 40 ml of ethanolic solution of $Cu(NO_3)_2 \cdot 3H_2O$ (0.03 M) was added [97] slowly to 40 ml of ethanolic NaOH solution (0.5 M) in a round-bottomed flask at 80 °C, followed by drop-wise addition of 60 ml of DIW. The contents were refluxed at 80°C for 24 h. The product was washed with DIW and ethanol. ***Nanowires***: In a typical synthesis [98], 1 g of $Cu(NO_3)_2$ was dissolved in 100 ml DIW, then 30 ml ammonia solution was added to the $Cu(NO_3)_2$ solutions under constant stirring. Then 1 M NaOH was added to the above solution to adjust pH at 9–10, resulting in blue precipitates of $Cu(OH)_2$. The precipitates were filtered with DIW and then again dissolved in 30 ml DIW and transferred it to sealed Teflon-lined stainless steel autoclave at 130°C for 10 h. Finally black precipitates of CuO were washed with DIW and absolute ethanol.

1.5.1.5 Synthesis of SiO_2@CuO nanocomposites:

SiO_2@CuO nanocomposites have been synthesized by Stober process as shown in figure 1.9. A mixture of DIW (20 ml), ethanol (60 ml), 0.5 g CuO and 1 ml of ammonia was taken in a beaker and sonicated for 1 hour to make uniform dispersion. A mixture (20 ml) of ethanol and tetraethyl orthosilicate (TEOS) of various amounts was added (80, 100, 120, 140 and 160 µl) drop wise to the above dispersion. It was stirred for 2h at room temperature and aged for 12 hours, centrifuged and washed with ethanol several times, dried under vacuum overnight to get the final SiO_2@CuO nanocomposites.

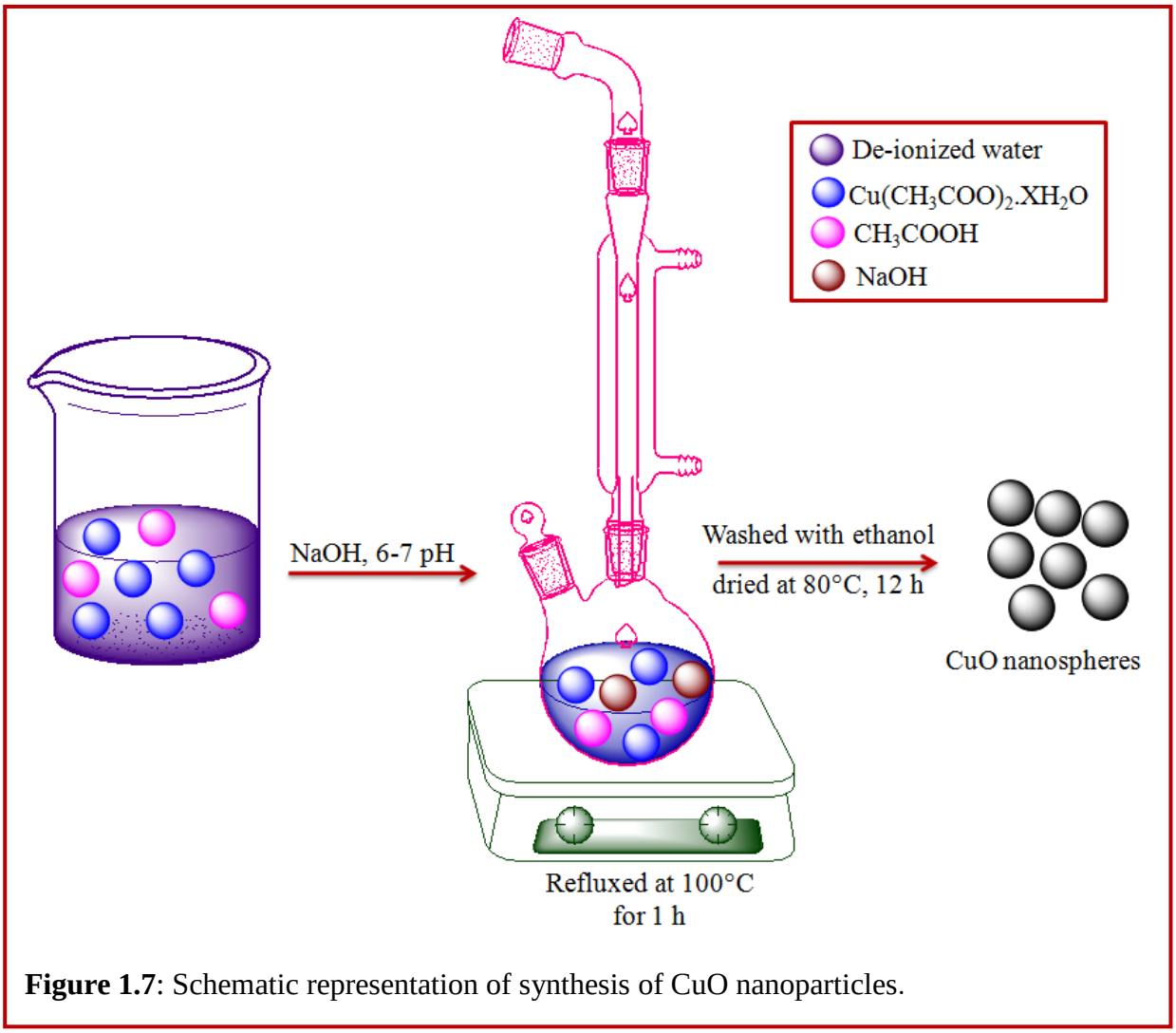

Figure 1.7: Schematic representation of synthesis of CuO nanoparticles.

1.5.1.6 Synthesis WO_3 nanoparticles: A 1 mmol of WCl_6 and $CO(NH_2)_2$ were mixed together in 40 ml of absolute [99] ethanol, stirred it for 1 hour, and then the solution was transferred into a Teflon-lined autoclave. The autoclave was then placed in a muffle furnace for 12 h at 180°C. The final product was washed with DIW and absolute ethanol 3-4 times and dried for 12 h at 60°C. The dried powder was then gradually calcined for 5 h at 450°C to get final product (figure 1.8). In a typical synthesis [100] of WO_3 nanorods, 0.825 g of $Na_2WO_4 \cdot 2H_2O$ and 0.292 g of NaCl were mixed in 20 ml of DIW (figure 1.8). After that 3 M HCl solution was added drop wise into the above mixture until the pH value reached at 2.0 with constant stirring. Then, the above mixed

was transferred into a Teflon-lined autoclave and placed in a muffle furnace for 24 h at 180 °C. After that product was obtained and washed repeatedly with DIW and ethanol.

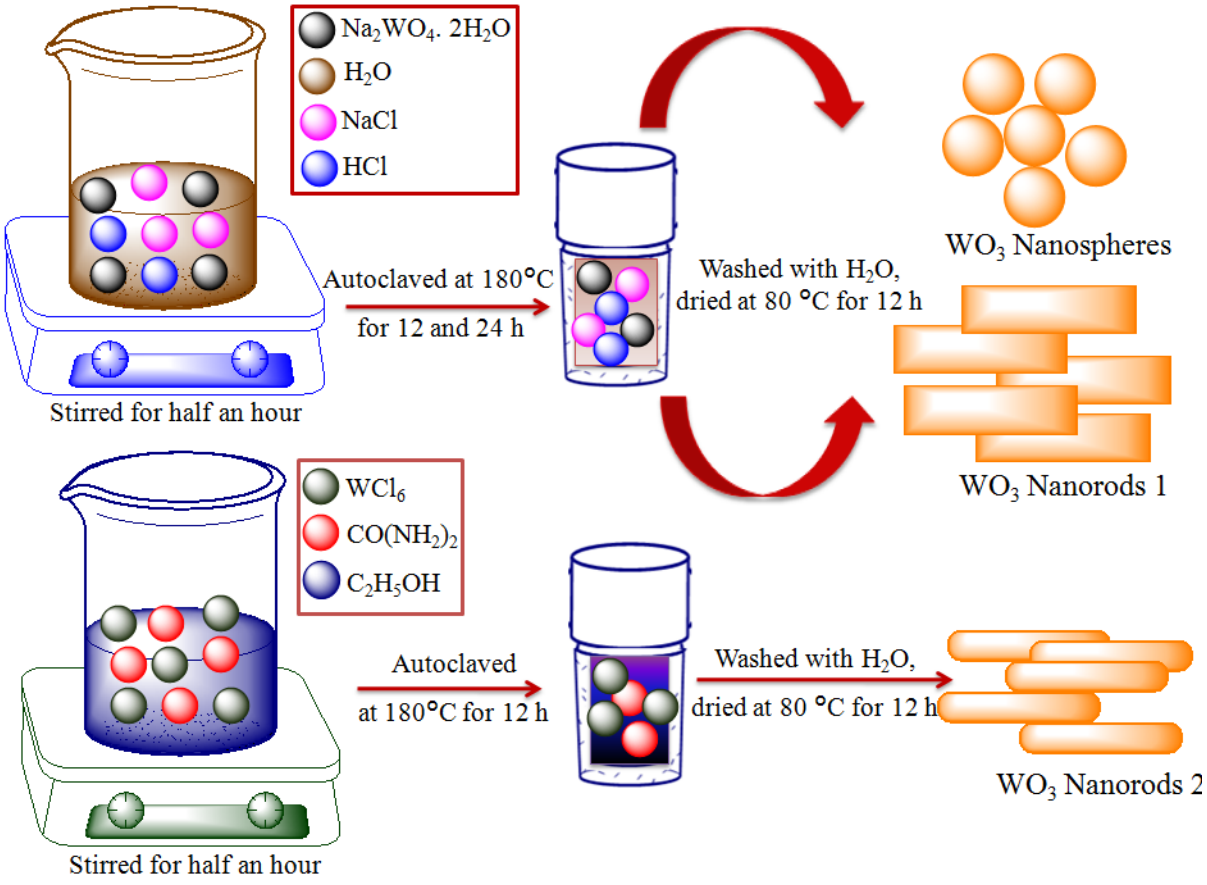

Figure 1.8: Schematic representation of synthesis of WO_3 nanoparticles.

1.5.1.7 Synthesis of SiO_2@WO_3 nanocomposites:

SiO_2@WO_3 nanocomposites have been synthesized by Stober process. A mixture of DIW (20 ml), ethanol (60 ml), 0.5 g WO_3 and 1 ml of ammonia was taken in a beaker and sonicated for 1 hour to make uniform dispersion. A mixture (20 ml) of ethanol and tetraethyl orthosilicate (TEOS) of various amounts was added (80, 100, 120, 140 and 160 µl) drop wise to the above dispersion. It was stirred for 2h at room temperature and aged for 12 hours, centrifuged and

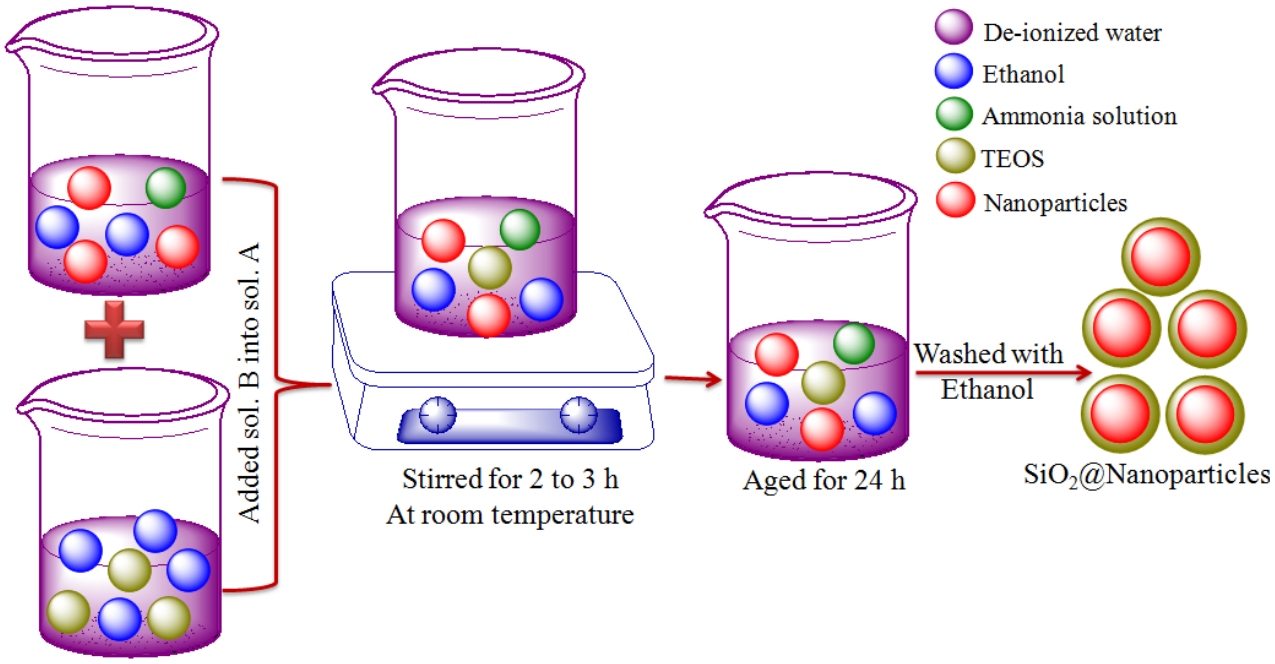

Figure 1.9: Schematic representation of SiO_2 coating over various nanoparticles.

washed with ethanol several times, dried under vacuum overnight to get the final $SiO_2@WO_3$ nanocomposites (figure 1.9).

1.5.2 Preparation of Nanofluids:

Nanofluids can be prepared by two methods, two-step method and single step method. In two step method, the nanoparticles are first synthesized and then dispersed into a base fluid as shown in figure 1.10. In single step method, particle's synthesis and dispersion takes place simultaneously directly into a base fluid; metallic based NFs are prepared by this

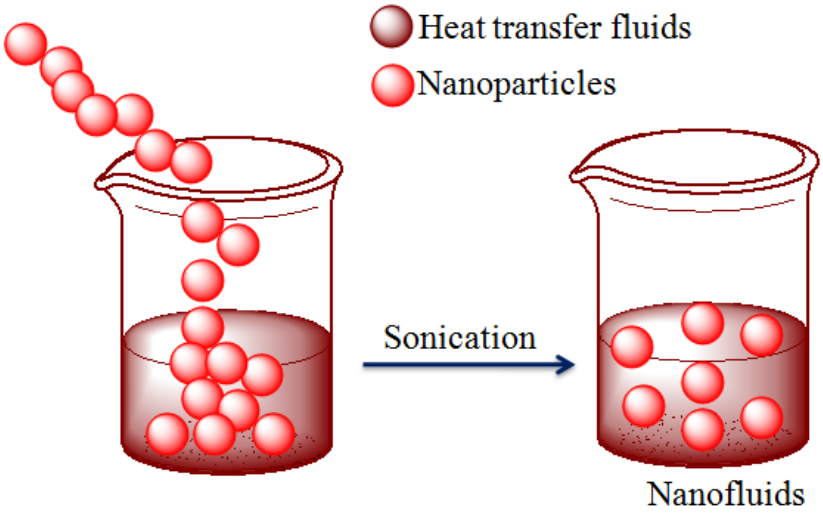

Figure 1.10: Schematic representation of preparation of nanofluids by two step method.

method. In this research two-step was adopted for preparation of NFs.

1.5.3 Thermal conductivity Measurement:

The KD-2 Pro (Decagon Devices, USA) thermal properties analyzer instrument was used for measurement of TC. The KS-1 sensor needle has been used for measurement of TC. The needle is made of stainless steel; it has length of 60 mm and a diameter of 1.3 mm. This needle gives the least disturbance to the sample during measurements. The accuracy for the measurement of TC by this needle is 5% in the range of 0.2– 2 W/m.K, which congregate the ASTM56 and IEEE57 standards. KS-1 sensor needle was inserted vertically into the 15 ml of given sample container and then readings were taken after every 15 minutes time interval at different temperatures for each sample. The instrument was calibrated with the known TC of glycerol, which has a value of 0.282 W/m.K; the experimental value was 0.280 W/m.K. The TC of the NFs was measured with different concentrations (0.01 to 10%) and temperature (15°C to 40°C) has been measured. Temperature controller with oil bath was used for the measurement of TC at various temperatures. The experimental setup for the measurement of TC was shown in figure 1.11.

Figure 1.11: Experimental setup for measurement of thermal conductivity.

1.5.4 Measurement of Density and Refractive index: The density of all the samples were measured (Density meter, DMA 35, Anton Paar, Austria) by density meter which has sample capacity of 1 ml. The accurate volume was determined with the uncertainty of ±0.1% using water and EG as reference liquids. Experimental setup is shown in scheme 6. The refractive index of all the samples was (Pocket Refractometer, Atago, PAL-RI, Japan) measured by refractometer with 0.3 ml sample capacity. The refractive index of DIW and EG was measured as a standard. A 0.3 ml of sample was taken in micropipette then added on the glass of refractometer by drop-wise and measure the refractive index of every sample. The experimental setup is shown in figure 1.12.

Figure 1.12: Experimental setup for measurement of density and refractive index.

1.5.5 Measurement of Viscosity: Viscosity has been measured by DV-III Ultra Programmable Rheometer. The sample capacity of instrument is 1 ml and temperature controller is also present in the instrument by which viscosity of samples can be measured at various temperatures.

1.5.6 Measurement of particle size distribution and zeta potential: The particle size (Dynamic Light Scattering, DLS) distribution and Zeta potential (Brook haven 7610 instrument) were measured using 1.5 ml aqueous suspension (0.01%) of samples after 30 min sonication.

1.5.7 Characterization techniques: As prepared NPs have been characterized by various techniques for the identification of their crystal structure, absorption, morphology, surface area, chemical composition, functional group, thermal stability and surface charge density.

1.5.7.1 Powder X-Ray Diffraction (XRD)

Powder X-ray diffraction (XRD) is a primary technique used for identification of phase, composition and crystal system of the materials; it can also give information on unit cell dimensions. XRD patterns also help in to calculate the crystallite size of the materials by using Scherrer's equation $D = k\lambda/\beta\cos\theta$, where k is a constant, λ is the X-ray wavelength, D is the crystallite size, θ is the diffraction angle and β is full width at maxima of the diffraction line. PANalytica X' pert PRO X-ray diffractometer with Cu Kα (λ = 1.54 Å) radiation was used for XRD pattern analysis. For the identification of crystal system, phase, composition and crystallinity of the materials this technique was used throughout the research. A smooth plain surface paper was used to press the powder samples into a sample holder. The XRD study was done from Sophisticated Analysis Instrumentation Laboratory (SAI Lab), Thapar University, Patiala, India.

1.5.7.2 Ultraviolet-Visible Spectrophotometer (UV-Vis spectrophotometer)

The measurement of the reduction of a beam of light after it passes through a sample was done by UV-Vis absorption spectroscopy. Absorption spectra give the information about size distribution, band gap and nanoparticles formation. The principle of this instrument is that when sample is exposed to light (having suitable energy for electronic transition within the molecule), required energy is absorbed and the transition of electron takes place from lower energy level to higher energy level. Analytic Jena, SPECORD 205 UV-Vis spectrophotometer was used in this research in order to examine the characteristic absorbance band of the synthesized NPs (TiO_2, CuO and WO_3). Aqueous suspension of all samples was analyzed in a 3.5 ml quartz cuvette in the detection range of 190-1100 nm.

1.5.7.3 Scanning Electron Microscopy (SEM)

The external morphology (shape and size) of all the samples were analyzed by scanning electron microscopy. Morphology, topography, crystallographic and composition information about the sample surface can be investigated from SEM images. A beam of electrons is focused on a selected area of a sample at the time of SEM analysis and therefore an exchange of energy from the electron beam to the sample surface takes place. The electron gun produces electron at the top are referred to as primary electrons and these electrons are then analyzed, amplified and translated into images. JSM-7600F (0.1 to 30 kV) instrument was used for SEM images analysis,

where samples were placed on a specimen stub with conducting tape and then coated with a thin layer of gold to reduce sample charging.

1.5.7.4 Energy Dispersive X-ray (EDX) Spectrophotometer Analysis

The chemical composition and elemental analysis of all the samples was analyzed by energy dispersive x-ray spectrophotometer. EDX is also helpful to recognize contaminants and their comparative concentrations on the surface of the samples, EDX examination was done on JEOL JSM-6510LB.

1.5.7.5 Transmission Electron Microscopy (TEM)

Transmission electron microscopy is used to identify finest structural details of individual particles and their statistical size and shape distribution in the samples. In this technique, a beam of electrons is transmitted through the sample and interacting with it, due to this interaction an image is formed then magnified and focused onto an imaging device. High resolution transmission electron microscopy (HR-TEM) becomes a valuable technique due to its high magnification by which lattice fringes of materials can be clearly seen. In this research, Hitachi-7500 transmission electron microscope at 120 KV was used to investigate the morphology of all the samples. Aqueous suspension of all the samples was dropped on copper grid coated with carbon film and then analyzed. Analysis was done at various sophisticated laboratory such as IIT-Mumbai, Panjab University, Chandigarh, and NIPER, Mohali, Punjab, India.

1.5.7.6 BET surface Area Analysis

Surface area of the prepared samples was analyzed by Brunauer, Emmett and Teller (BET) surface area analyzer by physical adsorption/desorption of N_2 gas on the solid surface of powder samples. Smartsorb 92/93 instrument was used for this purpose where 100 mg of samples were heat at 130 °C for 2 h.

1.5.7.7 Thermogravimetric Analysis (TGA)

The thermal stability of a material as function of time and temperature in an inert atmosphere was analyzed by TGA. When a material was heated weight lose takes place due to phase

changes, water lose, structural decomposition and gas evolution. This technique was used to measure the thermal stability of all the samples by using Shimadzu TGA50.

1.5.7.8 Fourier-Transform Infrared (FTIR) Spectroscopy

FT-IR spectroscopy was used to obtain information about Si-O-Si linkage with NPs. The working principle is based on the fact that bonds and groups of bonds vibrate at characteristic frequencies. When a sample is exposed with infrared radiations, absorbed infrared energy excites molecules into higher vibrational states, which is characteristic to that particular molecule. All the FT-IR analysis of the samples was carried out on FT-IR, Agilent Cary 630 spectrometer. The electromagnetic spectrum range was 400 nm to 4000 nm at the time of measurement.

1.5.7.9 Ultraviolet and Ar ion LASER

Ultraviolet (266 nm) and Ar ion LASER were used for the fragmentation of NPs into various size and shape. Ar ion continuous laser (Stellar-Pro, MODU LASER with multiline configuration) having energies in the range of 40-120 W and controllable monochromatic wavelengths i.e. 488 nm was used for the fragmentation of CuO NPs. For the fragmentation of WO_3 and TiO_2 NPs 266 nm wavelength was used.

1.5.7.10 KD2 Pro thermal properties analyzer

KD2 Pro was used for the measurement of TC throughout the research work. This instrument works on the principle of transient hot wire methods where a single needle plays a role of heater and temperature sensor. The system monitors the temperature of the sensor when a current passes through the heater, then analysis of the sensor temperature determines the TC.

1.5.7.11 Dynamic light scattering and zeta potential analyzer: It provides the hydrodynamic size of the NPs and was done by taking ≈ 1.5 ml of the dispersed particles in a cuvette. The zeta potential is crucial in determining the stability of a colloidal NPs suspension. All the particles in suspension exhibit some surface charge or zeta potential, the measurement and knowledge of which is significant for predicting stability and interactions among the reacting substrates. Zeta potential (ζ) measurements were carried out by Brookhaven 7610 instrument and sample was prepared by adding 1.5 ml sample in a 3.5 ml glass cuvette. It represents the surface charge of a

particle which arises due to the potential difference between the particle's surface and the surrounding medium.

References:

[1] N.V. Tsederberg, *Thermal Conductivity of Gases and Liquids*. 1965, Cambridge, Massachusetts: THE M.I.T. Press. 246.

[2] B.E. Poling, J.M. Prausnitz and J.P. O'Connell, *The Properties of Gases and Liquids*. 5th ed. 2001, Boston: The McGraw-Hill Companies.

[3] J.A. Dean, *Lange's Handbook of Chemistry*. 14th ed. 1992, New York: McGraw-Hill, Inc.

[4] S.U.S. Choi, Z.G. Zhang, W. Yu, F.E. Lockwood and E.A. Grulke, *Appl. Phys. Lett.* 2001, **79(14**), 2252-2254.

[5] R.B. Bird, W.E. Stewart and E.N. Lightfoot, *Transport Phenomena*. 2nd ed. 2002, New York: John Wiley & Sons, Inc. 895.

[6] H.U. Kang, S.H. Kim and J.M. Oh, *Exp. Heat Transfer.* 2006, **19(3),** 181-191.

[7] T. Tritt, ed. *Thermal conductivity: theory, properties, and applications*. 2004, Kluwer Academic/Plenum Publishers: New York. 290.

[6] C.L. Tien, A. Majumdar and F.M. Gerner, eds. *Microscale Energy Transport*. 1998, Taylor & Francis: Washington D.C. 395.

[9] C.L. Tien, ed. *Annual Review of Heat Transfer*. Vol. 7. 1996, Begell House, Inc: New York. 444.

[8] C.T. Nguyen, G. Roy, C. Gauthier and N. Galanis, *Appl. Therm. Eng.* 2007, **27**, 1501-6.

[9] K.V. Wong and O. Leon, *Adv. Mech. Eng.* 2010, **2010**, 1-11.

[10] S. Lee, S.U.S. Choi, S. Li and J.A. Eastman, *J. Heat Transfer.* 1999, **121**, 280-289.

[11] K. Khanafer and K. Vafai, *Int. J. Heat Mass Transfer.* 2011, **54**, 4410-4428.

[12] H.A. Mintsa, G. Roy, C.T. Nguyen and D. Doucet, *Int. J. Therm. Sci.* 2009, **48**, 363-371.

[13] J.A. Eastman, S.R. Phillpot, S.U.S. Choi and P. Keblinski, *Annu. Rev. Mater. Res.* 2004, **34**, 219-246.

[14] S.K. Das, S.U.S. Choi and H.E. Patel, *Heat Transfer Eng.* 2006, **27**, 3-19.

[15] J. Maxwell, (1873). *A treatise on electricity and magnetism*, volume 1. Clarendon Press.

[16] D. Lide, (2004). *CRC Handbook of Chemistry and Physics.* CRC press, 84 edition.

[17] R. Saidur, K. Leong and H. Mohammad, *Renew. Sust. Energy Rev.* 2011, **15**, 1646-1668.

[18] D. Wen, G. Lin, S. Vafaei and K. Zhang, *Particuology*, 2009, **7**, 141-150.

[19] W. Yu and H. Xie, *J. Nano Mat.* 2012, **2012**, 1-48.

[20] S. Choi and J. Eastman, *Enhancing thermal conductivity of fluids with nanoparticles* (1995).

[21] J. Eastman, S. Choi, S. Li, L. Thompson and S. Lee, *MRS Proceedings*, 1996, 457.

[22] S. Das, S. Choi, W. Yu and T. Pradeep, (2007). *Nanofluids: Science and Technology.* John Wiley & Sons, Inc., Hoboken, New Jersey, USA.

[23] M. Chandrasekar and S. Suresh, *Heat Transfer Eng.* 2009, **30**, 1136-1150.

[24] J. Fan and L. Wang, *J. Heat Trans.* 2011, **133**, 1-14.

[25] R.S. Vajjha and D.K. Das, *Int. J. Heat Mass Transfer.* 2009, **52**, 4675-82.

[26] D. Zhu, X. Li, N. Wang, X. Wang, J. Gao and H. Li, *Curr. Appl Phys.* 2009, **9**, 131–139.

[27] Y. Hwang, J.K. Lee, C.H. Lee, Y.M. Jung, S.I. Cheong, C.G. Lee, B.C. Ku and S.P. Jang, *Thermochim. Acta.* 2007, **455**, 70-74.

[28] P.D. Shima, J. Philip and B. Raj, *J. Phys. Chem. C.* 2010, **114**, 18825-18833.

[29] R. Singh and B. Pal, *J. Mol. Catal. A: Chem.* 2013, **371**, 77-85.

[30] M. Haruta, *Chem. Rec.* 2003, **3**, 75-87.

[31] R. Hao, R. Xing, Z. Xu, Y. Hou, S. Gao and S. Sun, *Adv. Mater.* 2010, **22**, 2729-2742.

[32] S. Kinge, M. Crego-Calama and D. N. Reinhoudt, *Chem. Phys. Chem.* 2008, **9**, 20-42.

[33] L.S. Li, J. Hu, W. Yang and A.P. Alivisatos, *Nano. Lett*., 2001, **1**, 349–351.

[34] J. Hu, L.S. Li, W. Yang, L. Manna, L.W. Wang and A.P. Alivisatos, *Science*, 2001, **292**, 2060-2063.

[35] R.G. Chaudhuri and S. Paria, *Chem. Rev.* 2012, **112**, 2373-2433.

[36] T. Ung, L.M. Liz-Marzan, and P. Mulvaney, *Langmuir*, 1998. 14, 3740-3748.

[37] G. Vigil, Z. Xu, S. Steinberg and J. Israelachvili, *J. Colloid Interface Sci.* 1994, **165**, 367-385.

[38] F. Kuspert, *Berichte* 1919, **35**, 2815.

[39] F. Mafune, J. Kohno, Y. Takeda and T. Kondow, *J. Phys. Chem. B.* 2002, **106**, 8555-8561.

[40] A. Takami, H. Kurita and S. Koda, *J. Phys. Chem. B.* 1999, **103**, 1226-1232.

[41] M. Sugiyama, H. Okazaki and S. Koda, *Jpn. J. Appl. Phys., Part 1*. 2002, **41**, 4666-4674.

[42] T. Yamada, Y. Asako, J.O. Gregory and M. Faghr, *Numer. Heat Transfer, Part A*. 2012, **61**,323-37.

[43] H. Xie, J. Wang, T. Xi and Y. Liu, *Int. J. Thermophys.* 2002, **23**, 571-80.

[44] P. He and R. Qiao, *J. Appl. Phys*. 2008, **103**, 094305-6.

[45] K.B. Anoop, T. Sundararajan and S.K. Das, *Int. J. Heat Mass Transf.* 2009, **52**, 2189-95.

[46] S.H. Kim, S.R. Choi and D. Kim, *ASME J. Heat Transf.* 2007, **129**, 298-307.

[47] J. Hong, S.H. Kim and D. Kim, *J Phys: Conference Series.* 2007, **59**, 301-4.

[48] G. Chen, W. Yu, D. Singh, D. Cookson and J. Routbort, *J. Nanopart. Res.* 2008, **10**, 1109-14.

[49] J. Eapen, R. Rusconi, R. Piazza and S. Yip, *ASME J. Heat Transf.* 2010, **132**, 102402.

[50] G. Okeke, S. Witharana, S.J. Antony and Y. Ding, *J. Nanopart. Res.* 2011, **13**, 6365-75.

[51] H.T. Zhu, C.Y Zhang, Y.M .Tang and J.X. Wang. *J. Phys. Chem C.* 2007,**111**, 1646-50.

[52] S. Kondaraju, E.K. Jin and J.S. Lee. *Phys Rev E.* 2010, **81**, 016304.

[53] P. Bhattacharya, S.K. Saha, A. Yadav, P.E .Phelana and R.S.Prasher. *J. Appl. Phys.* 2004, **95**, 6492-6494.

[54] D.H. Yoo, K.S .Hong and H.S. Yang. *Thermochim. Acta* .2007, **455**, 66-9.

[55] S.M.S. Murshed, K.C. Leong and C. Yang. *Int . J. Therm. Sci* . 2005, **44**, 367-73.

[56] T.K. Hong and H.S. Yang. *J . Korean. Phys. Soc.* 2005,**47**, S321-S324.

[57] J. Buongiorno, *J. Appl. Phys. 2009*, **106**, **094312**.

[58] S.M.S. Murshed, K.C. Leong, C. Yang, *Int. J . Therm. Sci.* 2005, **44**, 367-73.

[59] M. Kole and T.K. Dey. *J. Phys. D: Appl. Phys.* 2010, **43**, 315501-10.

[60] C.Y. Hong, C.C. Wu, Y.C. Chiu, S.Y. Yang, H.E. Horng and H.C. Yang, *Appl. Phys. Lett.* 2006, **88**, 212512-3.

[61] D. Wen and Y Ding, *IEEE Trans Nanotech.* 2006, **5**, 220-7.

[62] D. Li, B. Hong, W. Fang, Y. Guo and R. Lin, *Ind. Eng. Che. Res.* 2010, **49**, 1697-702.

[63] D.H. Yoo, K.S. Hong and H.S. Yang, *Thermochim. Acta.* 2007, **455**, 66-9.

[64] W. Yu, H. Xie, L. Chen and Y. Li. *Colloids. Surf . A.* 2010, **355,** 109-13.4

[65] T.P. Teng, Y.H. Hung, T.C. Teng, H.E. Moa and H.G. Hsu, *App. Therm. Eng.* 2010, **30**, 2213-8.

[66] H.E. Patel, T. Sundararajan and S.K. Das, *J. Nanopart. Res*. 2010, **12**, 1015-31.

[67] H.A. Mintsa, G. Roy, C.T. Nguyen and D. Doucet, *Int. J. Therm. Sci*. 2009, **48**, 363-71.

[68] R.S. Vajjha and D.K. Das, *Int. J. Heat . Mass. Transfer*. 2009, **52**, 4675-82.

[69] L.S. Sundar and K.V. Sharma, *Int. J. Nanoparticles*. 2008, **1**, 66-77.

[70] L.S. Sundar and K.V. Sharma, *Int. J. Dyn. Fluids*. 2008, **4**, 57-69.

[71] C.H. Li and G.P. Peterson, *J . Appl. Phys*. 2006, **99**, 084314.

[72] W. Duangthongsuk and S. Wongwises, *Exp. Therm. Fluid. Sci*. 2009, **33**, 706-14. 2

[73] Y.J. Hwang, Y.C. Ahn, H.S. Shin, C.G. Lee, G.T. Kim and H.S. Park, *Curr. Appl. Phys* 2006, **6**, 1068-1071.

[74] S. Sarkar, S. Ganguly, A. Dalal, P. Saha and S. Chakraborty, *Int. J. Heat Fluid Fl.* 2013, **44,** 624–634.

[75] H.E. Patel, T. Sundararajan and S.K. Das, *J. Nanopart. Res.* 2010, **12**, 1015-31.

[76] R. Gowda, H. Sun, P. Wang, M. Charmchi, F. Gao and Z. Gu, *Adv. Mech. Eng*. 2010, **2010**, 1-10.

[77] D.H. Yoo, K.S. Hong and H.S. Yang, *Thermochim. Acta*. 2007, **455**, 66-9.

[78] P. He and R. Qiao, *J. Appl. Phys*. 2008, **103**, 094305-6.

[79] S. Habibzadeh, A.K. Beydokhti, A.A. Khodadadi, Y. Mortazavi, S. Omanovic and M.S. Niassar, *Chem. Eng. J.* 2010, **156**, 471-8.

[80 D. Lee, J.W. Kim and B.G. Kim, *J. Phys. Chem. B*. 2006, **110**, 4323-8.

[81] L. Li, Y. Zhan, H. Ma and M. Yang, *Phys. Lett. A*. 2008, **372**, 4541.

[82] P. He and R. Qiao , *J. Appl. Phy*. 2008, **103**, 094305-6.

[83] H.U. Kang, S.H. Kim and J.M. Oh, *Exp. Heat. Transfer*. 2006, **19**, 181-91.

[84] K. Sinha, B. Kavlicoglu, Y. Liu, F. Gordaninejad and O.A. Graeve, *J. Appl. Phys*. 2009, **106**, 064307.

[85] X.J. Wang, D.S. Zhu and S. Yang, *Chem. Phys. Lett.* 2009, **470**, 107-11.

[86] M.J. Assael, I.N. Metaxa, J. Arvanitidis, D. Christofilos and C. Lioutas, *Int. J. Thermophys.* 2005, **26**, 647-64.

[87] K. Sinha, B. Kavlicoglu, Y. Liu, F. Gordaninejad and O.A. Graeve, *J. Appl. Phys.* 2009, **106**, 064307-1-7.

[88] D. Singh, E. Timofeeva, W. Yu, J. Routbort, D. France and D. Smith, *J. Appl. Phys.* 2009, **105**, 064306-1-6.

[89] K.J. Lee, S.H. Yoon and Y. Jang, *Small*. 2007, **3**, 1209-13.

[90] L. Chen, H. Xie, Y. Li and W. Yu, *Thermochim. Acta*. 2008, **477**, 21-4.

[91] H.T. Zhu, C.Y. Zhang, Y.M. Tang and J.X. Wang, *J. Phys. Chem. C*. 2007, **111**, 1646-50.

[92] R. Gowda, H. Sun, P. Wang, M. Charmchi, F. Gao and Z. Gu, *Adv. Mech. Eng.* 2010, **2010**, 1–10.

[93] N.R. Karthikeyan, J. Philip, B. Raj, *Mater. Chem. Phys*. 2008, **109**, 50-5.

[94] J.N. Nian and H. Teng, *J. Phys. Chem. B.* 2006, **110**, 4193.

[95] O.K. Park and Y.S. Kang, *Colloids Surf., A.* 2005, **257-258**, 261–265.

[96] J. Zhu, D. Li, H. Chen, X. Yang, L. Lu and X. Wang, *Mater. Lett.* 2004, **58**, 3324-3327.

[97] Y. Chang and H.C. Zeng, *Cryst. Growth Des.* 2004, **4**, 397-402.

[98] G.H. Du and G.V. Tendeloo, *Chem. Phys. Lett.* 2004, **393**, 64–69.

[99] Z.G. Zhao and M. Miyauchi, *J. Phys. Chem. C.* 2009, **113**, 6539–6546.

[100] J. Wang, E. Khoo, P.S. Lee and J. Ma, *J. Phys. Chem. C.* 2009, **113**, 9655-9658.

Section A:

Shape dependent thermal conductivity of TiO_2-ethylene glycol and de-ionized water based suspension

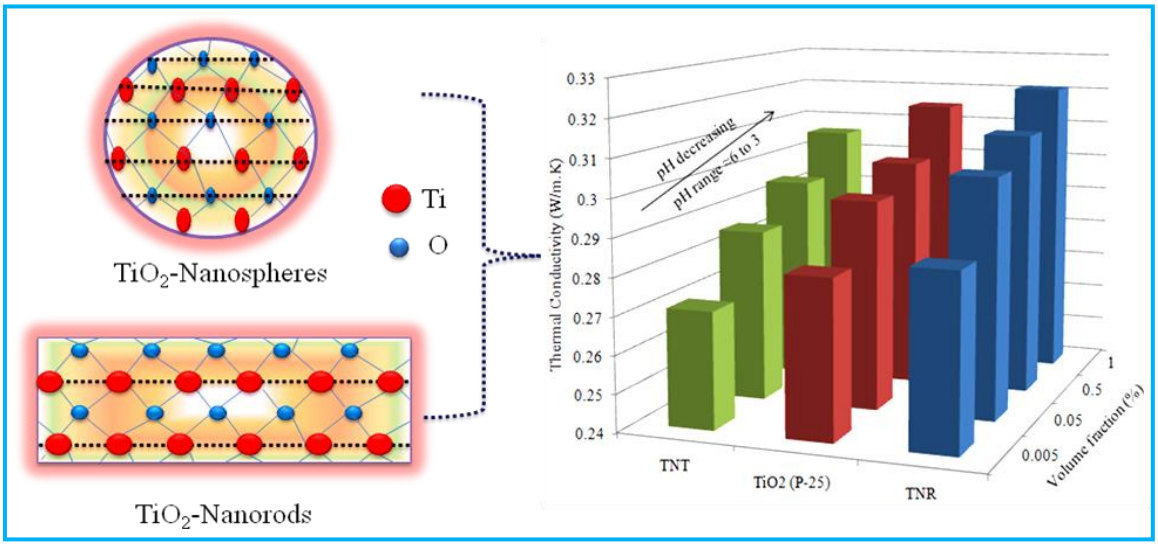

Abstract: This section demonstrates the importance of various shapes and crystal phases of TiO_2 nanostructures such as TiO_2 P-25 (70:30 anatase and rutile), as-prepared nanorods (pure anatase) and sodium titanate nanotubes (orthorhombic $Na_2Ti_2O_5.H_2O$ crystal) on the thermal conductivity of ethylene glycol and de-ionized water. It was observed that TiO_2 nanorods (L×W = 81-134 nm × 8-13 nm and surface area = 79 m^2g^{-1}) always showed higher thermal conductivity than porous nanotubes (L×W = 85-115 nm × 9-12 nm and surface area = 176 m^2g^{-1}) and commercial TiO_2 P-25 (30-55 nm surface area = 56 m^2g^{-1}),) which was explained by their differences in crystallinity, crystal phases, compactness, surface exposed atoms, surface area and much greater mean free path of longitudinal phonon vibrations along its lateral dimensions. The subsequent effect of sonication time from 5-10 h results into the breakdown of TiO_2 nanorods cluster (42 to 28 nm) with the instantaneous increase in negative zeta potential values from -31 to -45 mV, respectively, which seems to be an additional cause for enhancement in its thermal conductivity.

2.1 Introduction

A nanofluid is a two-phase mixture in which the continuous phase is usually a liquid (de-ionized water, ethylene glycol or oils) and the dispersed phase is extremely fine NPs [1-5]. Nanofluids are considered as a good candidate for heat transfer applications due to their superior thermophysical properties (*thermal conductivity, specific heat and viscosity, etc*.) than conventional heat-transfer fluids and can be used for cooling applications in nuclear reactors, transportation industry, electronics and biomedical [6-9]. A variety of factors such as volume fraction, size, shape, nature of NPs, pH, temperature, Brownian motion and aggregation of NPs have been proposed to play the vital roles in TC [10-13] of NFs. Viscosity and TC of NFs are also dependent on the physicochemical and structural features of nanomaterials and solvents [14-17].

Over the past few years, many research groups have been attempting to develop fluids which give improved cooling efficiency for thermal systems as compared to conventional fluids [18, 19]. The dispersion of μm to mm particles in fluids showed superior thermophysical properties, but they have their own limitations such as clogging of microchannels etc [16]. Nanoparticles due to their extremely small size, higher surface atom exposure, high surface to volume ratio and larger surface area may increase the heat transfer efficiency, improves the long-term stability and reduces the clogging of microchannels. High thermal conductive materials such as CNTs, Cu, Ag, Au, CuO, TiO_2 and Al_2O_3 spherical particles have been extensively studied [20-25]. Choi et al. [1] found 20% increase in heat transfer rate of CuO NPs in DIW and Eastman et al. showed 40% increment in TC by using CuO NPs in EG [5]. Das et al. [26] reported the four-fold increase in TC over a temperature range of 21-51 °C of Al_2O_3 (38.4 nm) and CuO (28.6 nm) NPs dispersion in DIW. In recent years, TiO_2 is considered as a suitable NF's material due to its light weight, hydrophilicity, non-toxicity, stability and reasonable TC etc. For example, aqueous suspension of TiO_2 and Al_2O_3 NPs [20] displayed approximately 11% enhancement in TC than base fluids at loading of 4.3 vol% NPs. The heat-transfer efficiency and flow characteristics of TiO_2 aqueous based NFs were also studied by He et al. [27]. Murshed et al. [28] reported 30-33% increase in TC at loading of 5 vol.% TiO_2 nanospheres (diameter ~15 nm) and nanorods (width = 10 nm and length = 40 nm) in DIW. Although, suspensions of spherical particles have been mostly investigated, but not much information of cylindrical shape NPs is known for

exhibiting high TC in EG and DIW based dispersion. As the change in geometric morphology led to alternation in surface properties and exposed surface atoms, thermophysical properties of NFs will be expected to be significantly changed [29]. Quantum dots, nanorods, nanotubes potentially exhibits superior *optoelectronic and photophysical properties* as compared to its spherical particles due to the increased delocalization of charge carriers along the long axis of the cylindrical particles [30-33]. Therefore, the effect of lengthy and anisotropic TiO_2 nanorods and nanotubes depending on their size and shape, volume fraction, sonication time, temperature, dispersion stability, and electrokinetic parameters (zeta potential, ζ) in DIW and EG based dispersion are comparatively studied for better heat transfer performance.

2.2 Experimental section

2.2.1 Materials and methods

The various shapes of TiO_2 NPs have been synthesized; the detail description is given in **Chapter 1**, **section 1.5.1.2**.

2.2.2 Characterizations

As synthesized NPs were characterized by various techniques, the details of the techniques are given in **Chapter 1**, **section 1.5.7**.

2.2.3 Preparation of Nanofluids

Nanofluids were prepared by two-step methods as mentioned in **Chapter 1, section 1.5.2**.

2.2.4 Thermal conductivity measurement

The TC measurement has been done by KD2 Pro, experimental details are given in **chapter 1**, **section 1.5.3**.

2.3 Results and Discussion

2.3.1 Structural and morphological characterization

Powder X-ray diffraction (figure 2.1) pattern of as synthesized TiO_2 nanostructures revealed that the crystal structures of TiO_2 P-25 belongs to anatase : rutile (70:30) mixture and TiO_2 nanotubes prepared [34] from TiO_2 P-25 having crystal planes (1 1 0) and (0 2 0) at 2θ values of 24.05^o and 48.07^o which matches with the crystal planes of $Na_2Ti_2O_5.H_2O$ (orthorhombic) as reported in literature [35]**.** However, TiO_2 nanorods belong to tetragonal crystal structure and showed the diffraction peaks at 2θ values 25.1^o, 37.5^o, 47.7^o, 53.4 and 54.9^o corresponding to (1 0 1), (0 0 4), (2 0 0), and (2 1 1) planes for the characteristic anatase phase of titania (JCPDS 21-1272) having lattice parameters (a = b = 3.80 Å and c = 9.56 Å) is in good agreement with the earlier report [36] and verified the appearance of pure anatase phase in TiO_2 nanorods.

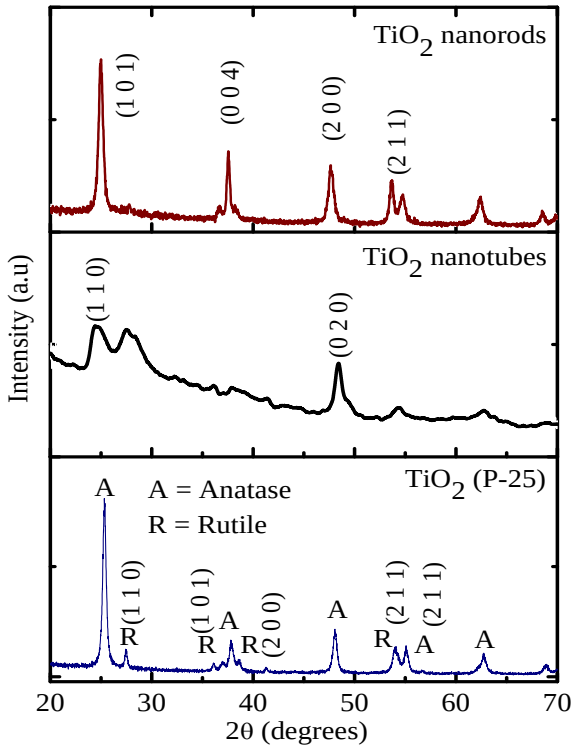

Figure 2.1: XRD patterns of TiO_2 P-25, nanorods and nanotubes.

The TEM images of figure 2.2 (a-b) showed some cubical and irregular spherical shapes of commercial TiO_2 P-25 NPs have an average size of 30-55 nm. Rice like TiO_2 nanorods of length 81-134 nm and diameter 8-13 nm have been observed in the TEM photographs of figure 2.2 (c-d). Similar TiO_2 nanorods morphology having diameter 6-10 nm and length 50-70 nm was also synthesized by both Nian et al. [34] and Christy et al. [37]. Tube like hollow lengthy TiO_2 nanotubes particles of width 9-12 nm, length 85-115 nm and wall thickness ~1 nm is observed in the TEM images of figure 2.2 (e-f). Such type of TiO_2 nanotubes with diameter 70-100 nm and 14-50 nm wall thickness were also prepared by Hoyer et al. [38]. The BET (Brunaer-Emmett-Teller) surface area analysis for nanotubes, nanorods and TiO_2 P-25 (176, 79 and 56 m^2g^{-1}) has been done and it was found that the difference in surface area of as prepared NPs is due to their morphologies. The nanotubes displayed higher surface area due to its hollowness from inner side and porous surface which was also shown in TEM images. The decreased surface area (176 to 79 m^2g^{-1}) occurred due to structural changes from TiO_2 nanotubes to nanorods formation indicating

the collapse [39] of hollow nonotubes together at higher temperature (175°C) autoclaving for 48 hours.

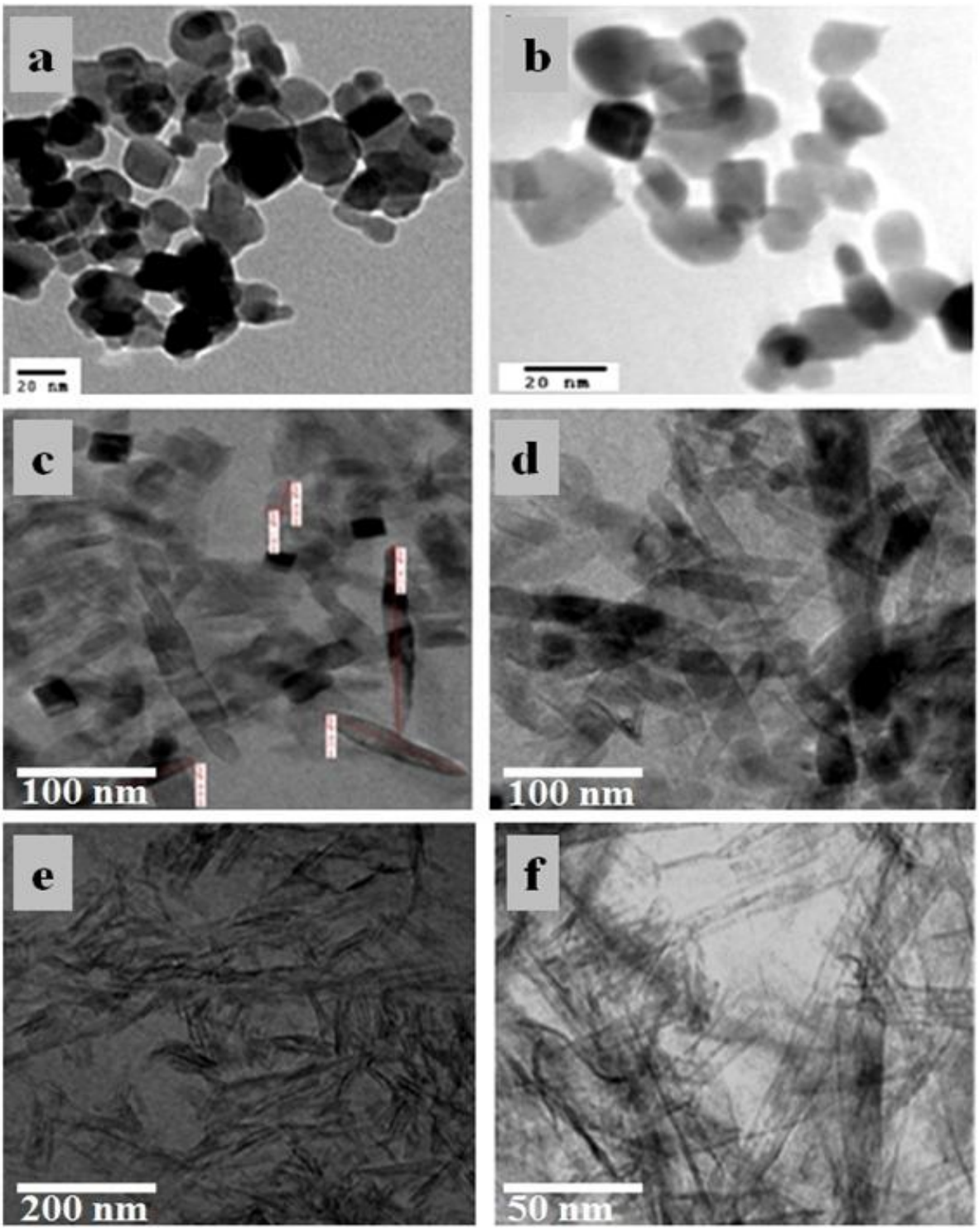

Figure 2.2: TEM images of TiO_2 (a and b) P-25, (c and d) nanorods (TNR) and (e and f) nanotubes (TNT).

2.3.2 Influence of volume fraction, shape and pH on TC of TiO_2-DIW based dispersion

The variation in TC of different TiO_2 nanostructures in DIW based dispersion with volume fraction 0.005 to 1% at temperature 25.12 ±0.03 °C after 5 h sonication is presented in figure 2.3. The experimental results showed that TC increases with increase in volume fraction and decrease in pH. At dilute suspension (0.005%-0.05%) of TiO_2 NPs, there is a sudden increase (7-16%) in TC and it gradually improved with increasing TiO_2 NPs concentration up to 1% and decreasing pH. TiO_2 nanorods dispersion exhibits high TC as compared to TiO_2 P-25 and TiO_2 nanotubes suspension and pH is gradually reduced from initial 6.65 to 3.66 with the increasing amount (0.005 to 1%) of TiO_2 NPs in DIW without the addition of any acid.

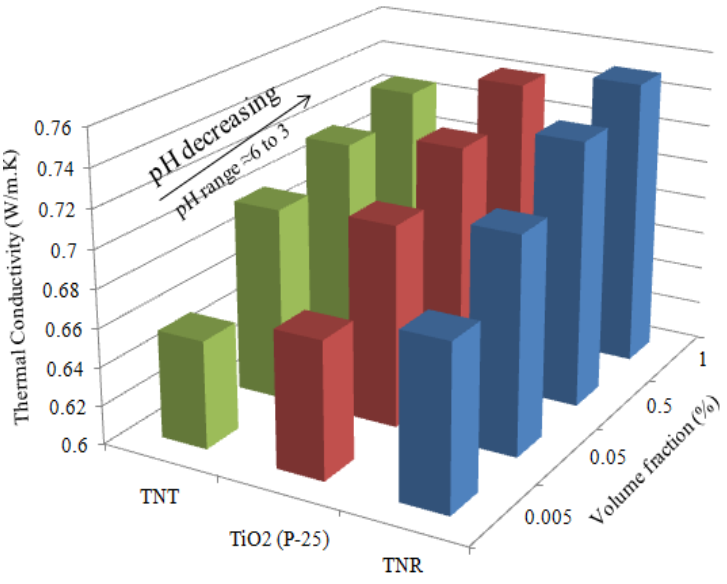

Figure 2.3: Change in TC of DI water as a function of nanoparticles shape, concentration and pH (at 25.12 ± 0.03 °C).

The TC of EG is also investigated for low temperature cooling applications because of its lowest freezing point (-13 °C) and higher viscosity than DIW. Figure 2.4 shows the relative variation in TC with concentration (0.005% to 1%) of TiO_2 nanorods, TiO_2 P-25 and TiO_2 nanotubes dispersed in EG after 5 h sonication at 25.16 ±0.03 °C. All the TiO_2 nanostructures dispersed in EG significantly

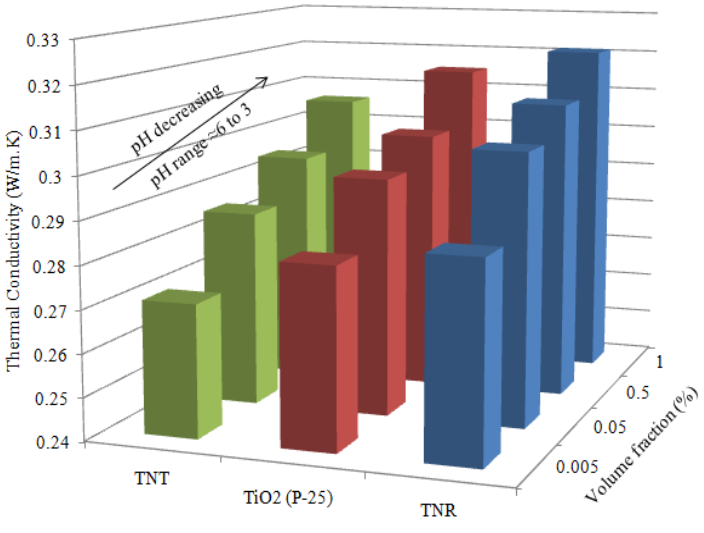

Figure 2.4: Change in TC of ethylene glycol as a function of nanoparticles shape, concentration and pH (at 25.16 ± 0.03 °C).

improved the TC with increase in volume fraction and decease in pH (5.58 to 3.54). The TiO_2 nanorods dispersed in EG again displayed higher TC than TiO_2 P-25 and nanotubes for all volume fractions. At loading of 1 vol%, the enhancement in TC was observed 27% for TiO_2 nanorods-EG based suspension and 23% for aqueous TiO_2 nanorods based suspension.

The mixture of EG and water was verified superior for heat transfer applications (decrease the freezing point of base fluids up to -34 °C) in cold region where EG and DIW separately does not

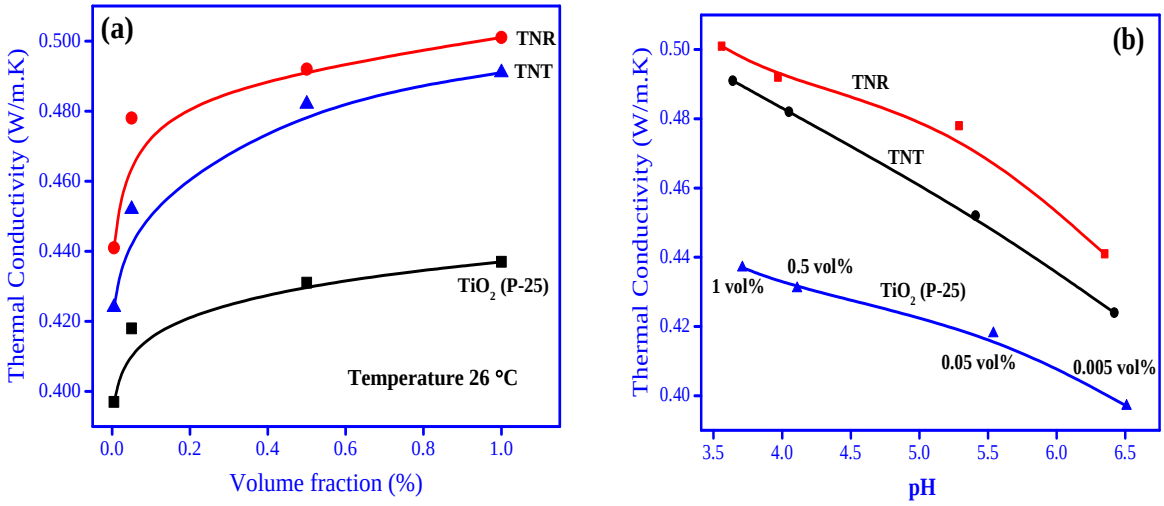

Figure 2.5: Variation in thermal conductivity of 1:1 DI water and ethylene glycol mixture as a function of **(a)** nanoparticles concentration at 26 ± 0.03 °C and **(b)** pH.

work properly. The TC of DI water and EG mixture (1:1) was found to be 0.350 ±5 W/m.K at 26 ± 0.5 °C, which was considerably increased after dispersion of TiO_2 NPs as shown in figure 2.5 (a). At loading of low volume fraction (0.005 to 0.05 vol%) of TiO_2 nanorods, TiO_2 P-25 and nanotubes in DI water and EG mixture exhibited a sharp increase in TC and then gradually increased at the higher volume fraction, this might be due to slower Brownian motion and some phonon scattering between solid phase in case of higher volume fraction. The long cylindrical shape exhibited marked improvement in TC of DI water and EG mixture based NFs as compared to the commercial cubical morphology of TiO_2 P-25 particles. Figure 2.5 (b) clearly revealed that with the increase in dispersion (0.005-1 vol%) of TiO_2 nanoparticles in mixed base fluids, the thermal conductivity was gradually improved with decrease in pH from 6.5 to 3.5.

Thus, it is demonstrated that TiO_2 nanorods based NFs showed always higher thermal conductivity than nanotubes and TiO_2 P-25 because of the compactness in structure, less interparticles distance, higher geometric surface area per particle, and strong phonon vibrations

in nanorods structure. As heat-transfer is a surface phenomenon, then it is obvious to use the particles with higher surface area where a large percentage of atoms reside on the surface and make them accessible for the thermal interaction [40]. The estimated geometric surface area per-particle is ~9420 nm^2 for nanorods, ~5805 nm^2 for nanospheres and ~12685 nm^2 for nanotubes, and the number of surface exposed TiO_2 molecules is found to be more (ca. ~14,845) for nanorods as compared to TiO_2 P-25 nanoparticles (~5,243). The specific surface area of TiO_2 P-25 (56 m^2g^{-1}) is also lesser than TiO_2 nanorods (79 m^2g^{-1}) and hence nanorods showed higher thermal conductivity. Although TiO_2 nanotubes has more surface molecules (~17,135), more surface area (176 m^2g^{-1}) than nanorods (79 m^2g^{-1}), but its porous/amorphous surface structure and lacking of compactness or poorly connected TiO_2 particle obstructs the efficient heat transfer from one TiO_2 unit to another**.** Thus, it is evident that nanorod having pure anatase phase exhibited more thermal conductivity than the mixed anatase-rutile phases of TiO_2 P-25 and sodium titanate nanotube possessing orthorhombic crystal structure.

The TC increases with increase in concentration of NPs because solid has a thousand-time higher thermal conductivity than liquids. The high surface charge density help in production of strong repulsive forces which further improved the dispersion stability of particles in base fluids, therefore, it is important to measure zeta potential and pH of the suspension. In this study, as the NFs become more acidic (lower pH), far from its point of zero charge (PZC) at a higher volume fraction of TiO_2 NPs, more and more charges have accumulated on the particle surface and thereby prevent the coagulation with the concurrent increase in dispersion stability and thermal conductivity.

2.3.3 Effect of temperature on thermal conductivity

Figure 2.6 shows the change in TC of

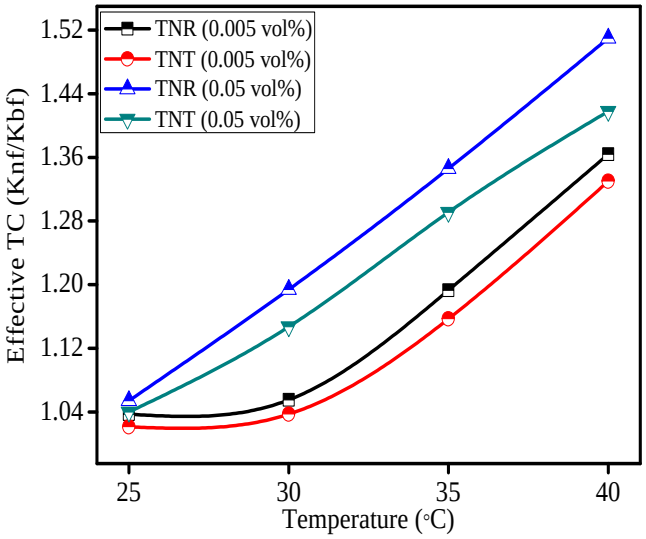

Figure 2.6: Effect of temperature on the thermal conductivity of TiO_2 nanorods and nanotubes dispersed in DI-water at two different volume fractions (0.005 vol% and 0.05 vol%).

TiO_2-water based dispersion as a function of temperature, shape and particle volume fractions. The experimental data showed that the TC of NFs increased with increase in temperature and particle concentration. For both volume fractions (0.005 and 0.05%), TiO_2 nanorods DI water suspension shows more increase in thermal conductivity than TiO_2 nanotubes DI water suspension. The heat- transfer rate depends on the temperature gradient and thermal conductivity of the material, the heat capacity and phonon vibration of TiO_2 NPs increased by a rise in temperature and assists the rapid heat transfer from one particle to another.

2.3.4 Effect of sonication time on the dispersion stability, zeta potential and TC

Ultrasonication is a common way to breakdown agglomerated cluster particles and promotes dispersion of NPs into base fluids. This is verified with the DLS and zeta potential (ζ) measurements as a function of sonication time. With an increased sonication time from 2 to 10 h, the cluster of agglomerated particles becomes smaller and lighter, therefore, suspend more uniformly in base fluid. For volume fraction 0.05% at a different sonication time (2 to 10 h), the dispersion of TiO_2 nanorods and TiO_2 P-25 in DI water clearly showed that the thermal conductivity significantly increased from 23.6% to 51.23% and from 12.13% to 31.31%, respectively, as seen in figure 2.7. Thus more pronounced effect of TiO_2 nanorods than TiO_2 P-25 dispersion because of the superior suspension stability owing to breakdown of relative larger aggregates particle into smaller particles. This fact is further clarified by DLS particles size distribution and ζ analysis (figure 2.8). The large aggregation of NPs can increase the probability of settlement, clogging of microchannels, and also decreases the thermal conductivity of NFs. If the particles have a sufficiently high repulsion due to high surface charge, the suspensions will exist in a

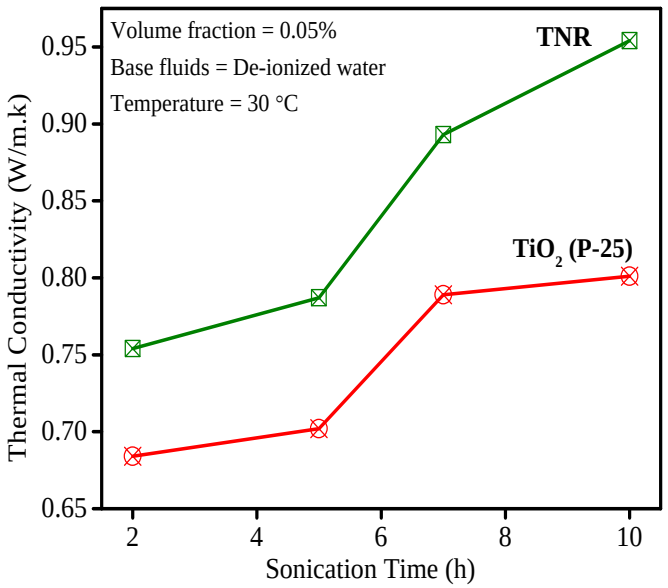

Figure 2.7: Influence of sonication time on the thermal conductivity of TiO_2 nanorods and TiO_2 P-25 dispersed in DI water.

stable state for longer time. The concentration of counter ions increased close to the surface due to increase in net charge of the particles at the surface, therefore, an electrical double layer formed around the each particle and the potential that formed at this boundary is known as the Zeta potential [41].

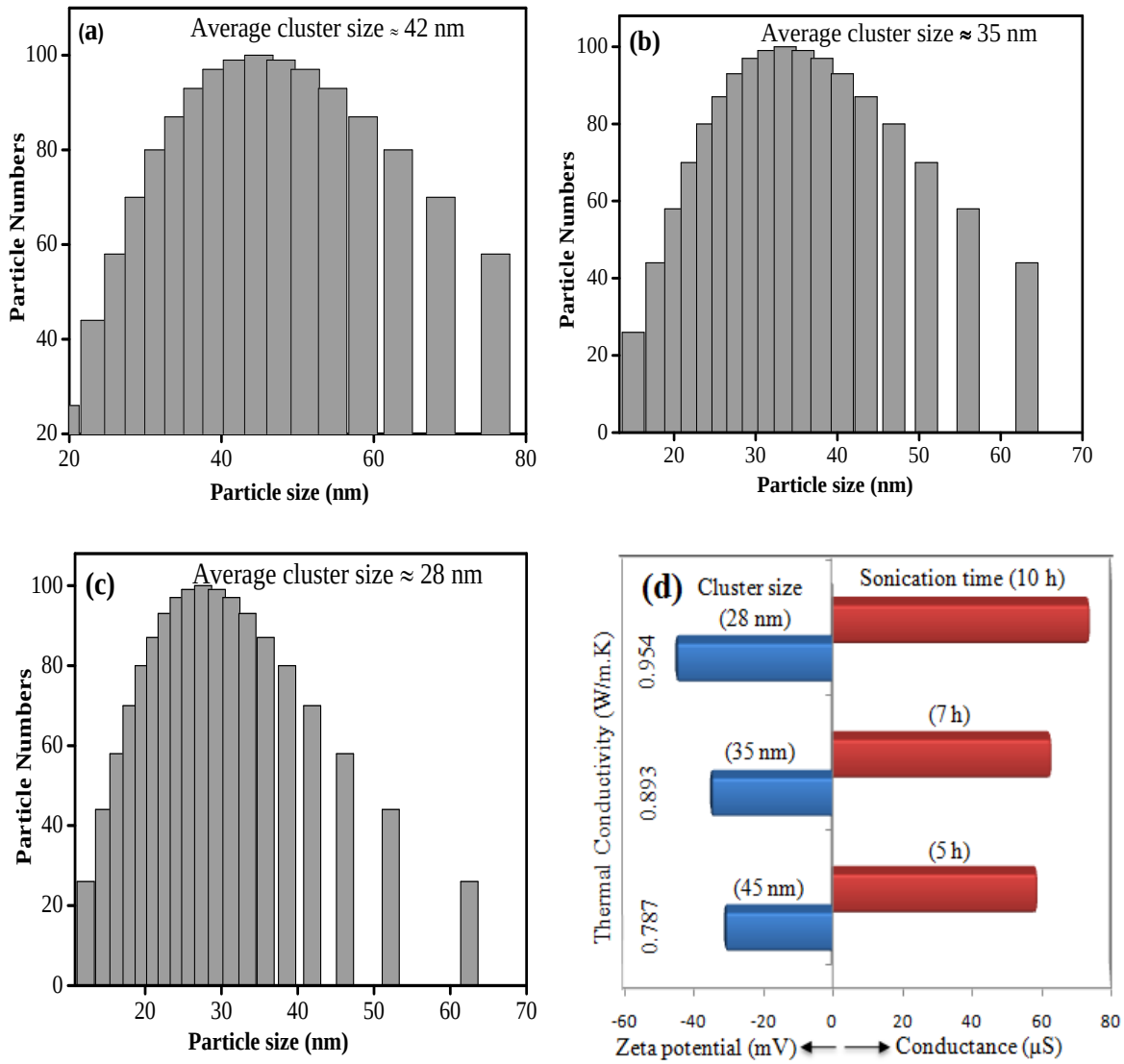

Figure 2.8: Particle size distribution of TiO_2 nanorods (0.05 vol. %) in DI-water measured by DLS after sonicated for **(a)** 5 h, **(b)** 7 h, **(c)** 10 h and **(d)** variation in thermal conductivity, zeta potential and conductance with average particle cluster size and sonication time.

Figure 2.8 shows that with increasing sonication time from 5 to 10 h, the TiO_2 nanorods cluster size gradually decreased from 42 nm (5 h) to 28 nm (10 h) with a corresponding increase in conductance (59 to 74 μS) and ζ values from -31 mV to -45 mV, respectively. Due to breakdown of aggregated clusters of TiO_2 nanorods by strong and irregular shock of ultrasonic waves with increasing sonication time, thermal conductivity is greatly improved as shown in fig. 7. DLS (fig. 8) results provide an evidence for breakdown of larger clusters into smaller one by ultrasonication. The measured negative ζ values indicated the good stability of TiO_2 nanoparticle dispersions which causes to exhibit high thermal conductivity because colloids with high (40 to 60 mV) positive and negative ζ values are electrically stabilized, while colloids with low ζ value tend to coagulate or flocculate and reduced the thermal conductivity.

2.4 Conclusions

In summary, the anisotropic shapes of TiO_2 NPs influence the TC of NFs as a function of their morphological difference. Anisotropic shapes showed 20-27% enhancement in thermal conductivity only at lower volume fraction (0.05 to 1 vol%), but in literature same enhancement is shown at higher volume fraction (3 to 8 vol%). Due to small interparticles distance, high compactness, high surface atom exposure and much greater mean free path of longitudinal phonons of TiO_2 nanorods, it shows always higher thermal conductivity than porous TiO_2 nanotube and TiO_2 P-25. EG always shows higher dispersion stability than DI water because of higher viscosity of EG. So it is concluded here that optimization of experimental conditions, anisotropic shape, appropriate theoretical models and long term dispersion stability of NPs is very essential for cooling applications.

Section B:

SiO_2@TiO_2 nanocomposites for enhanced thermal conductivity and dispersion stability in de-ionized water

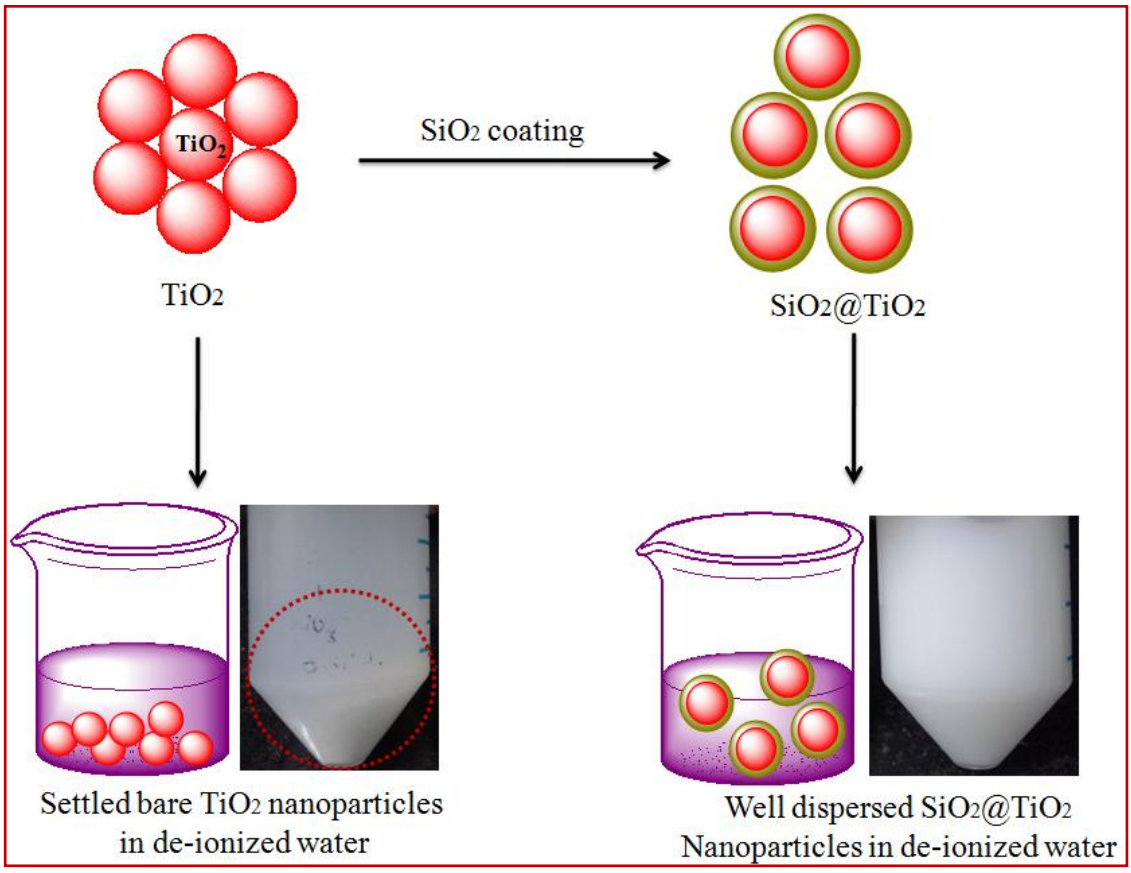

Abstract: This research presents the synthesis of bare and SiO_2 coated TiO_2 nanoparticles and investigate their effect on thermal conductivity of de-ionized water; as prepared nanoparticles were characterized by powder X-ray diffraction, Fourier transform infrared spectroscopy and transmission electron microscopy etc. These nanoparticles were dispersed in de-ionized water at various volume fractions (0.01%) and studied their thermophysical (density, thermal conductivity, refractive index etc) properties. The experimental results showed that a thin layer of SiO_2 coating (3-6 nm) over TiO_2 nanostructures exhibit superior dispersion (0.5 vol%) stability as evident by steady zeta potential (-30 ↔ -36 mV), no significant change in particle-size (95↔133 nm) distribution, density (1.001↔0.998 g/cm^3) and refractive index (1.336↔1.333) etc. Thin Si-OH

layer over surface imparts superior hydrophilicity, larger surface area for effective solute-solvent (SiO_2@TiO_2-H_2O) interaction for improved colloidal stability. Thereby, thermal conductivity is found to be quite stable (0.625↔0.614 W/m.K) up to 2-3 months, whereas aqueous suspension of bare TiO_2 particles quickly settles down. Depending on the thickness of SiO_2 layer and volume fraction of SiO_2@TiO_2, a maximum of 8-10% increment of thermal conductivity was achieved at 0.01 vol.%.

2.5 Introduction

The low TC of heat transfer fluids is a primary issue in the cooling systems [42]. To overcome this drawback, the TC of these fluids can be enhanced by dispersing suitable metal and metal oxide nanoparticles (Al_2O_3, CuO, SiO_2 and TiO_2 etc) in it as reported [43-46] in many review articles. The nanoparticles (NPs) have higher surface-area-to-volume ratio and surface active atoms which not only improve the heat transfer efficiency but also increased the dispersion stability. As heat transfer takes place generally through the surface atoms [47], anisotropic nanoparticles having more surface exposed atoms can further alter the material's [48,49] properties significantly for improved heat conduction capacity. For example, Murshed *et al.* [50] dispersed spherical and cylindrical TiO_2 nanoparticles (1-5%) in de-ionized water (DIW) and found 30-33% enhancement in TC. Some research groups reported an enhancement of 28-31% in TC [51,52] for aqueous CuO (1-5%) and Al_2O_3 suspension.

It is well-known that NPs aggregate and precipitate with passage of time unless it is effectively passivated with suitable surface active agents, and difficult to re-disperse in water due to their high surface [53] energy. The aggregation of NPs results not only the clogging of microchannels [54] but also decreasing the TC of heat transfer fluids. Studies to date have shown that the charge of NPs in base fluids, interaction between the particles and dispersant directly affect the stability of the suspension. For example, Jiang *et al*. [55] and Li *et al.* [56] showed that the most important factors affecting the stability of carbon nanotubes and Cu/H_2O suspensions were the NP's concentration, viscosity of base liquid, pH value and dispersant type etc. Saterlie *et al.* [57] studied the effect of different surfactants (SDBS, PVP, CTAB and oleic acid) on long term dispersion (0.55%) stability and TC of Cu/H_2O suspension. However, it suppressed the TC that decline gradually due to chemical interaction and charge imbalance resulting into coagulation of NPs with passage of time. Both *et al.* [58] tried to improve dispersion stability of SiO_2 supported Ag NPs (15-20 nm) in transformer oil up to one hour without using any surfactant. An enhancement in TC

of 15% was observed when 0.60 wt% silver was supported on 0.07 wt% SiO_2. As this context, SiO_2@TiO_2 nanocomposites have been synthesized and studied their impact on dispersion stability and thermal conductivity for longer time. Optimization of shell thickness around TiO_2 has been also investigated for maximum thermal conductivity and dispersion stability.

2.6 Experimental Section

2.6.1 Materials and methods

The various shapes of bare and SiO_2@TiO_2 NPs have been synthesized; the detail is given in Chapter 1, **section 1.5.1.2 and 1.5.1.2**.

2.6.2 Characterizations

As synthesized NPs were characterized by different techniques, the details of the techniques are given in Chapter 1, **section 1.5.7**.

2.6.3 Preparation of Nanofluids

Nanofluids were prepared by two-step methods as mentioned in Chapter 1, **section 1.5.2**.

2.6.4 Thermal conductivity, density and refractive index analysis of SiO_2@TiO_2 suspension:

The TC measurement has been done by KD2 Pro, experimental details are given in chapter 1, **section 1.5.3 and 1.5.4**.

2.7 Results and Discussion:

2.7.1 Structural and Morphological characterization

Figure 2.9 (a-b) shows the powder x-ray diffraction (XRD) patterns of bare and SiO_2@TiO_2 nanocomposites. XRD pattern shows formation of both anatase and rutile phase. For the bare TiO_2, peaks at 2θ (25.5, 48.5 and 37.7) are well matched with anatase phase, JCPDS 02-0406. The peaks with lesser intensity (at 2θ = 27.6 and 36.2) are well matched with rutile phase of TiO_2. The XRD patterns of SiO_2@TiO_2 nanocomposites are same as pure TiO_2 as shown in figure 2.9 (b), it clearly indicates the absence of characteristic peaks of SiO_2. The reason for absence of SiO_2 peaks in the

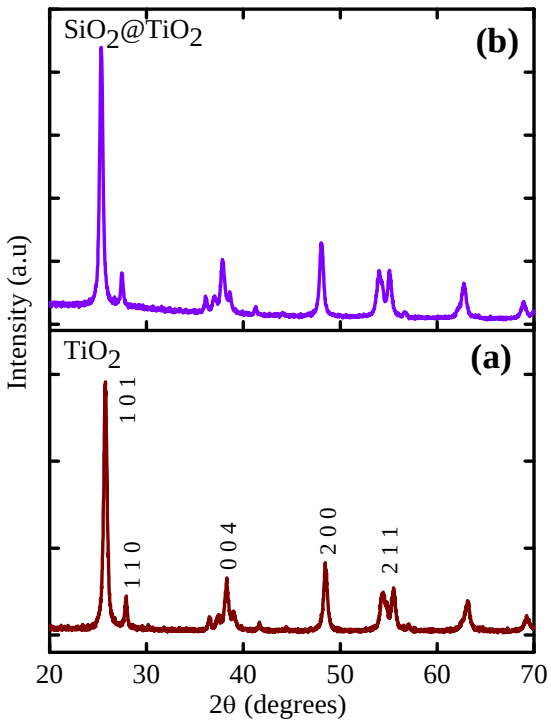

Figure 2.9: Powder x-ray diffraction pattern of **(a)** TiO_2 and **(b)** SiO_2@TiO_2.

XRD pattern is low concentration of SiO_2 in the sample. For the confirmation of presence of SiO_2 in the sample, transmission electron microscopy (TEM) and high resolution transmission electron microscopy (HR-TEM) has been done (figure 2.10, 2.11 and 2.12). Figure 2.10 (a-f) shows the TEM images of bare TiO_2 nanospheres with diameter 25-30 nm and nanorods with width 25-40 nm and length 0.3-0.5 µm. Figure 2.11 (b-c) shows the TEM and HR-TEM images of SiO_2@TiO_2 nanocomposites where a thin layer of SiO_2 coating with thickness of 2-5 nm can clearly differentiate from TiO_2 NPs. The Figure 2.11 (c) shows clear crystalline lattice fringes for both SiO_2 and TiO_2 NPs, their corresponding elemental composition is also shown in figure 2.11 (d). The TEM images of SiO_2@TiO_2 nanorods are shown in figure 2.12 (a-c) where SiO_2 coating over TiO_2 nanorods can be clearly seen, the thickness of the SiO_2 was found to be 3-5 nm.

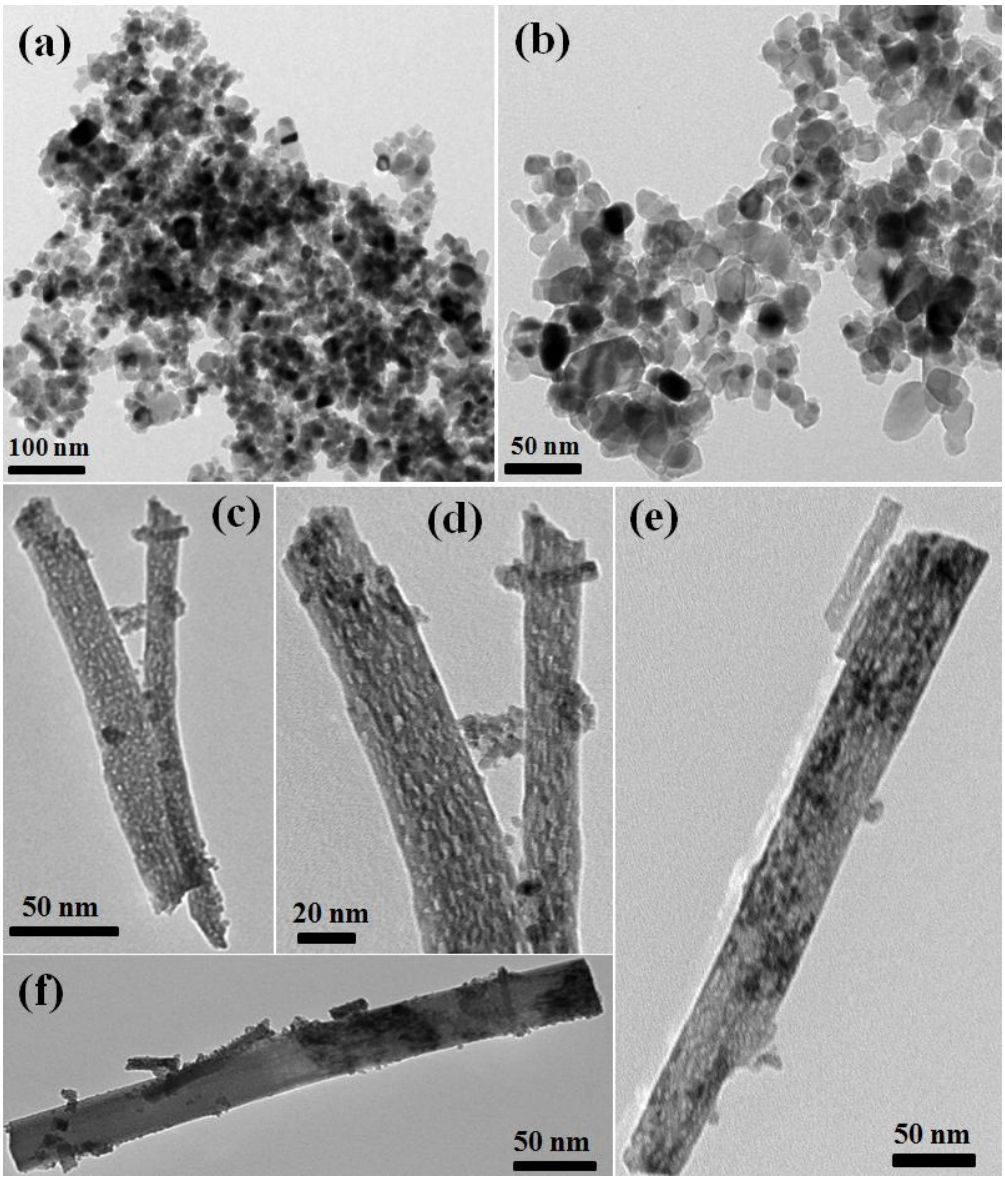

Figure 2.10: TEM images of (a-b) TiO_2 nanospheres (c-f) TiO_2 nanorods.

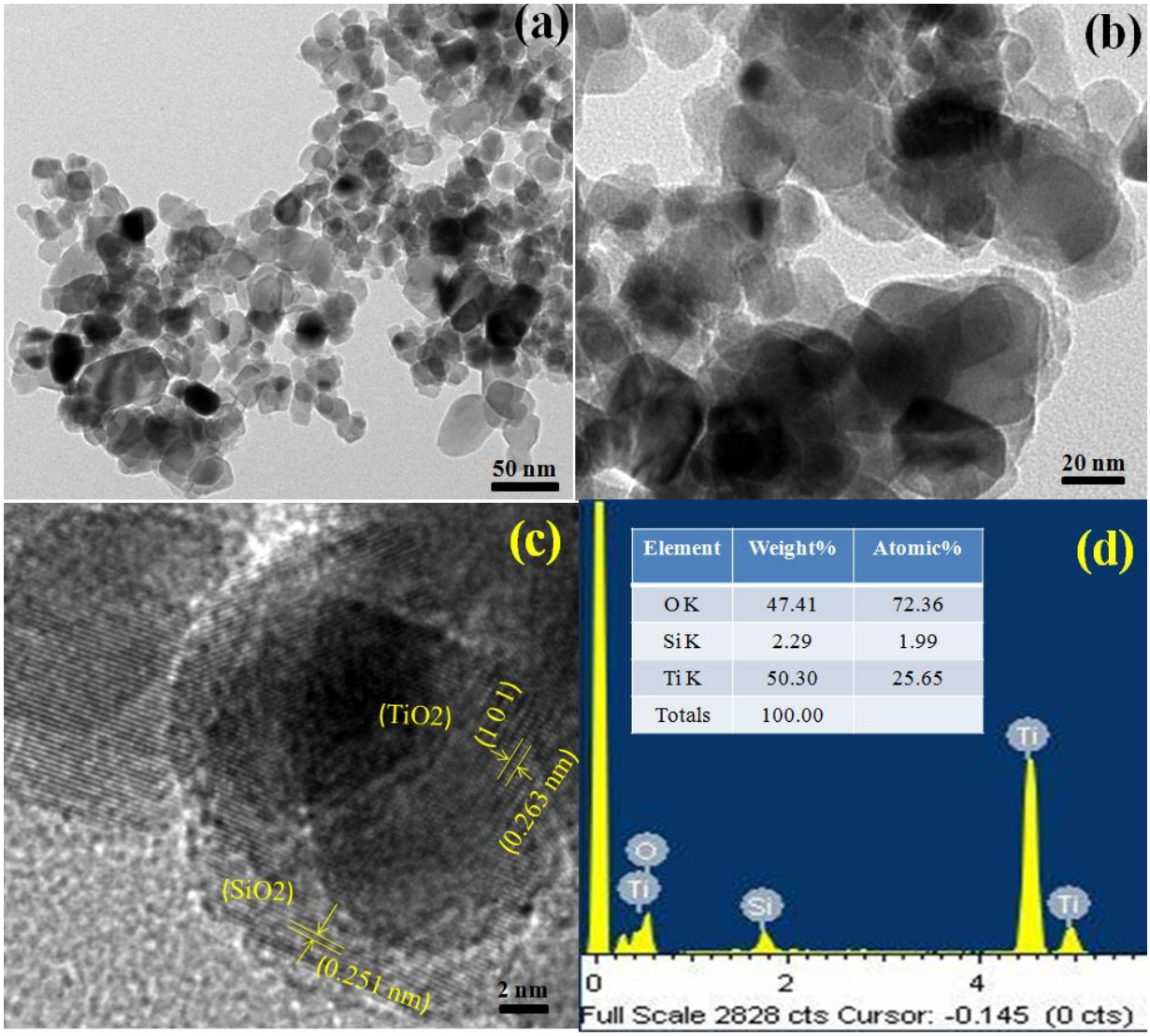

Figure 2.11: HR-TEM images of **(a)** bare TiO_2 and **(b-c)** SiO_2@TiO_2 nanocomposites. **(d)** EDS of SiO_2@TiO_2 nanocomposites.

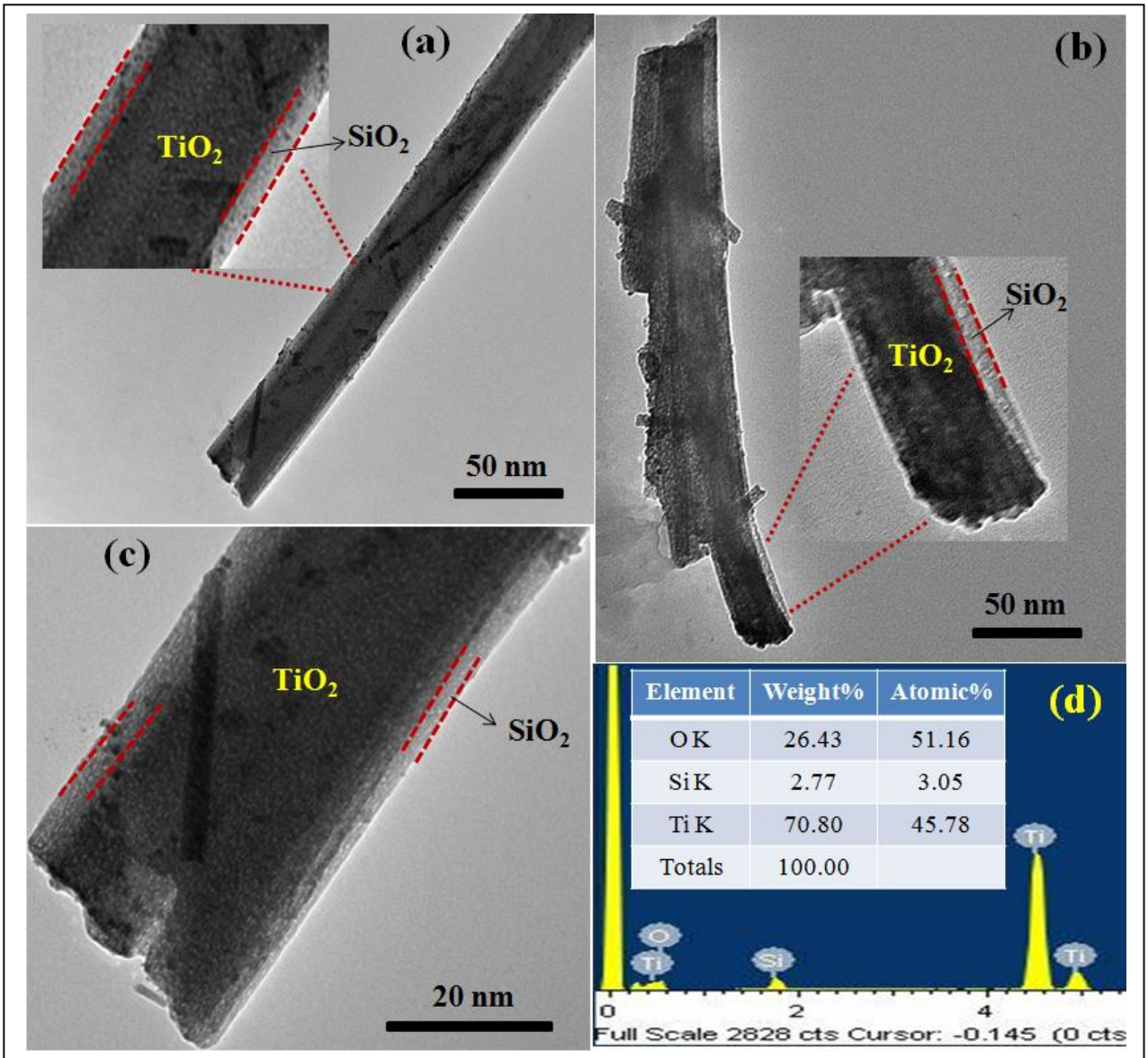

Figure 2.12: TEM images of **(a-c)** SiO_2@TiO_2 nanorods. **(d)** EDS of SiO_2@TiO_2 nanorods.

2.7.2 Fourier Transform Infrared Spectroscopy and particle size distribution analysis

The verification of SiO_2 in SiO_2@TiO_2 nanocomposites has also been done by Fourier Transform Infrared Spectroscopy (FTIR) as shown in figure 2.13 (a). The FT-IR spectra of SiO_2@TiO_2 NPs showing the vibrational stretching peak at ~1076 cm^{-1} for Si-O-Si formation relative to no such band in bare TiO_2, therefore, this is another evidence for presence of SiO_2 in SiO_2@TiO_2 nanocomposites. Particle size distribution was also done for both bare and SiO_2@TiO_2 NPs as

shown in figure 2.13 (b). It was found that the hydrodynamic size of bare TiO_2 (86 nm) NPs increases after the SiO_2 coating and reaches to 96 nm.

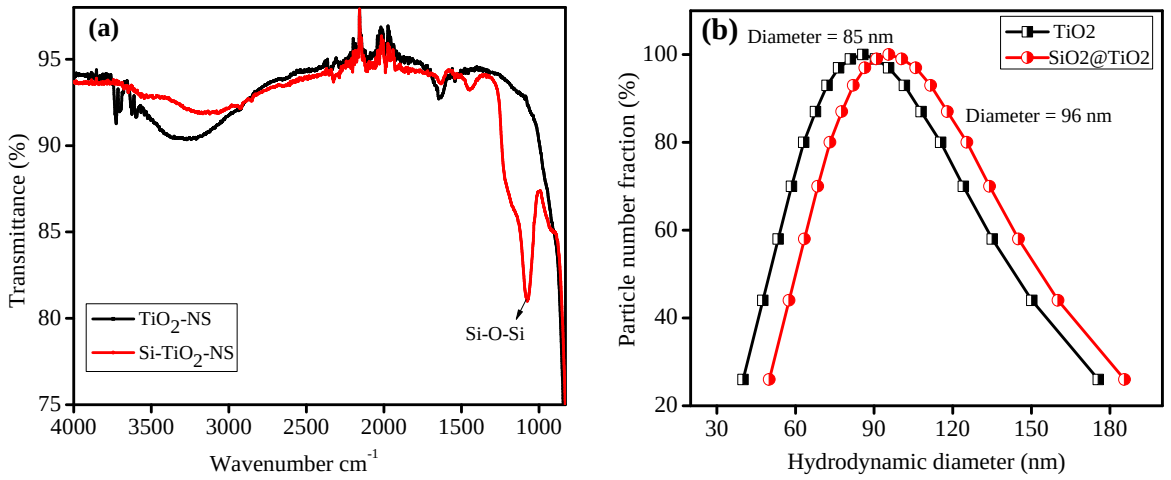

Figure 2.13: **(a)** FT-IR absorption spectra and **(b)** particle size distribution of TiO_2 and SiO_2@TiO_2 in aqueous suspension.

2.7.3 Thermogravimetric analysis

Thermal stability analysis has been done for bare TiO_2 and SiO_2@TiO_2 nanocomposites as shown in figure 2.14. From figure 2.14, it was observed that bare TiO_2 shows 3 stages of weight loss, one at ~100°C, second at ~500°C and third at ~750°C. In the first stage it losses ~4% weight, in second stage it losses ~2% and finally it losses ~3% weight. In case of SiO_2@TiO_2 nanocomposites only two stage of weight loss occurred, first at temperature 200°C and second at 500°C, after that there is no weight loss.

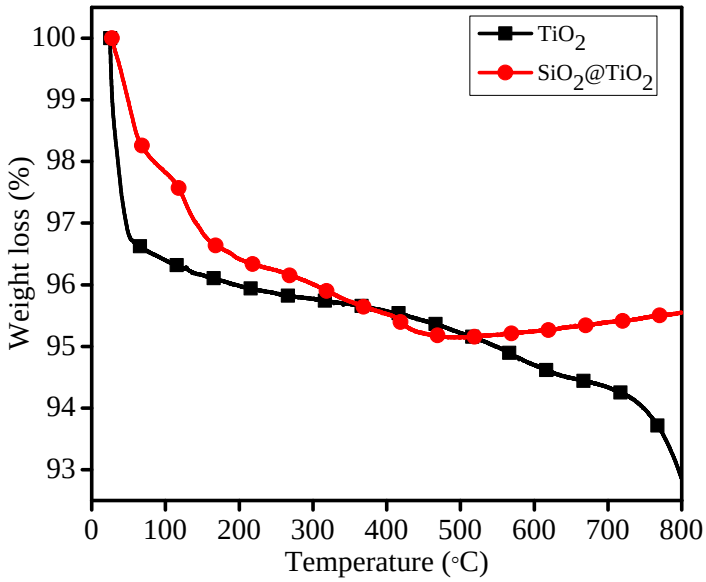

Figure 2.14: TGA of the as-synthesized bare and SiO_2 coated TiO_2 nanoparticles measured at a heating rate of 1°C/min in nitrogen.

2.7.4 Effect of silica coating and shape on thermal conductivity

Figure 2.15 (a-b) showed the comparative study of effect of bulk TiO_2, nanoparticles of TiO_2 and nanocomposities of SiO_2@TiO_2 on thermal conductivity of de-ionized. All the samples were sonicated for 30 min before the measurement of thermal conductivity. It was observed that when equal volume fraction (0.05%) of bulk, NPs and nanocomposites of TiO_2 have been dispersed in de-ionized water, they showed enhancement in TC but SiO_2@TiO_2 nanocomposites displayed higher enhancement in effective TC than others. It was observed that thermal conductivity increases with the increase in shell thickness of SiO_2 up to certain concentration but after that it decreases the TC (figure 2.15a-b), this is due to more thickness of SiO_2 which hamper that TC of TiO_2 at higher concentration. Thus, it clearly indicate that optimization of shell thickness is crucial parameter for enhancement in thermal conductivity and dispersion stability. Experimental results also showed that SiO_2@TiO_2 nanorods based aqueous suspension showed higher enhancement (20%) in TC than SiO_2@TiO_2 nanospheres (15%) at same temperature (23°C) and volume fraction (0.05%) as shown in figure 2.15 (a-b).

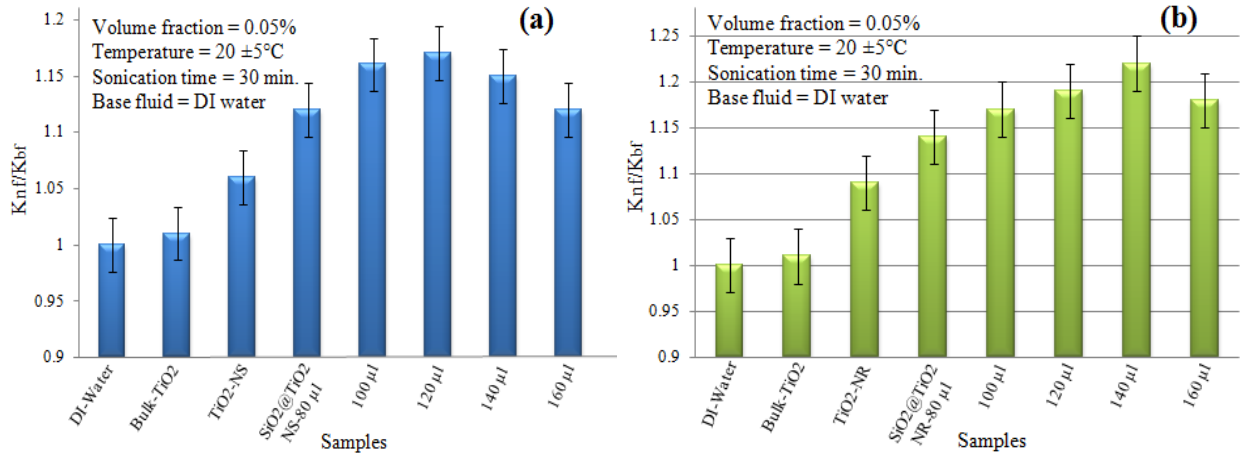

Figure 2.15: Influence of thickness of SiO_2 shell over TiO_2 **(a)** nanospheres and **(b)** nanorods for maximum enhancement in thermal conductivity.

2.7.5 Evaluation of dispersion stability of aqueous suspension of SiO_2@TiO_2 nanocomposites by measuring TC, density and refractive index and their corresponding photographs

In this section evaluation of dispersion stability has been studied. The sample (SiO_2@TiO_2) which

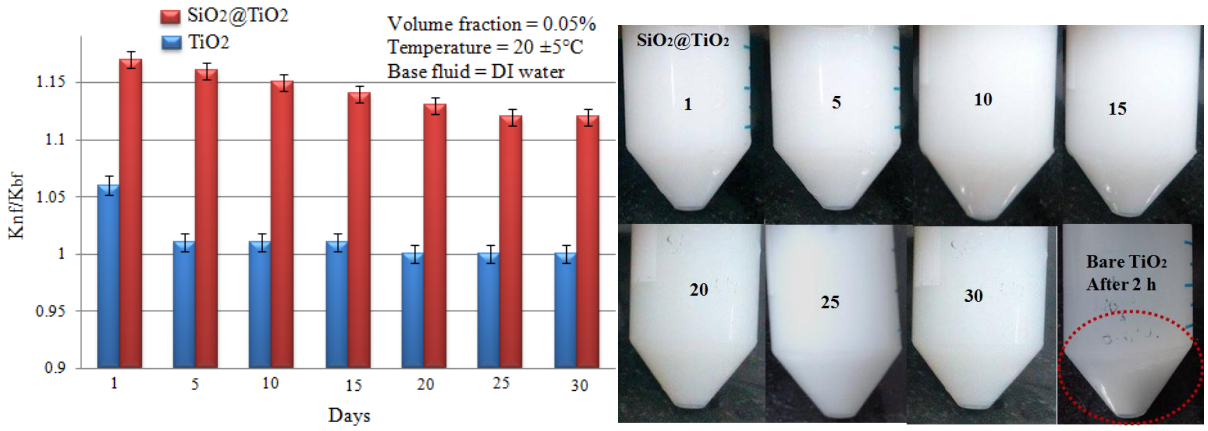

Figure 2.16: Variation in thermal conductivity of SiO_2 coated TiO_2 aqueous suspension with the passage of time (0-30 days after preparation of samples) and Photographs of these SiO_2@TiO_2 aqueous suspensions.

showed maximum enhancement in thermal conductivity was preserved for further study of dispersion stability. After optimization of silica thickness, dispersion stability has been investigated for approximate 1 month by measuring TC, density and refractive index. Figure 2.16 showed the effect of dispersion stability and thermal conductivity with passage of time. It was found that bare TiO_2 based suspension showed sharp decrease in thermal conductivity and reaches the TC of water after 1-2 days as shown in figure 2.16, but in case of SiO_2@TiO_2 based nanocomposites suspension there is only 4-5% decrease in TC enhancement even after 1 month. It was observed that for first

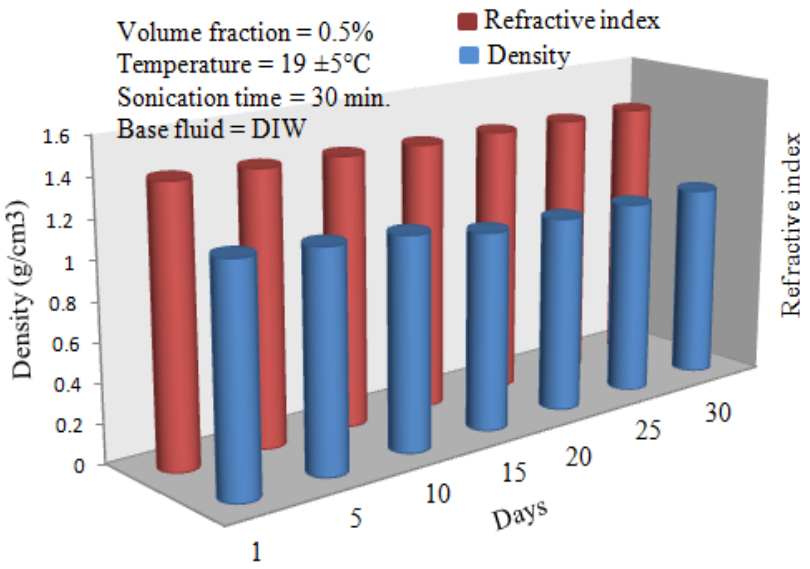

Figure 2.17: Variation in density and refractive index of SiO_2 @TiO_2 aqueous suspension with the passage of time (0-30 days after preparation of samples).

10 days the decrease in TC was ~3% but after that there was only 1-2% decrease in TC. Photographs of all the samples have been also taken by time to time to see any visual settling of NPs as shown in figure 2.16. For further confirmation of dispersion stability of the same sample, the density and refractive index measurement have been done with passage of time (1-30 days) as shown in figure 2.17. The experimental results showed that there is not much change in density and refractive index with time (1-30 days) which clearly indicate the longer dispersion stability of NPs as shown in figure 2.17. For the measurement of density and refractive index upper part of the suspension has been taken. Photographs of all the samples also showed that with the passage of time the upper part of suspension become lighter in color, so there is slight decrease in density and refractive index.

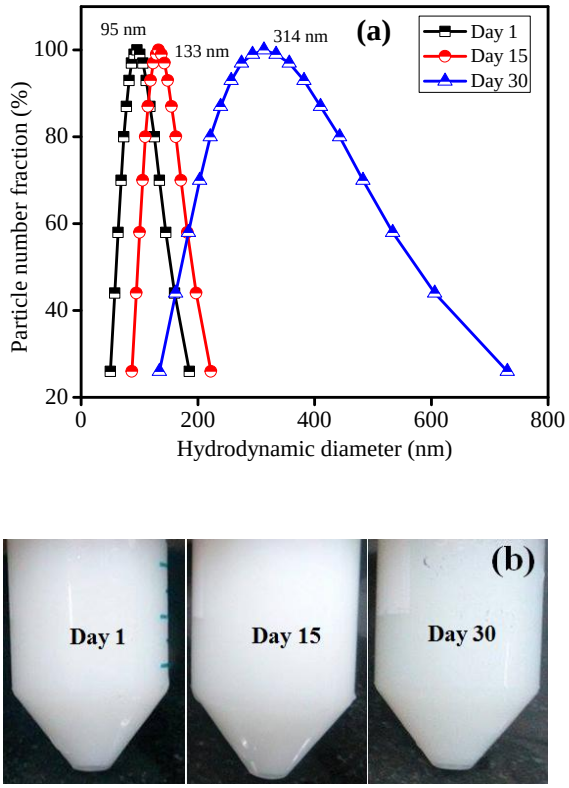

Figure 2.18: (a) Particle size distribution of SiO_2@TiO_2 nanocomposites in aqueous suspension after 1, 15 and 30 days**. (b)** Photographs of these samples.

2.7.6 Evaluation of dispersion stability of aqueous suspension of SiO_2@TiO_2 nanocomposites by measuring particle size distribution and zeta potential

The dispersion stability of the same sample was also evaluated by measuring particle size distribution and zeta potential. Figure 2.18 (a) showed that with the passage of time (1-30 days), the hydrodynamic size of SiO_2@TiO_2 suspension increased from 95 to 304 nm and their corresponding photographs are also shown in figure 2.18 (b). Figure 2.19

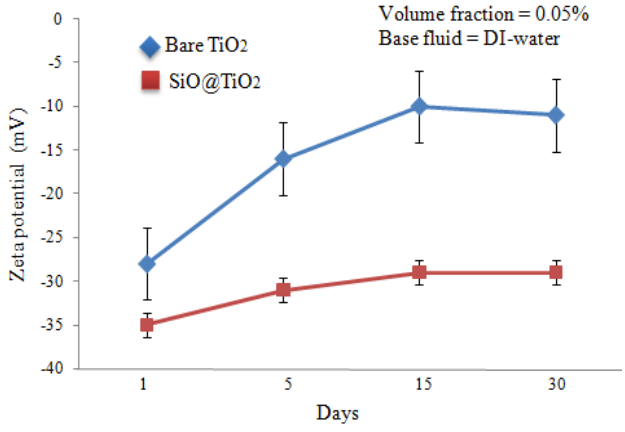

Figure 2.19: Change in zeta potential of bare and SiO_2@TiO_2 nanoparticles dispersed in de-ionized after 1, 5, 15 and 30 days.

displayed the change in zeta potential with passage of time (1-30 days). It was found that bare TiO_2 suspension showed much change in zeta potential values -28 to -11 which indicate the aggregation of TiO_2 NPs in base fluids, but SiO_2@TiO_2 suspension showed small change in zeta potential value -36 to -30 which indicate the stability of suspension for longer time.

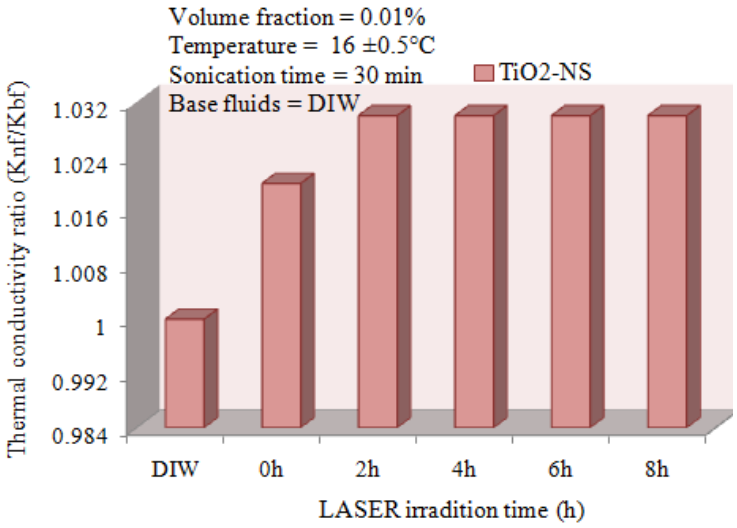

Figure 2.20: Effect of LASER irradiation on thermal conductivity of aqueous suspension of TiO_2 nanoparticles.

2.7.7 Effect of LASER irradiation on thermal conductivity:

Figure 2.20 showed the effect of LASER irradiation on thermal conductivity of TiO_2 NPs based aqueous suspension. It was found that after 2 h irradiation of suspension, there is slight increase in thermal conductivity but after that there is no change in thermal conductivity even after 8 h of LASER irradiation.

2.8 Conclusions

In summary, the beneficial effect of a thin layer of SiO_2 coating over TiO_2 nanostructures for superior dispersion stability and thermal conductivity are investigated with the supportive evidences of particle size distribution, zeta potential, density and refractive index analysis as indicator parameter for stable suspension. As a result, SiO_2 coated composite particles always exhibited higher TC than bare NPs dispersion which generally undergoes quick agglomeration and precipitation. Further optimization of SiO_2 shell thickness is important for exhibiting long term dispersion stability and maximum enhancement in thermal conductivity. It was also found that lengthy nanorods based suspension exhibit more enhancements in TC than spherical NPs.

References:

[1] S.U.S. Choi, *ASME FED*, 1995, **66**, 99-105.

[2] S.M.S. Murshed, K.C. Leong and C. Yang, *Appl. Therm. Eng.* 2008, **28**, 2109-2125.

[3] S.M.S. Murshed, K.C. Leong and C. Yang, *Int. J. Therm. Sci.* 2008, **47**, 560-568.

[4] S. Lee, S.U.S. Choi, S. Li and J.A. Eastman, *J. Heat Transfer*. 1999, **121**, 280-289.

[5] J.A. Eastman, S.U.S Choi, S. Li, W. Yu and L.J. Thompson, *Appl. Phys. Lett.* 2001, **78**, 718-720.

[6] K.V. Wong and O. Leon, *Adv. Mech. Eng.* 2010, **2010**, 1-11.

[7] S. Lee, S.U.S. Choi, S. Li and J.A. Eastman, *J. Heat Transfer*. 1999, **121**, 280-289.

[8] K. Khanafer and K.Vafai, *Int. J. Heat Mass Transfer.* 2011, **54**, 4410-4428.

[9] S.J. Palm, G. Roy and C.T. Nguyen, *Appl. Therm. Eng.* 2006, **26**, 2209-2218.

[10] S.P. Jang and S.U.S. Choi, *Appl. Phys. Lett.* 2004, **84**, 4316-4318.

[11] W. Evans, J. Fish and P. Keblinski, *Appl. Phys. Lett.* 2006, **88**, 1-3.

[12] C.H. Chon, K.D. Kihm, S.P. Lee and S.U.S. Choi, *Appl. Phys. Lett.* 2005, **87**, 1-3.

[13] X. Wang and A. Mujumdar, *Int. J. Therm. Sci*. 2007, **46**, 1-19.

[14] X.F. Li, D.S. Zhu, X.J. Wang, N. Wang, J.W. Gao and H. Li, *Thermochim. Acta*. 2008, **469**, 98-103.

[15] M. Sakamoto, Y. Kanda, M. Miyahara and K. Higashitani, *Langmuir* 2002, **18**, 5713-5719.

[16] J.C. Maxwell, A Treatise on Electricity and Magnetism, third ed., Clarendon Press, Oxford, UK, 1891.

[17] W. Duangthongsuk and S. Wongwises, *Exp. Therm. Fluid Sci.* 2009, **33**, 706-714.

[18] I. Mudawar and T.M. Anderson, *ASME J. Electron. Packag.* 1993, **115**, 89–99.

[19] T.M. Anderson and I. Mudawar, *ASME J. Heat Transfer* 1989, 111, 752–759.

[20] H. Masuda, A. Ebata, K. Teramae and N. Hishinuma, *Netsu Bussei (Japan)* 1993, **4**, 227-233.

[21] B.C. Pak and Y.I. Cho, *Exp. Heat Transfer*. 1998, 11, 151-170.

[22] S. Lee, S.U.S. Choi, S. Li and J.A. Eastman, *Trans. Am. Soc. Mech. Eng.* 1999, **121**, 280-289.

[23] Y. Ding, H. Alias, D. Wen and R. Williams, *Int. J. Heat Mass Transfer*. 2006, **49**, 240-250.

[24] G. Paul, J. Philip, B. Raj, P.K. Das and I. Manna, *Int. J. Heat Mass Transfer.* 2011, **54**, 3783-3788.

[25] D. Zhou, *Int. J. Heat Mass Transfer*. 2004, **47**, 3109-3117.

[26] S.K. Das, N. Putta, P. Thiesen and W. Roetzel, *ASME Transactions, J. Heat Transfer*. 2003, 125, 567-574.

[27] Y. He, Y. Jin, H. Chen, Y. Ding, D. Cang and H. Lu, *Int. J. Heat Mass Transfer.* 2007, **50**, 2272-228.

[28] S.M.S. Murshed, K.C. Leong and C. Yang, *Int. J. Therm. Sci.* 2005, **44**, 367-373.

[29] M. Chandrasekar, S. Suresh, and A.C. Bose, *Exp. Therm. Fluid Sci.* 2010, **34**, 210-216.

[30] S.K. Pradhan, P.J. Reucroft, F. Yang and A. Dozier, *J. Crystal Growth.* 2003, **256**, 83-88.

[31] M. Gratzel, *J. Photochem. Photobiol. C.* 2003, **4**, 145-153.

[32] S.H. Kang, J.Y. Kim, H.S. Kim and Y.E. Sung, *J. Ind. Eng. Chem.* 2008, **14**, 52-59.

[33] H. Zhang, G.R. Li, L.P. An, T.Y. Yan, X.P. Gao and H.Y. Zhu, *J. Phys. Chem. C.* 2007, 111**,** 6143-6148.

[34] J.N. Nian and H. Teng, *J. Phys. Chem. B* 2006, **110,** 4193-4198.

[35] I.S. Grover, S. Singh and B. Pal, *Appl. Surf. Sci.* 2013, **280**, 366-372.

[36] X. Chen and S.S. Mao, *Chem. Rev.* 2007, **107**, 2891-2959.

[37] P.D. Christy, N. Melikechi, N.S.N. Jothi, A.R.B. Suganthi and P. Sagayaraj, *J. Nanopart. Res.* 2010, **12**, 2875-2882.

[38] P. Hoyer, *Langmuir* 1996, **12**, 1411-1413.

[39] T. Nanba, S. Masukawa, J. Uchisawa and A. Obuchi, *Catal. Lett.* 2004, **93**, 195-201.

[40] X. Chen, S. Shen, L. Guo, and S.S. Mao, *Chem. Rev.* 2010, **110**, 6503-6570.

[41] M.J.P. Gallego, C. Casanova, R. Paramo, B. Barbes, J.L. Legido and M.M. Pineiro, *J. Appl. Phys.* 2009, **106**, 1-8.

[42] J.A. Eastman, S.R. Phillpot, S.U.S. Choi and P. Keblinski, *Annu. Rev. Mater. Res.* 2004, **34**, 219-246.

[43] W. Yu, D.M. France, J.L. Routbort and S.U.S. Choi, *Heat Transfer Eng.* 2008, **29**, 432-460.

[44] P. Keblinski, J.A. Eastman and D.G. Cahill, *Mater. Today.* 2005, **8**, 36-44.

[45] L.S. Sundar and K.V. Sharma, *Int. J. Nanoparticles.* 2008, **1**, 66-77.

[46] R.S. Vajjha and D.K. Das, *Int. J. Heat Mass Transfer.* 2009, **52**, 4675-82.

[47] P.D. Shima, J. Philip and B. Raj, *J. Phys. Chem. C.* 2010, **114**, 18825-18833.

[48] R. Singh and B. Pal, *J. Mol. Catal. A: Chem.* 2013, **371**, 77-85.

[49] M. Haruta, *Chem. Rec.* 2003, **3**, 75-87.

[50] S.M.S. Murshed, K.C. Leong and C. Yang, *Int. J. Therm. Sci.* 2005, **44**, 367-73.

[51] H.T. Zhu, C.Y. Zhang, Y.M. Tang and J.X. Wang, *J. Phys. Chem. C.* 2007, **111**, 1646-50.

[52] J.W. Gao, R.T. Zheng, H. Ohtani, D.S. Zhu and G. Chen, *Nano. Lett.* 2009, **9**, 4128-32.

[53] D. Lee, J.W. Kim and B.G. Kim, *J. Phys. Chem. B.* 2006, **110**, 4323–4328.

[54] A. Ghadimi, R. Saidur, and H.S.C. Metselaar, *Int. J. Heat Mass Transfer.* 2011, **54**, 4051-4068.

[55] W. Jiang, G. Ding and H. Peng, *Int J. Therm. Sci.* 2009, **48**, 1108-15.

[56] X.F. Li, D.S. Zhu, X.J. Wang, N. Wang, J.W. Gao and H. Li, *Thermochim Acta.* 2008, **103**, 469-98.

[57] S.M. Saterlie, H. Sahin, B. Kavlicoglu, Y. Liu and A.O. Graeve, *Chem. Mater.* 2012, **24**, 3299-3306.

[58] S.S. Botha, P. Ndungu and B.J. Bladergroen, *Ind. Eng. Chem. Res.* 2011, **50**, 3071–3077.

Section A

Anisotropic CuO nanostructures of different size and shape exhibit thermal conductivity superior than typical bulk powder

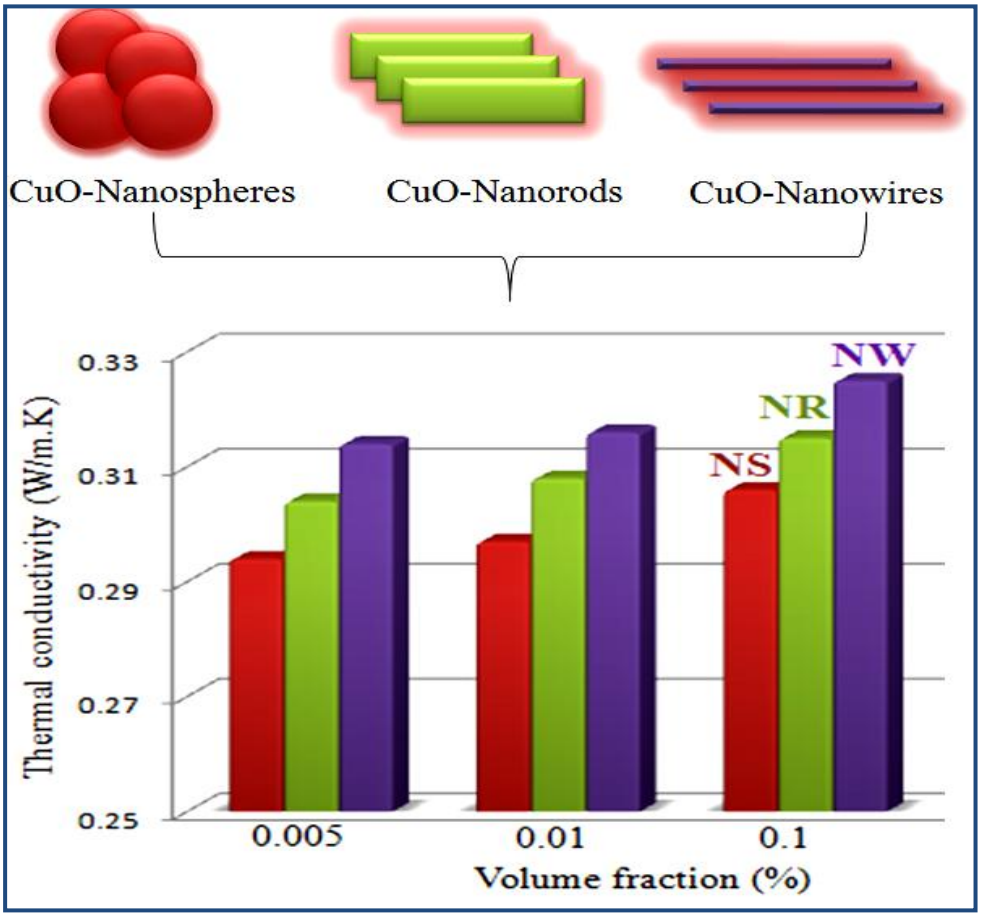

Abstract: This work demonstrates the preparation of monoclinic crystalline CuO nanospheres (5-10 nm), nanorods (L × W = 100-140 nm × 30-40 nm) and nanowires (200-210 nm × 2-5 nm) for the study of thermal conductivity when dispersed in de-ionized water and ethylene glycol (0.005-0.1 vol.%). It has been observed that CuO nanorods and nanowires having surface area 53 and 61 m^2/g, respectively, always displayed higher thermal conductivity than CuO nanospheres possessing lower surface area (41 m^2/g) which attributed to the differences in their per-particle surface area, percentage of surface exposed atoms, anisotropic lengthy shape and large phonon-mean-free paths. The experimental results revealed higher thermal conductivity than obtained from theoretical models due to particle shape effect as expected from Hamilton-Crosser equation. It has also been found that density is directly proportional to thermal conductivity and increases with the increase in volume fraction. The decrease in aggregated particle size (130–104 nm) and an increase in zeta potential value (−32 to −37 mV) of CuO nanospheres cause more stability of CuO dispersion with 3-6 h of sonication.

3.1 Introduction

Nanocrystalline semiconductor particles have drawn considerable interest in recent years because of their special properties such as a large surface-to-volume ratio, higher activity, and special electronic and optical properties as compared to [1-3] the bulk materials. The oxides of transition metals are an important class of semiconductors having applications in magnetic storage, solar energy transformation, [4,5] electronics and catalysis. The CuO is a narrow band gap material used for photoconductive and photothermal applications having higher TC (32 W/m.K) and heat capacity (520 J/mol.K) than other oxides of [6-8] transition metals. Over the past decade, [9] a new dimension has been added to colloid chemistry due to the proposition that suspended particles may significantly enhance the thermal properties of cooling liquids. After suspending nanometer-sized crystalline CuO in water, an increase in TC of the mixture was observed [10]. Recently many research groups [11,12] worked with different size of CuO nanoparticles (NPs) for increased TC in heat transfer applications. Some research groups [13-17] observed 10 to 30% enhancement in TC for CuO at different (1 to 5%) volume fractions and a maximum increase in TC of approximately 20% was observed for 4 vol% CuO NPs of average size 35 nm dispersed in EG. Density [18] is another significant property of a fluid that affects the friction factor, pump loss, Reynolds number, etc. Said et al. [19] has investigated the density of Al_2O_3, ZnO_2 and

Sb_2O_4:SnO_2 EG-water based suspensions and compared the results with proposed formula of Pak and Chao [20].

It is expected that TC is not only closely related to NPs size but also to their geometric shapes, anisotropicity and lengthy dimension [21]. The size dependent catalytic activity of Cu nanoclusters for the reduction of oxygen has been reported by Wei and Chen et al. [22] and also used for methylene blue-hydrazine reduction by Shen et al. [23]. By changing the shape of NPs, the number of surface exposed atoms, per-particle surface area, edges or corners of unsaturated surface atoms will be changed and accordingly altering the properties of materials. As heat transfer takes place mostly on the surface of a material [24], hence conduction will also be improved depending on NPs geometric surface morphology. Literature reveal that although most of the studies are carried out using spherical CuO NPs, much information about the TC of anisotropic lengthy CuO nanostructure is not available. The study of electrophoretic behavior through measurement of the zeta potential (ζ) and dynamic light scattering (DLS) becomes important parameter for understanding the dispersion behavior of NPs in a liquid medium and has not been investigated much. In this context, various size and shapes of CuO NPs were prepared to investigate their comparative TC depending on variation in surface area, morphology and dispersion stability in DI water and EG in-correlation with observed zeta potential and particle size distribution. The experimental results of TC for spherical and non-spherical particles have compared with theoretical model of Maxwell and Hamilton-Crosser. The as-prepared materials can be used for cooling applications like transportation, nuclear reactor and defense etc and also for energy storage in solar collector.

3.2 Experimental Section

3.2.1 Materials and methods

The various shapes of CuO NPs have been synthesized; detail description is given in **Chapter 1**, **section 1.5.1.4.**

3.2.2 Characterizations

As synthesized NPs were characterized by various techniques, the details of the techniques are given in **Chapter 1**, **section 1.5.7.**

3.2.3 Preparation of Nanofluids

Nanofluids were prepared by two-step methods as mentioned in **Chapter 1, section 1.5.2**.

3.2.4 Thermal conductivity measurement

The TC measurement has been done by KD2 Pro, experimental details are given in **chapter 1**, **section 1.5.3**.

3.3 Results and Discussion

3.3.1 Structural and morphological characterization

Typical XRD patterns of the CuO nanostructures in figure 3.1 showed that all peaks indexed to monoclinic CuO (space group *C*2/*c*) crystal phase as per JPCDS Card No. 80-1268, without any impurity peaks of Cu $(OH)_2$ and Cu_2O indicating high purity of CuO NPs. All CuO NPs exhibit different intensities and broadness of XRD peaks suggesting change in nanocrystal size (grain size) of CuO nanospheres (~5 nm), nanorods (~10 nm) and nanowires (~25 nm) as calculated by the Debye-Scherrer equation $d=k\lambda/\beta\cos\theta$ using the average values of (0 0 2) (2θ =35.5°) and (2 0 0) (2θ = 38.8°) planes, where k is the Debye-Scherrer [25] constant (0.89), θ is diffraction angle, and β is full width at half-maximum introduced by grain size. In particular, low Miller-indexed (002) and (200) reflections show strongest peaks indicating the preferential crystal planes of the nanorods and nanowires. The difference in intensity of related peaks for the three CuO nanostructures may be due to texture effect as well as the dimension/morphological

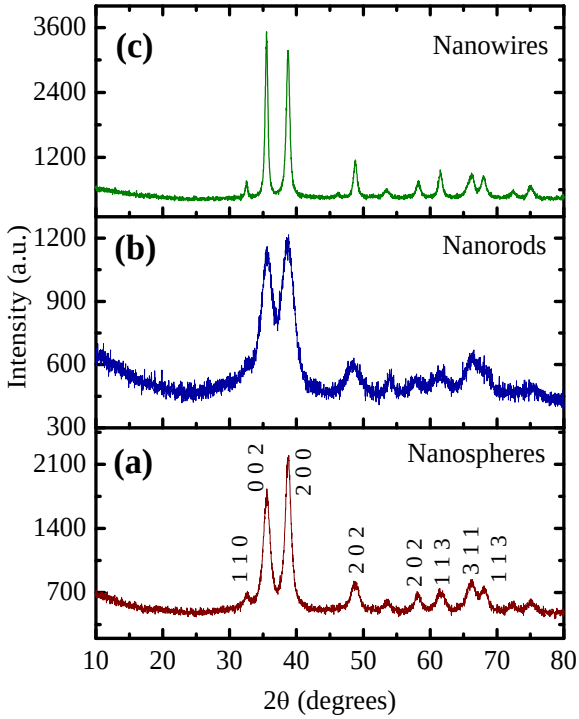

Figure 3.1: XRD patterns of CuO **(a)** nanospheres (NS) **(b)** nanorods (NR) and **(c)** nanowires (NW).

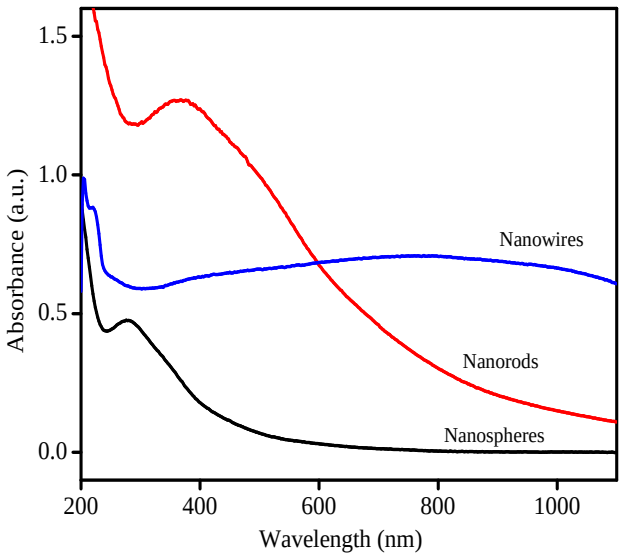

Figure 3.2: UV-visible absorption spectra of CuO nanospheres (NS), nanorods (NR) and nanowires (NW).

alternation in a certain direction. Similar results show variation of morphology and growth direction leading to the change in intensity of the XRD peaks are reported by Singh et al. [26].

The absorption spectra showed a broad peak at 290 nm with absorption edge at 426 nm (figure 3.2) for CuO nanospheres and its estimated band-gap (E_g = 2 eV) for 5-10 nm particle is reported to much larger than bulk CuO (1.65 eV). This blue-shift in energy gap is attributed to the enhancement of quantum confinement effect resulting from decrease in size of the NPs. The observed broad absorption band is probably due to the dominant surface-related defects for intra-gap states. Ovchinnikov et al. [27] have described the role of electronic defects due to presence of dopants or valence defects (O vacancies and Cu^{+}) in CuO NPs leading to the development of intra-band states.

The SEM images revealed the spherical morphology (figure 3.3a) of CuO NPs that seems to be agglomerated. Figure 3.3b showed that CuO nanorods are stacked together in a bundle like structure with an aspect ratio of 25-50 and many lengthy CuO nanowires are found in figure 3.3c-d. To further confirm their exact shape and dimensions, TEM analysis was carried out. As shown in figure 3.4a and 3.4b, the CuO nanospheres were uniformly dispersed with average diameter of 5-10 nm. The CuO nanowires of length 150-200 nm and diameter 5-10 nm are randomly

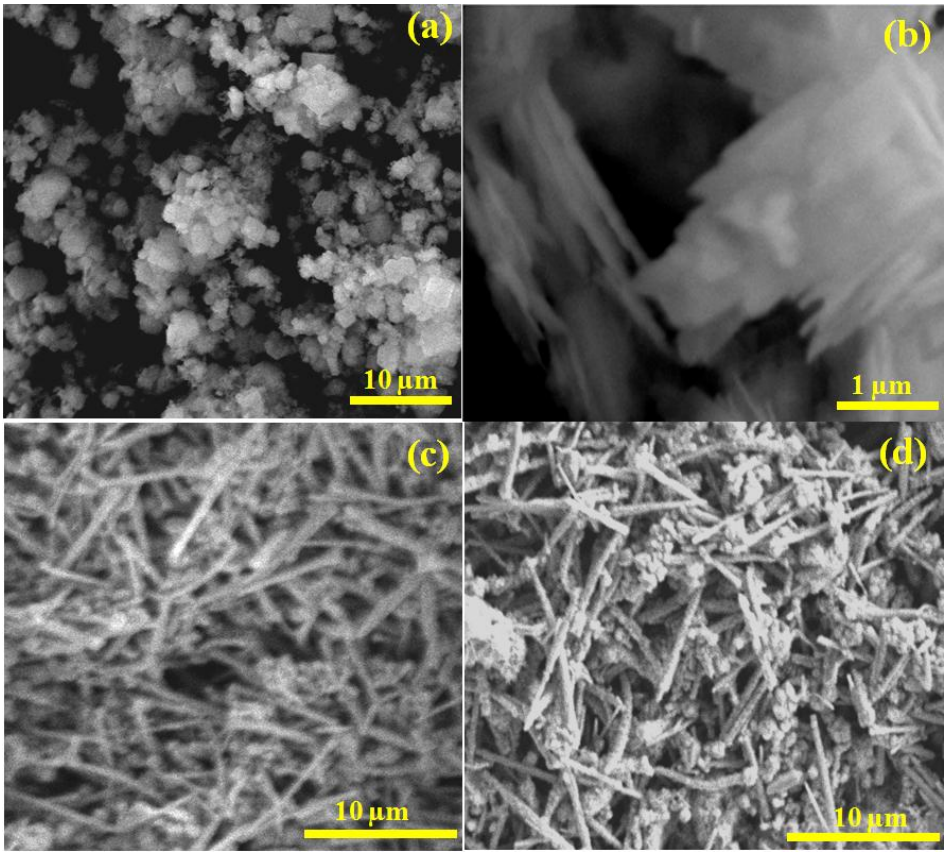

Figure 3.3: SEM images of CuO **(a)** nanospheres (NS) **(b)** nanorods (NR) and **(c-d)** nanowires (NW).

agglomerated as observed in figure 3.4c-d. The TEM images (figure 3.5) of CuO nanorods of diameter 80-90 nm and length 0.5-1 µm are tightly packed in a bundle like shape. The surface area of CuO nanowires 61 m^2g^{-1} is higher than 53 and 41 m^2g^{-1} for nanorods and nanospheres, respectively and is accordance with their difference in geometric dimension and surface morphology.

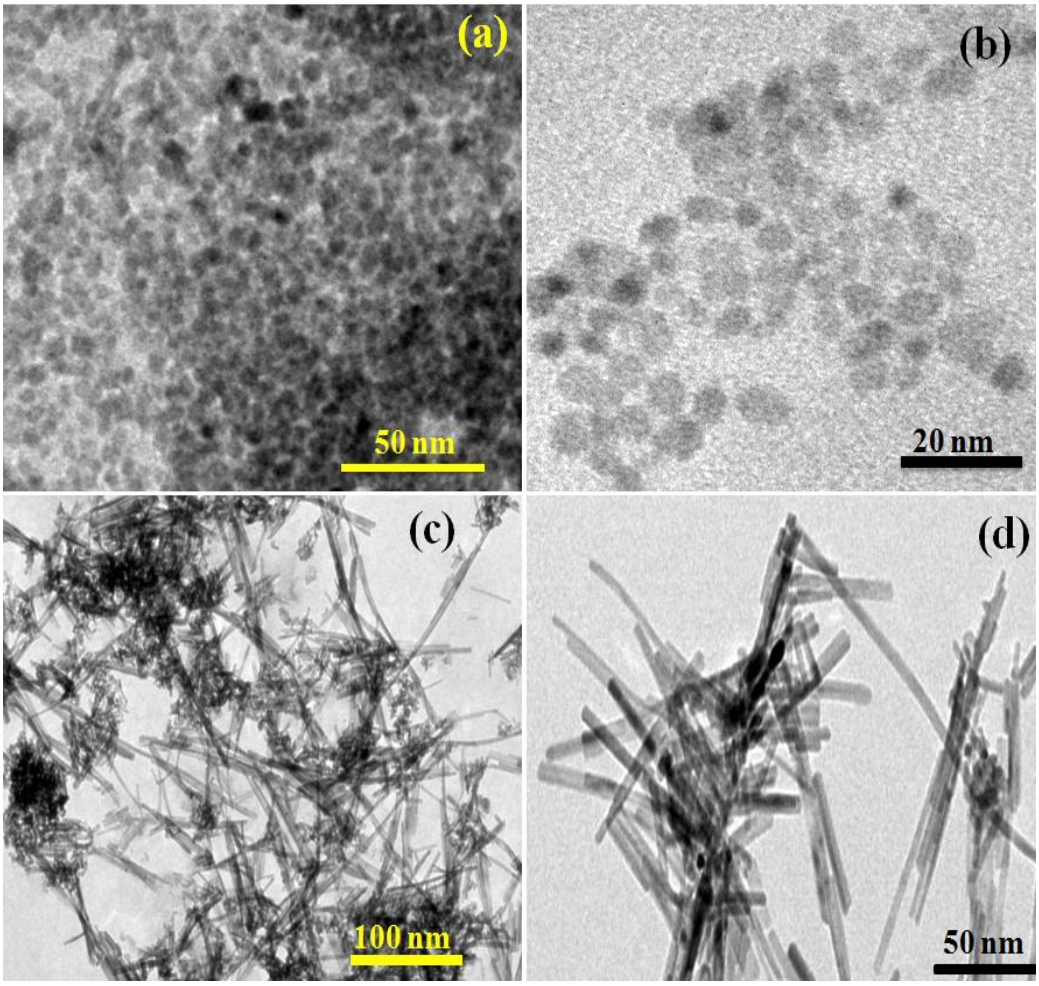

Figure 3.4: TEM images of CuO **(a-b)** nanospheres (NS) and **(c-d)** nanowires (NW).

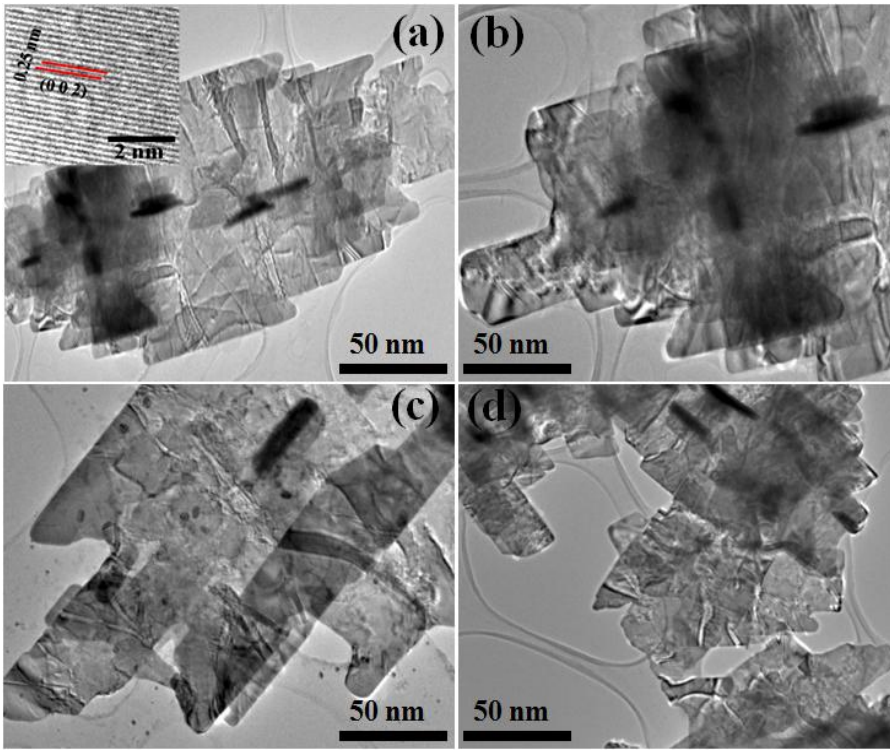

Figure 3.5: TEM and HRTEM images of CuO nanorods (NR).

3.3.2 Effect of volume fraction and shape on thermal conductivity

Thermal conductivity of CuO-DI water and EG suspension is shown in figure 3.6a-b revealed that TC increases with the increase in volume fractions (0.005 to 0.1 vol%) and sonication time (3 to 6 h). The CuO nanowires and nanorods dispersed both in DI water and EG showed more enhancements in TC than nanosphere dispersion. In suspension of CuO nanowires-DI water, the TC enhancement was found to be 22.05% with respect to pure DI water, and 28.45% with respect to EG at same volume fraction (0.1 vol%). The higher TC observed for lengthy nanorods and nanowires can be attributed to less interparticles distance, higher geometric surface area of per particle (28638 nm^2 for nanowires and 57727 nm^2 for nanorods as compared to 254 nm^2 of nanospheres), percentage of surface exposed atoms, anisotropic lengthy shape and rigidity in shape make a regular structural network in DI-water that help in rapid transfer of phonon vibration from one particle to other particles. The number of unsaturated atoms at edges/corners

increase by changing the shape of particle from spheres to wire/rods and will also facilitate the improved heat transfer rate. The higher TC enhancement in EG dispersion is due to its more viscosity making better suspension and decrease in settling rate of NPs but in case of DI water, the NPs are not much suspended and they easily settle down. This, in turn, leads to more particle-to-particle interaction in a given period of time and increase the phonon vibration rate per particle. As a result, heat is more readily transferred from EG to the particles than from DI water to particles. The ultrasonications also help in the breakdown of large NP clusters into smaller ones leading to enhancement in TC with increase in sonication time. It has been reported [28] that TC increases up to 30% for CuO nanosphere dispersion in EG (1-5 vol%), however, in this work TC was found to be 25-28% for anisotropic shapes of CuO in EG dispersion even at very low volume fractions (0.01 to 0.1%).

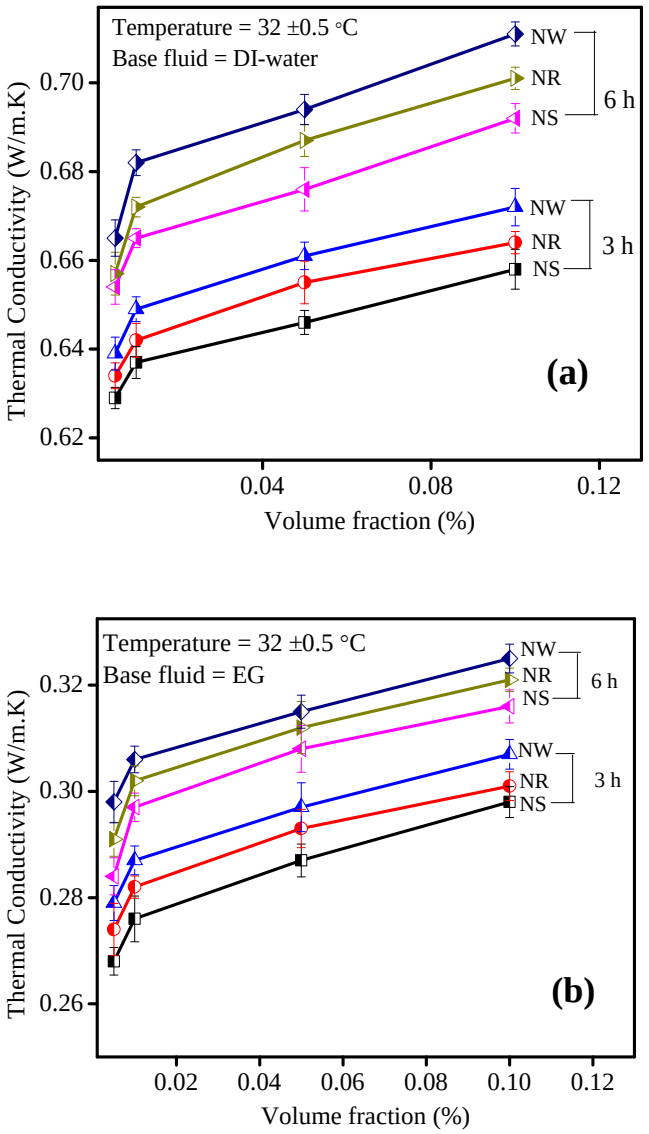

Figure 3.6: Change in Thermal conductivity as a function of shape, sonication time and volume fraction **(a)** CuO nanoparticles dispersed in DI water **(b)** CuO nanoparticles dispersed in ethylene glycol (EG).

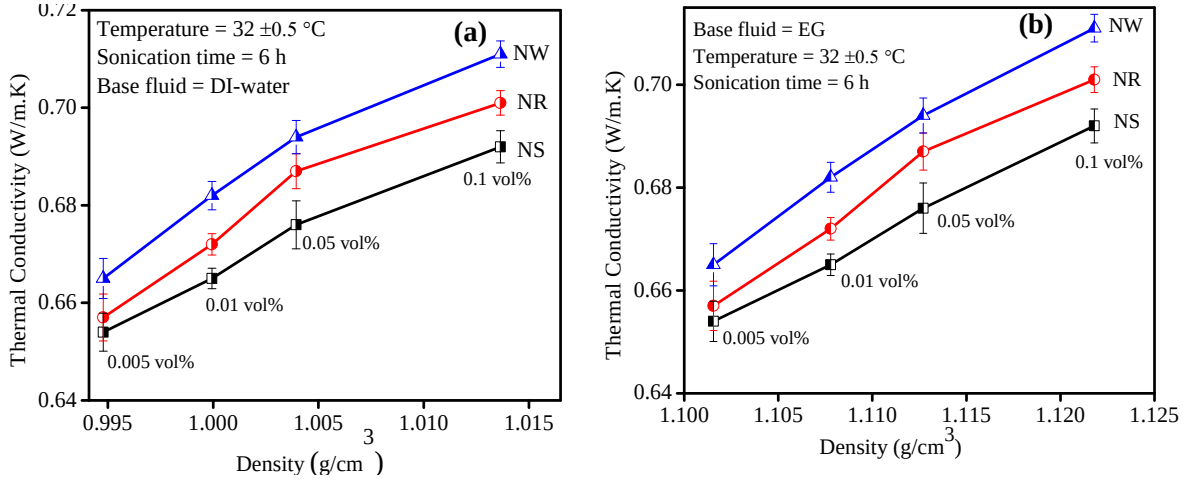

Figure 3.7: Variation in thermal conductivity as a function of density **(a)** CuO nanoparticles dispersed in DI water **(b)** CuO nanoparticles dispersed in EG.

Change in TC as a function of density is presented in fig. 7a-b at 32 ±5% °C. The density of DI - water and EG has been measured without the addition of NPs and found that Ethylene glycol showed higher density than DI-water due to its viscous nature. In DI-water and EG dispersion of NPs, the density increases with increase in volume concentration of NPs. The density of dispersion was calculated according to Pak and Cho's equation [20]

$$\rho_{nf} = \phi\rho_p + (1-\phi)\rho_w \qquad (1)$$

Where ϕ and ρ_p are the volume fraction and density of the nanoparticles respectively, and ρ_w is the density of the base fluid.

3.3.3 Effect of sonication time on particle size distribution

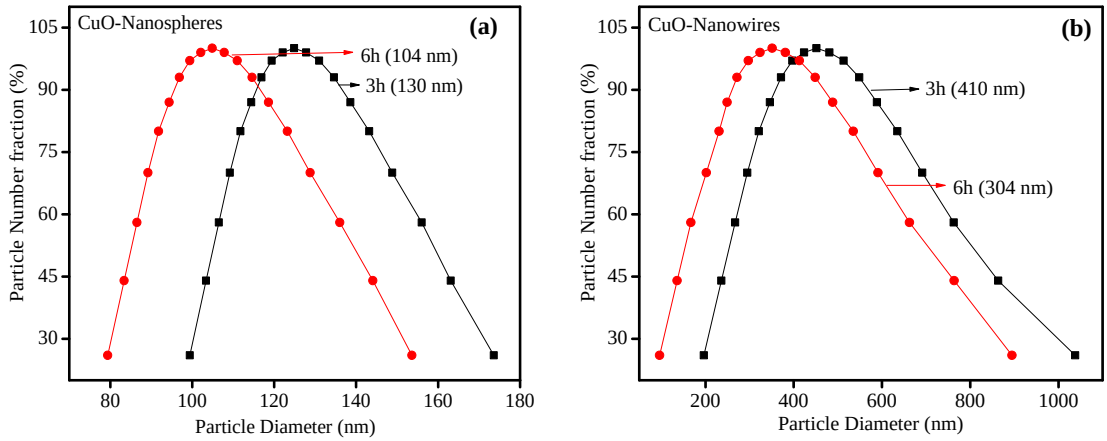

Figure 3.8: Particle size distribution of **(a)** CuO-NS+DIW and **(b)** CuO-NR+DIW at two different sonication time (3 and 6 hours).

Figure 3.8 (a-b) revealed that by increasing the duration of sonication from 3 to 6 h, the aggregated size distribution of particle decreases from 130 to 104 nm in case of CuO nanospheres and 410 to 304 nm for CuO nanowires which directly affect the TC. The decrease in aggregated particle size is due to strong sonic waves breaking large clusters into smaller ones after increasing the time duration of sonication. Furthermore, the surface charges of NPs also play a very important role in the dispersion stability. The measured negative ζ (-32 and -37) values indicated the good stability of CuO NPs dispersions which causes to exhibit high TC due to effective suspension for longer time.

3.3.4 Theoretical models

The Maxwell model [29] was developed to determine the effective TC of liquid-solid suspensions for low volumetric loading of the spherical particles. This model is applicable to statistically homogeneous and low volume fraction liquid-solid suspensions with randomly dispersed and uniform size spherical particles.

$$\frac{k_{eff}}{k_f} = \frac{k_p + 2k_f + 2\phi\left(k_p - k_f\right)}{k_p + 2k_f - \phi\left(k_p - k_f\right)} \qquad (2)$$

Where k_p and k_f are the conductivities of the particle material and the base fluid respectively, and ϕ is volume fraction of NPs**.**

Hamilton and Crosser [30] modified Maxwell's model to determine the effective TC of non-spherical particles by applying a shape factor.

$$\frac{k_{eff}}{k_0} = \frac{k_p + (n-1)k_0 + (n-1)\left(k_p - k_0\right)\phi}{k_p + (n-1)k_0 - \left(k_p - k_0\right)\phi} \qquad (3)$$

Where k_p and k_0 are the conductivities of the particle materials and the base fluid, and ϕ is the volume fraction of NPs. Thus, according to this model, suspensions of particles with high shape factor (elongated and thin) should have higher thermal conductivities.

Prasher *et al.* [31] considered dynamic contribution of NPs in their TC model for suspensions. However, their model contains three unknown empirical or fitting parameters. In addition, dynamic contribution was coupled with Maxwell's model without taking into account the effect of interfacial layer in their model. Besides particle volume fraction, particles size, temperature, particles dispersions and particle movement should be taken into account in developing model for the effective TC of suspension. Prasher *et al.*´s model is expressed as

$$\frac{k_{eff}}{k_f} = \left(1 + A\phi_p \,\mathrm{Re}^m \,\mathrm{Pr}^{0.33}\right)\frac{(1+2\alpha) + 2\phi_p(1-\alpha)}{(1+2\alpha) - \phi_p(1-\alpha)} \qquad (4)$$

Where $\alpha = 2R_b k_f / d_p$, d_p is the particle diameter, R_b is interfacial resistance, and A and m are empirical parameters.

As predicted by Maxwell and Prasher et al. model (figure 3.9a), the TC increases with increase in volume fraction, but our experimental results showed more enhancement in TC than these models. The effect of non-spherical particles on TC was explained by Hamilton-Crosser model as shown in figure 3.9 (b), TC increases with increase in volume fraction, here again our experimental results showed more enhancement in TC than theoretical model.

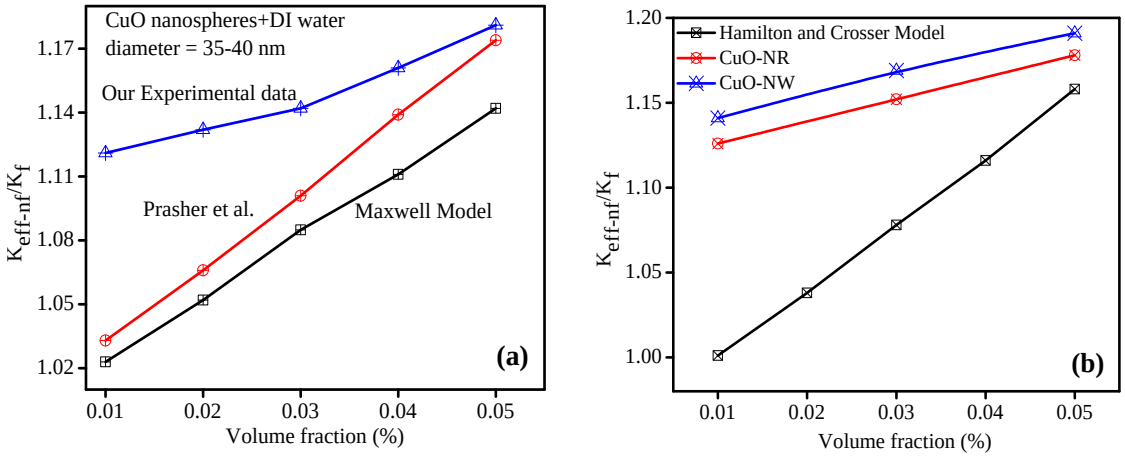

Figure 3.9 (a-b): Thermal conductivity ratio comparison between theoretic model's predictions and our experimental data of CuO-de-ionized based nanofluids.

3.4 Conclusions

In the present study, anisotropic shapes (nanowires and nanorods) of CuO nanostructures based dispersion showed higher enhancement in thermal conductivity than spherical shaped CuO based dispersion as expected by Hamilton-Crosser model. The experimental results displayed higher thermal conductivity than theoretically predicated models. It is concluded here that with the increase in volume fraction, the thermal conductivity and density also increased. The effective thermal conductivity is also well correlated with zeta potential values and particle size distribution data. The extended sonication time helps in breakdown of large clusters into smaller sized particles which enhances the thermal conductivity.

Section B:

SiO_2@CuO nanocomposites for enhanced thermal conductivity and dispersion stability in de-ionized water

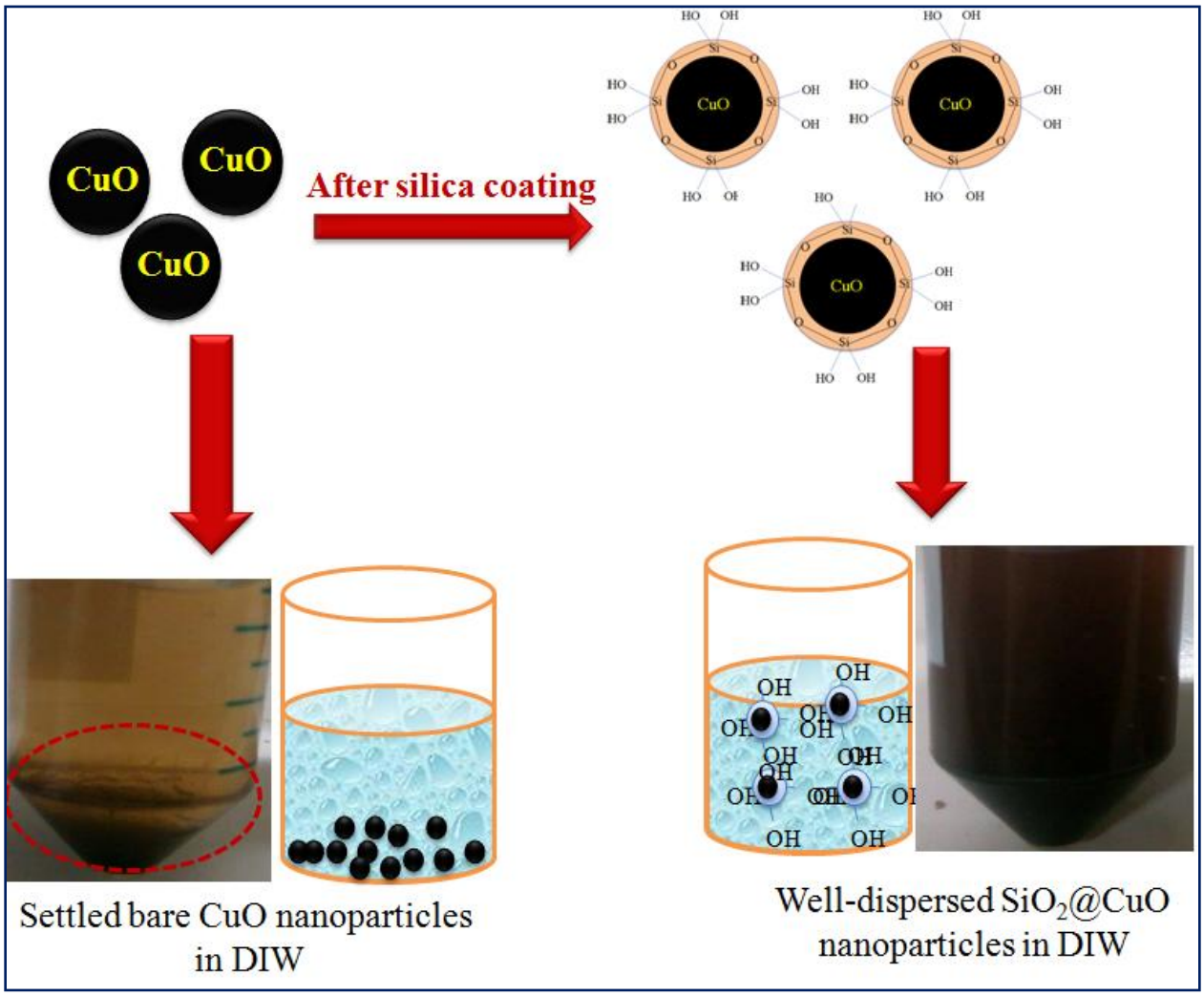

Abstract: This research demonstrates the synthesis of bare and SiO_2 coated CuO nanoparticles and investigate their effect on thermal conductivity of de-ionized water. The samples were characterized by powder X-ray diffraction, Fourier transform infrared spectroscopy and transmission electron microscopy etc. The nanoparticles were dispersed (0.01 vol.%) in de-ionized water and sonicated for half an hour before the measurement of thermophysical properties. The experimental results showed that a thin layer of SiO_2 coating (2-6 nm) over CuO nanoparticles display superior dispersion stability as marked by steady zeta potential (-31 ↔ -40 mV) and density (1.003↔1.002 g/cm^3). Thin Si-OH layer over surface imparts superior hydrophilicity, larger surface area for effective solute-solvent (SiO_2@CuO-H_2O) interaction for improved colloidal stability. Thereby, thermal conductivity is found to be quite stable (0.625↔0.614 W/m.K) up to 2-3 months, whereas aqueous suspension of bare CuO nanoparticles quickly settles down. Depending on the thickness of SiO_2 layer and concentration of SiO_2@CuO, a maximum of 8-10% enhancement in thermal conductivity was achieved.

3.5 Experimental section

3.5.1 Materials and methods

SiO_2@CuO nanocomposites have been synthesized; detail procedure is given in **Chapter 1**, **section 1.5.1.5.**

3.5.2 Characterizations

As synthesized nanocomposities were characterized by various techniques, the details of the techniques are given in **Chapter 1**, **section 1.5.7.**

3.5.3 Preparation of Nanofluids

Nanofluids were prepared by two-step methods as mentioned in **Chapter 1, section 1.5.2**.

3.5.4 Measurement of thermal conductivity and density

The TC measurement has been done by KD2 Pro, experimental details are given in **chapter 1**, **section 1.5.3** and **1.5.4**.

3.6 Results and Discussion:

3.6.1 Structural and Morphological Characterization

Figure 1 (a-b) shows the powder x-ray diffraction (XRD) patterns of bare and SiO_2@CuO nanocomposites. The XRD pattern of bare CuO NPs is discussed in section A. The XRD patterns of SiO_2@CuO nanocomposites are same as pure CuO as shown in figure 3.10 (b), it clearly indicates the absence of characteristic peaks of SiO_2. The reason for absence of SiO_2 peaks in the XRD pattern is low concentration of SiO_2 in the sample.

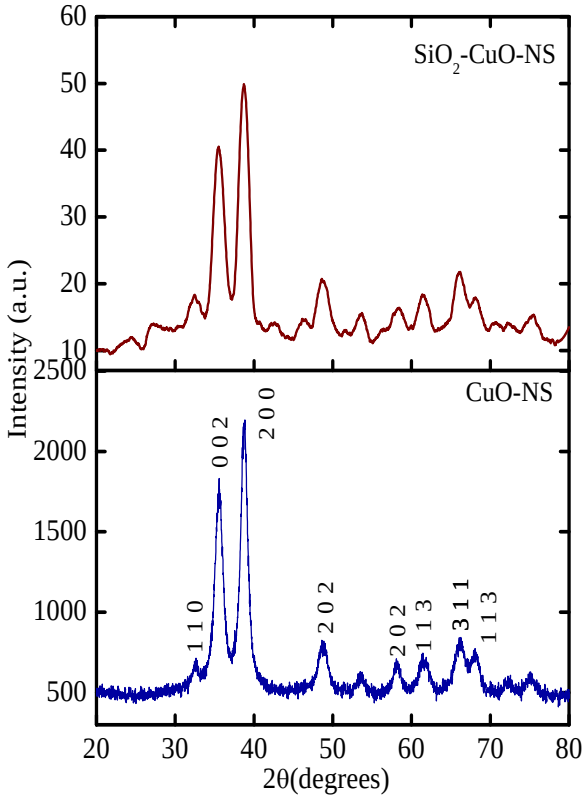

Figure 3.10: XRD patterns of bare and SiO_2 coated CuO nanoparticles.

The verification of SiO_2 in SiO_2@CuO nanocomposites has also been done by Fourier Transform Infrared Spectroscopy (FTIR) as shown in figure 3.11. The FT-IR spectra of SiO_2@CuO NPs showing the vibrational stretching peak at ~1025 cm^{-1} for Si-O-Si formation relative to no such band in bare CuO, thus, this is an evidence for presence of SiO_2 in SiO_2@CuO nanocomposites.

The TEM images of SiO_2@CuO nanocomposites are shown in figure 3.12 (a-c). The images show the clear coating of SiO_2 over CuO NPs, the thickness of SiO_2 shell was found to be 2-5 nm. Confirmation of presence of SiO_2 in the samples has also been done by energy dispersive x-ray spectroscopy (EDS) as shown in figure 3.12 (d), EDS spectra shows 2-4 wt% of Si in SiO2@CuO nanocomposites.

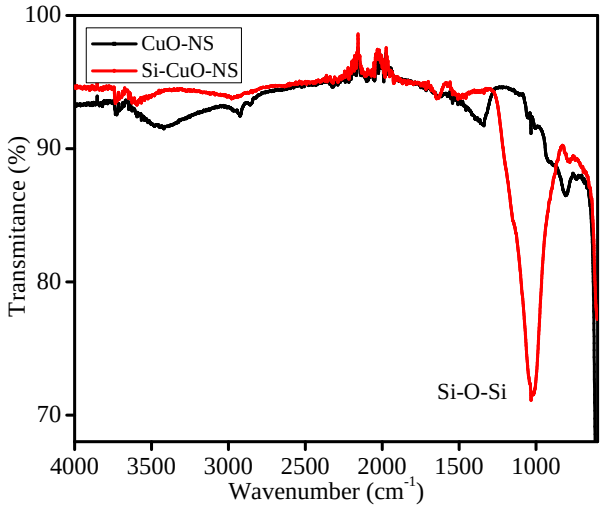

Figure 3.11: FT-IR absorption spectra of bare and SiO2@CuO nanocomposites.

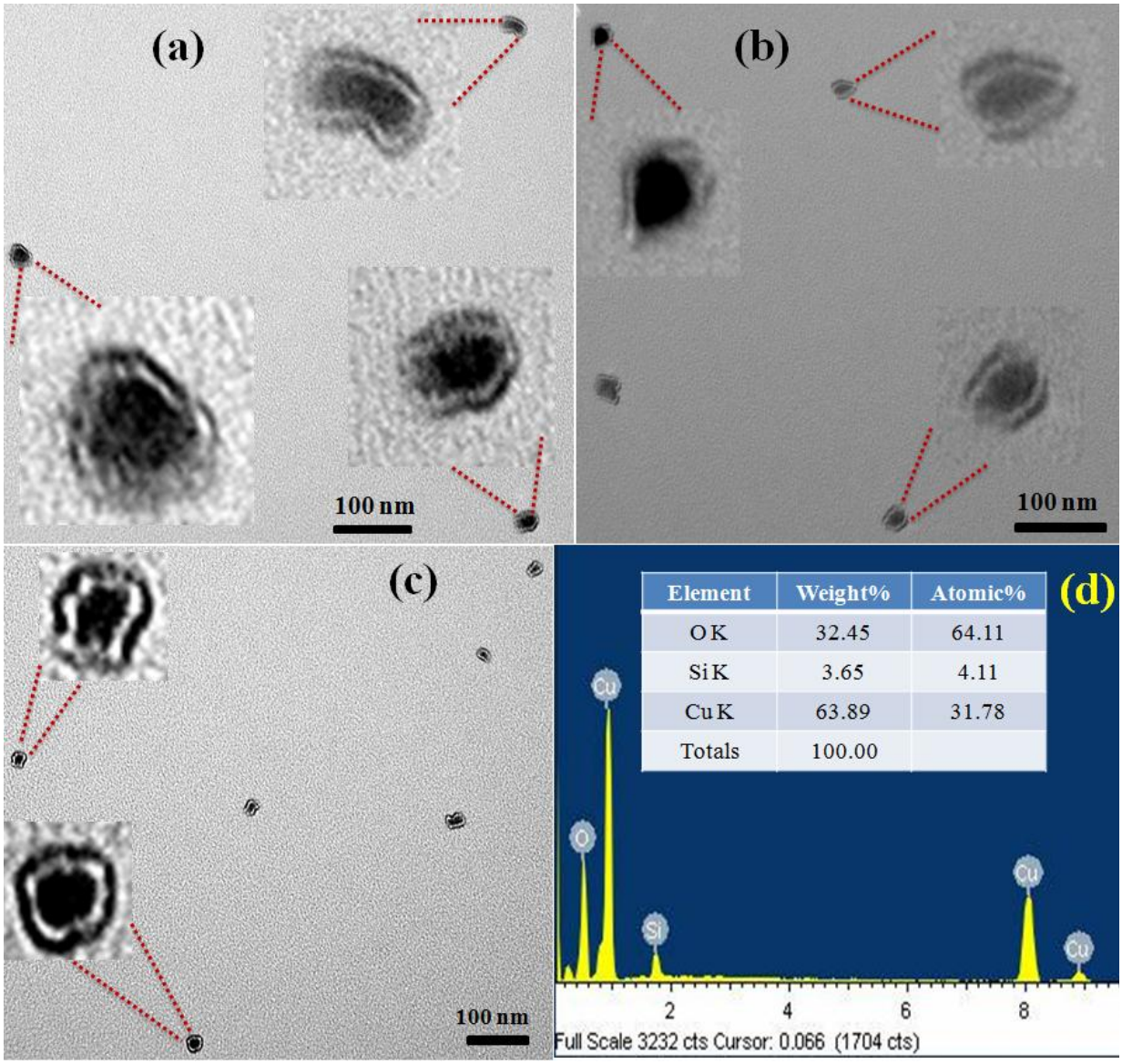

Figure 3.12: TEM images of SiO_2@CuO nanospheres.

3.6.2 Effect of silica coating on thermal conductivity:

The optimization of SiO_2 layer thickness over CuO nanoparticles for maximum enhancement in thermal conductivity has also been studied as presented in figure 3.13. This figure also shows the comparative enhancement in thermal conductivity after dispersion of bulk particles, bare and SiO_2@CuO nanoparticles. It was found that SiO_2@CuO NPs dispersion showed higher thermal conductivity than bulk particle and bare CuO NPs dispersion. Due to this enhancement in thermal conductivity, optimization of SiO_2 shell thickness over CuO nanoparticles is very important. This experiment has been done by varying the amount of SiO_2 precursor in the reaction samples. It was observed that a certain shell thickness showed maximum enhancement in thermal conductivity and after that it decreases the thermal conductivity as clearly presents in figure 3.13, this is due to more concentration of SiO_2 which hamper the thermal conductivity of CuO core particles.

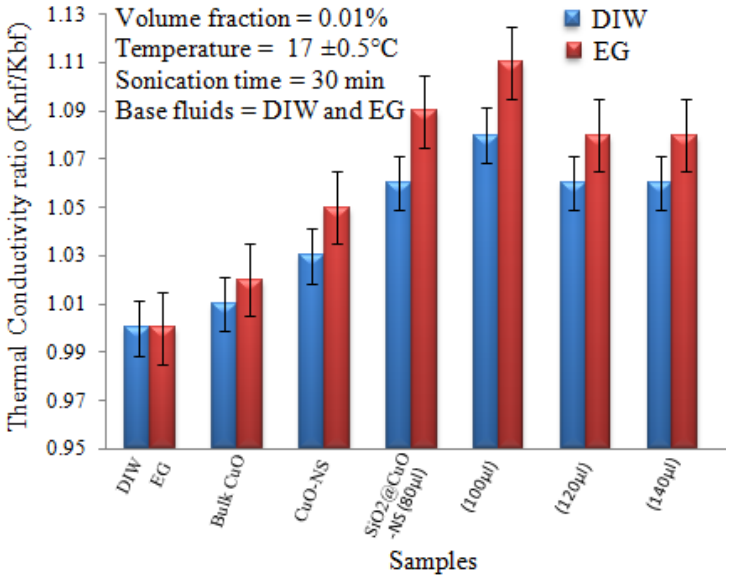

Figure 3.13: Optimization of silica coating around CuO nanospheres for maximum enhancement in thermal conductivity and dispersion stability in DI water and EG.

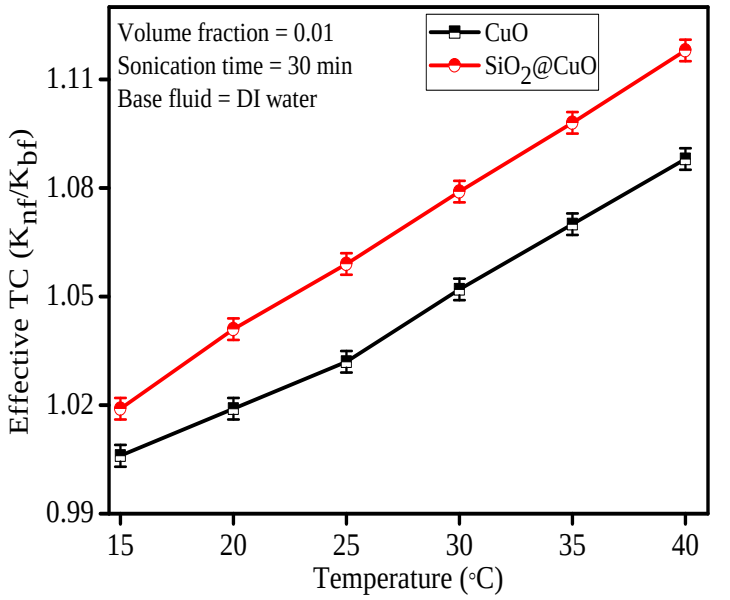

Figure 3.14: Effect of temperature on thermal conductivity of bare and SiO_2 coated CuO aqueous suspension.

3.6.3 Effect of temperature on thermal conductivity: The thermal conductivity increases with increase in temperature as shown in figure 3.14. With the increase in temperature the kinetic energy and Brownian motion of the particles increase which directly increase the thermal conductivity of the suspension. At loading of 0.01 vol% of SiO_2@CuO in de-ionized water, the enhancement in thermal conductivity was increased from ~8-18% at 15-40°C. It was observed that SiO_2 coated CuO suspension showed more enhancements in thermal conductivity than bare CuO nanoparticles suspension.

3.6.4 Evaluation of dispersion stability of aqueous suspension of SiO_2@CuO nanocomposites by measuring TC, density, zeta potential and their corresponding photographs:

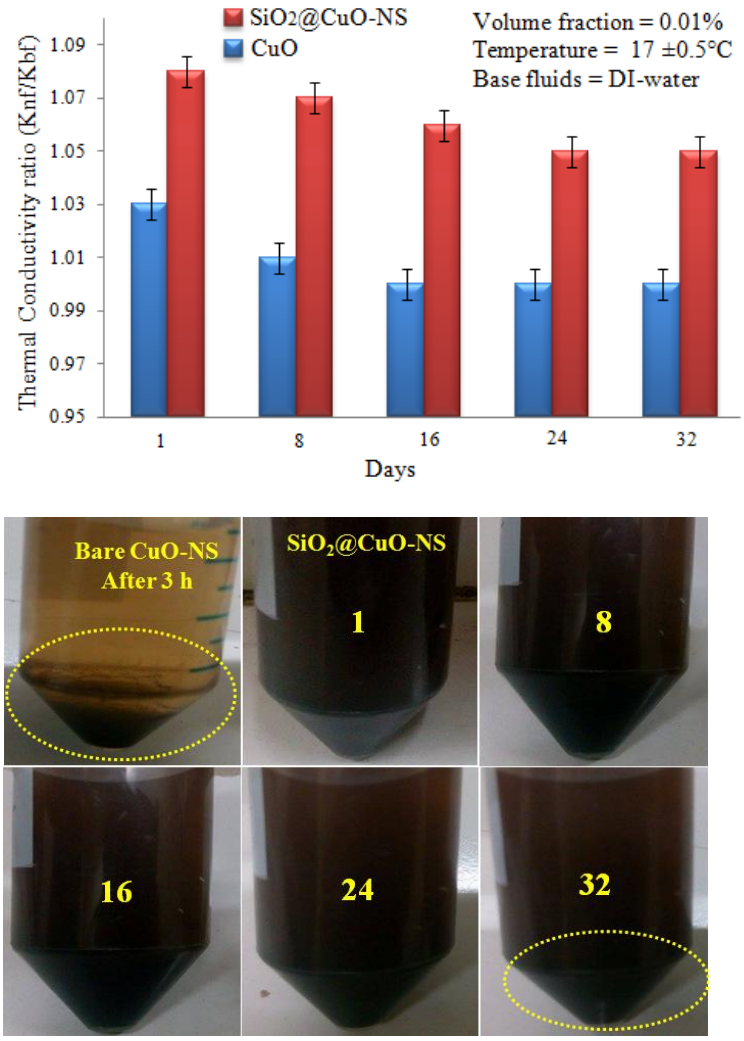

Figure 3.15: Variation in thermal conductivity of SiO_2 coated CuO aqueous suspension with the passage of time (0-30 days after preparation of samples) and Photographs of these SiO_2@CuO aqueous suspensions

In this section evaluation of dispersion stability has been studied. The sample (SiO_2@CuO) which showed maximum enhancement in thermal conductivity was preserved for further study of dispersion stability. After optimization of silica thickness, dispersion stability has been investigated for approximate 1 month by measuring TC, density and zeta potential. Figure 3.15 shows the effect of dispersion stability and thermal conductivity with passage of time. It was found that bare CuO NPs based suspension showed sharp decrease in thermal conductivity and reaches the TC of water after 1-2 days as shown in figure 3.15, but in case of SiO_2@CuO based nanocomposite suspension there was only 3-4% decrease in TC enhancement even after 1 month. It was observed that for first 15 days the decrease in TC was ~4% but after that there was only 2-3% decrease in TC. Photographs of all the samples have been also taken by time to time to see any visual settling of NPs in base fluids (figure 3.15). For further confirmation of dispersion stability of the same sample, the density measurement has been done with passage of time (1-30 days) as shown in figure 3.16. The experimental results showed that

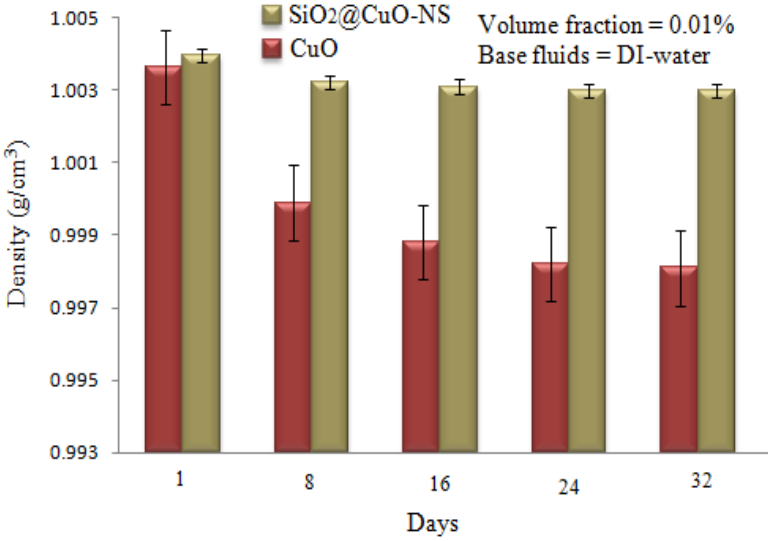

Figure 3.16: Change in density of SiO_2 @CuO aqueous suspension with the passage of time (0-30 days after preparation of samples).

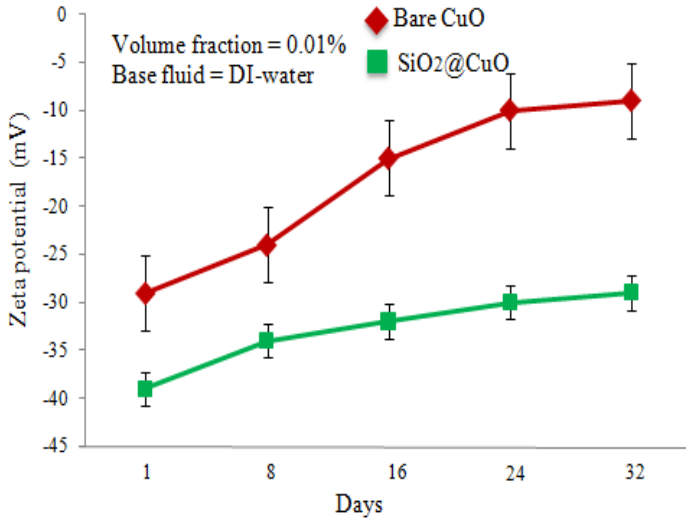

Figure 3.17: Change in zeta potential of bare and SiO_2@CuO nanocomposites dispersed in de-ionized (after 1, 5, 15 and 30 days).

there is not much change in density with time (1-30 days) which clearly indicate the longer dispersion stability of NPs (figure 3.16). Figure 3.17 displayed the change in zeta potential with passage of time (1-30 days). It was found that bare TiO_2 suspension showed much change in zeta potential values -29 to -9 which indicate the aggregation of CuO NPs in base fluids, but SiO_2@CuO suspension showed small change in zeta potential value -40 to -32 which indicate the stability of suspension for longer time.

3.6.5 Effect of LASER irradiation on thermal conductivity:

Figure 3.18 showed the effect of LASER irradiation on thermal conductivity of CuO NPs based aqueous suspension. It was found that thermal conductivity does not show any change after 2-8 h LASER irradiation, this might due to coagulation of particles by laser heat or insufficient energy to breakdown the particles into smaller size.

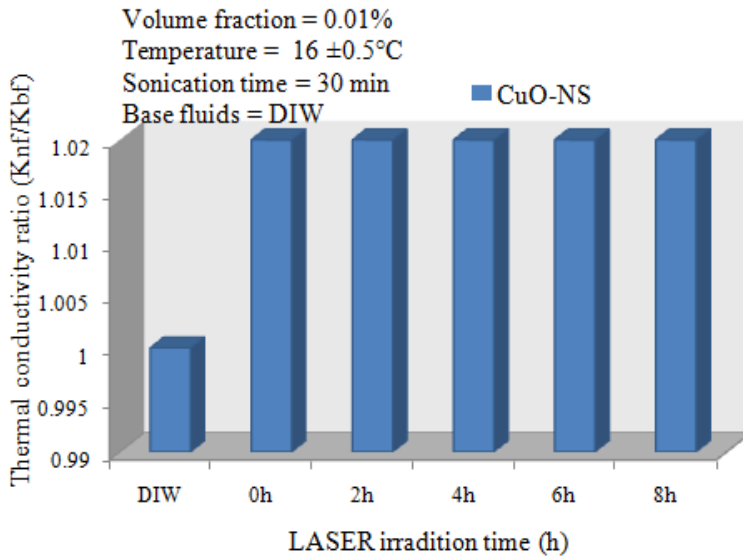

Figure 3.18: Effect of LASER irradiation on thermal conductivity of aqueous suspension of CuO nanoparticles.

3.7 Conclusions

In this study, the beneficial effect of a thin layer of SiO_2 coating over CuO nanostructures for superior dispersion stability and thermal conductivity are investigated with the supportive evidences of particle size distribution, zeta potential, density and refractive index analysis as indicator parameter for stable suspension. As a result, SiO_2 coated composite particles always exhibited higher TC than bare NPs dispersion which generally undergoes quick agglomeration and precipitation. Further optimization of SiO_2 shell thickness is important for exhibiting long term dispersion stability and maximum enhancement in thermal conductivity. It was also found that lengthy nanorods based suspension exhibit more enhancements in TC than spherical NPs. Thermal conductivity enhancement can be further increased by increasing the volume fraction of SiO_2@CuO nanocomposites.

References:

[1] Z. Fei, P. Lu, X. Feng, B. Sun and W. Ji, *Catal. Sci. Technol.* 2012, **2**, 1705-1710.

[2] P.K. Khanna, S. Gaikwad, P.V. Adhyapak, N. Singh and R. Marimuthu, *Mater. Lett.* 2007, **61,** 4711-4714.

[3] Z. Yang, J. Xu, W. Zhang, A. Liu, S. Tang, Z. Yang, J. Xu, W. Zhang, A. Liu and S.J. Tang, *Solid State Chem*. 2007, **180,** 1390-1396.

[4] H.T. Zhu, C.Y. Zhang, Y.M. Tang and J.X. Wang, *J. Phys. Chem. C.* 2007, **111,** 1646–1650.

[5] G. Qiu, S. Dharmarathna, Y. Zhang, N. Opembe, H. Huang and S.L. Suib, *J. Phys. Chem. C*. 2012, **116,** 468-477.

[6] M.L. Kantam, T. Ramani, L. Chakrapani and B.M. Choudary, *Catal. Commun*. 2009, **10,** 370–372.

[7] M.S. Hassan, T. Amna, O.B. Yang, M.H. El-Newehy, S.S. Al-Deyab and M.S. Khil, *Colloids Surf. B,* 2012, **97,** 201-206.

[8] J. Liu, J. Jin, Z. Deng, S.Z. Huang, Z.Y. Hu, L. Wang, C. Wang, L.H. Chen, Y. Li, G.V. Tendeloo and B.L.J. Su, *J. Colloid Interface Sci*. 2012, **384,** 1-9.

[9] S. Lee, S.U.S. Choi, S. Li and J.A. Eastman, *J. Heat Transfer*.1999, **121,** 280-289.

[10] J.A. Eastman, S.U.S. Choi, S. Li, G. Soyez, L.J. Thompson and R.J. DiMelfi, *Mater. Sci. Forum*, 1999, **312,** 629-34.

[11] P.D. Shima, J. Philip and B. Raj, *Appl. Phys. Lett*. 2010, **97,** 153113-3.

[12] A.S. Teja, M.P. Beck, Y.Yuan and P. Warrier, *J. Appl. Phys.* 2010, **107,** 114319-4.

[13] H. Hong, X. Luan, M. Horton, C. Li and G.P. Peterson, *Thermochim. Acta*. 2011, **525,** 87-92.

[14] H. Xie, J. Wang, T. Xi, Y. Liu, F. Ai and Q. Wu, *J. Appl. Phys.* 2002, **91,** 4568–4572.

[15] M.S. Liu, M.C.C. Lin, I.T. Huang and C.C. Wang, *Chem. Eng. Technol.* 2006, **29,** 72-77.

[16] L.P. Zhou, B.X. Wang, X.F. Peng, X.Z. Du and Y.P. Yang, *Adv. Mech. Eng.* 2010, **2010,** 172085-4.

[17] J. Wensel, B. Wright, D. Thomas, W. Douglas, B. Mannhalter, W. Cross, H. Hong, J. Kellar, P. Smith and W. Roy, *Appl. Phys. Lett.* 2008, **92,** 023110-3.

[18] A.D. Sommers and K.L. Yerkes, *J. Nanopart. Res.* 2010, **12,** 1003-1014.

[19] Z. Saida, M. Sajid, H.A. Kamyara and R. Saidura, *Earth and Environmental Science*. 2013, **16,** 012002-1-4.

[20] B.C. Pak and Y.I. Cho, *Exp. Heat Transfer.* 1998, **11**, 151-170.

[21] S.M.S. Murshed, K.C. Leong and C. Yang, *Int. J. Therm. Sci*. 2005, **44,** 267-373.

[22] W. Wei and W. Chen, *Int. J. Smart Nano Mater*. 2013, **4**, 62-71.

[23] J.S. Shen, Y.L. Chen, Q.P. Wang, T. Yu, X.Y. Huang, Y. Yanga and H.W. Zhang, *J. Mater. Chem. C*. 2013, **1**, 2092-2096.

[24] P.D. Shima, J. Philip and B. Raj, *J. Phys. Chem. C*. 2010, **114,** 18825-18833.

[25] D.P. Singh, A.K. Ojha and O.N. Srivastava, *J. Phys. Chem. C*. 2009, **113,** 3409-3418.

[26] I.S. Grover, S. Singh and B. Pal, *Appl. Surf. Sci.* 2013, **280**, 366–372.

[27] S.G. Ovchinnikov, B.A. Gizhevskii, Y.P. Sukhorukov, A.E. Ermakov, M.A. Uimin, E.A. Kozlov, Y. Kotov and A.A.V. Bagazeev, *Phys. Solid State* 2007, **49,** 1116-1120.

[28] X. Wang, X. Xu and S.U.S. Choi, *J. Thermophys Heat* Transfer 1999, **13,** 474-480.

[29] J.C. Maxwell, *Clarendon: Oxford, U.K.*, 1881; Vol. 1.

[30] R.L. Hamilton and O.K. Crosser, *Ind. Eng. Chem. Fundam.* 1962, **1,** 187-191.

[31] R. Prasher, P. Bhattacharya and P.E. Phelan, *Phys. Rev. Lett*. 2005, **94,** 025901-1-025901-4.

Section A:

WO_3 nanostructures of different size and shape for improved dispersion stability and thermal conductivity in aqueous suspension

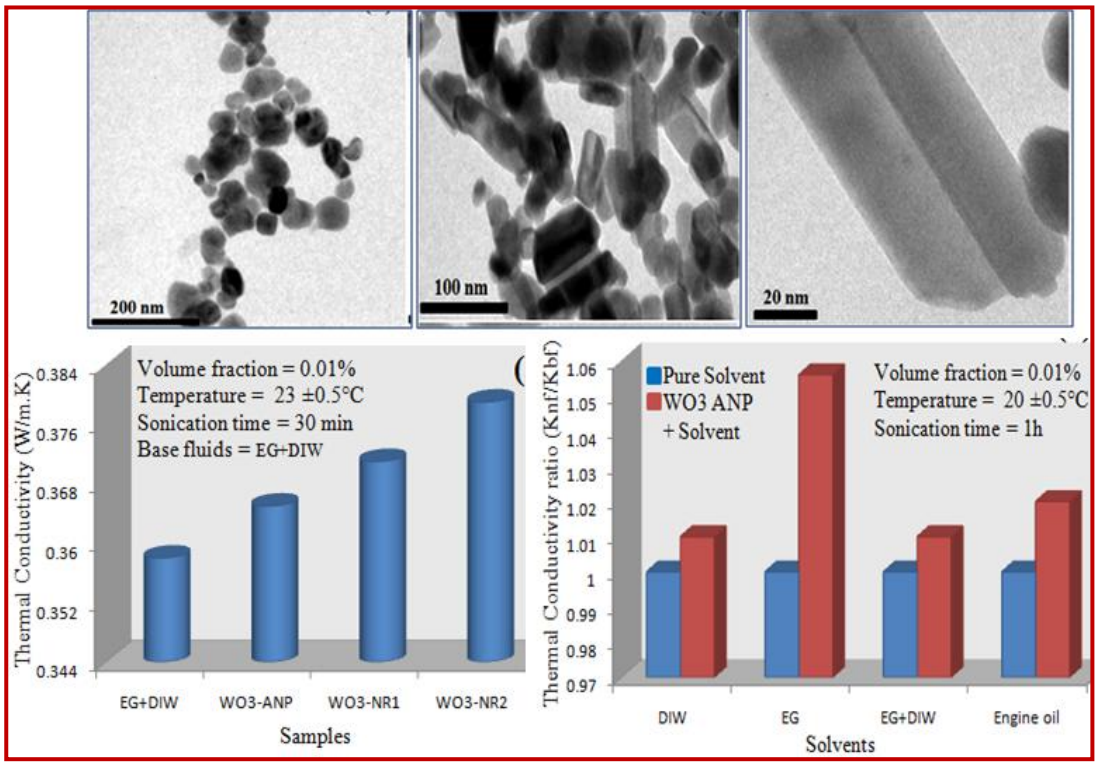

Abstract: This work presents the preparation of different anisotropic (cubic, spherical and rod shaped) nanoparticles of WO_3 (monoclinic and hexagonal crystal structure) and studied their relative thermal conductivity in de-ionized water and ethylene glycol. Experimental results showed that thermal conductivity increases (7-12%) with the increase in volume fraction (0.01-1%) and density. WO_3 nanorods having surface area 61 m^2g^{-1} showed higher (10-12%) increment in thermal conductivity than WO_3 anisotropic nanoparticles (6-8%) possessing lower surface area 41 m^2g^{-1} which attributes to the differences in their surface exposed atoms, long phonon mean free path and lengthy shape factor etc. The results also showed that choice of stabilizer for better thermal conductivity and dispersion stability depend upon the nature of stabilizers and nanoparticle's interaction with stabilizer. Sodium dodecyl sulfate was found to be best stabilizer for WO_3-de-ionized suspension as compared to other stabilizers (CTAB, Triton-x-100, PVP, PVA and Oleic acid). The dispersion behavior of WO_3-de-ionized water suspension was also investigated under different pH values (2-12). The point of zero charge (1.5-2) of WO_3-de-ionized water suspension was identified in terms of colloidal stability.

4.1 Introduction

Metal oxides nanoparticles (NPs) such as ZnO, ZrO_2, MgO, Al_2O_3, SiO_2, TiO_2, CuO, WO_3, CeO_2 etc play a key role in physics, chemistry and materials science for their bendable technological applications in the fabrication of piezoelectric devices, microelectronic circuits, sensors, fuel cells, coatings, energy conversion, catalysis and adsorption [1-5]. These metal oxide NPs exhibit special chemical and physical properties due to their tiny sizes and a high density of edge or corner surface sites [6,7]. The metal oxide NPs of different shapes have drawn special attention because of their exceptional structural flexibility combined with a variety of properties and potential applications [8,9]. The size and shape dependent optical and catalytic properties have studied to a large extent, however, thermophysical properties such as specific heat, thermal conductivity etc are rarely studied as a function of their morphology and surface functionality. In this context, various metal oxides also have attracted much interest for heat transfer application using nanofluids possessing dispersed metal oxide NPs in a suitable base liquid (water, ethylene glycol and engine oil) because of their higher stability, easily availability, non-toxicity, high thermal conductivity and heat capacity etc [10,11]. In many research articles, enhanced thermal conductivity (TC) of metal oxide NPs (Al_2O_3, CuO, SiO_2 and TiO_2 etc) based nanofluids has

been reported [12-14]. For example, suspension of cylindrical and spherical TiO_2 NPs showed 30-33% enhancement in TC as reported by [15] Murshed et al. An enhancement in TC for cylindrical shaped metal oxide (TiO_2 and CuO) NPs suspended in DIW (0.1%) at 25°C was found to be 15-17% by [16,17] Pal et al. WO_3 suspension showed 13.8% enhancement in TC reported by [18] Yoo et al. for a particle loading of 0.3%. The aqueous suspension of CuO (1-5%) and Al_2O_3 showed 28-31% enhancement in TC as reported by different research groups [19,20].

It is well recognized that TC is not only closely related to naoparticle's size but also to [21] their morphologies. As heat transfer takes place typically on the surface of a material [22], therefore the heat conduction can be improved with the alteration of NPs morphology. With the change in morphology of NPs, the number of surface exposed atom, edges or corners of surface atoms can be changed and thereby the properties of material alter accordingly. Literature reveals that although most of the studies are carried out using spherical metal oxides (CuO, Al_2O_3, ZnO, WO_3 and TiO_2 etc) NPs, but not much information about the TC of anisotropic lengthy WO_3 nanostructure is available. Therefore, various size and shape of WO_3 NPs were prepared to investigate the comparative TC depending on the variation in surface area, morphology and dispersion stability in DIW, EG and engine oil. The study particle size distribution and surface charge through measurement of the ζ potential and DLS becomes important parameter for understanding the dispersion behavior of NPs in a liquid medium and the effect of stabilizers and pH have been studied here. The experimental results of TC for spherical and non-spherical NPs have compared with theoretical models such as Maxwell and Hamilton-Crosser etc.

4.2. Experimental Section

4.2.1 Materials and Methods:

The synthesis of various shapes of WO_3 nanoparticles have been done, detailed description is given in **Chapter 1 section 1.5.1.6**.

4.2.2 Characterizations

As synthesized NPs were characterized by various techniques, the details of the techniques are given in **Chapter 1**, **section 1.5.7**.

4.2.3 Preparation of Nanofluids

Nanofluids were prepared by two-step methods as mentioned in **Chapter 1, section 1.5.2.**

4.2.4 Measurement of thermal conductivity, density and refractive index:

The experimental details are given in **Chapter 1, section 1.5.3, 1.5.4.**

4.3. Results and Discussion

***4.3.1 Structural, optical and morphological characterizations*:** Powder x-ray diffraction pattern of as prepared WO_3 NPs are displayed in figure 4.1 (a-c). The WO_3 nanorods1 (NRs1, figure 4.1c) are of typical wurtzite (hexagonal) structure with lattice constants of $a = b = 0.7298$ nm and $c = 0.3899$ nm. All diffraction peaks of WO_3 NRs1 shown in figure 4.1c well indexed with standard pattern of WO_3 (JCPDS No. 33-1387). The XRD patterns shown in figure 4.1 (a-b) are well indexed with the XRD pattern of monoclinic WO_3 JCPDS file No. 43-1035, strong diffraction peaks also indicate the good crystallinity of the samples. As prepared samples were also characterized by UV-Vis spectrophotometer as shown in figure 4.2. It was observed that WO_3 anisotropic nanoparticles (ANPs) showed band edge emission at 371 nm which further red-shifted for nanorods indicating the large size. The shifting of absorption edge in case of nano-sized WO_3 NPs to higher energies as compare to that of bulk WO_3 signifying a widening of the energy gap caused by quantum size effects [23], the wavelength at

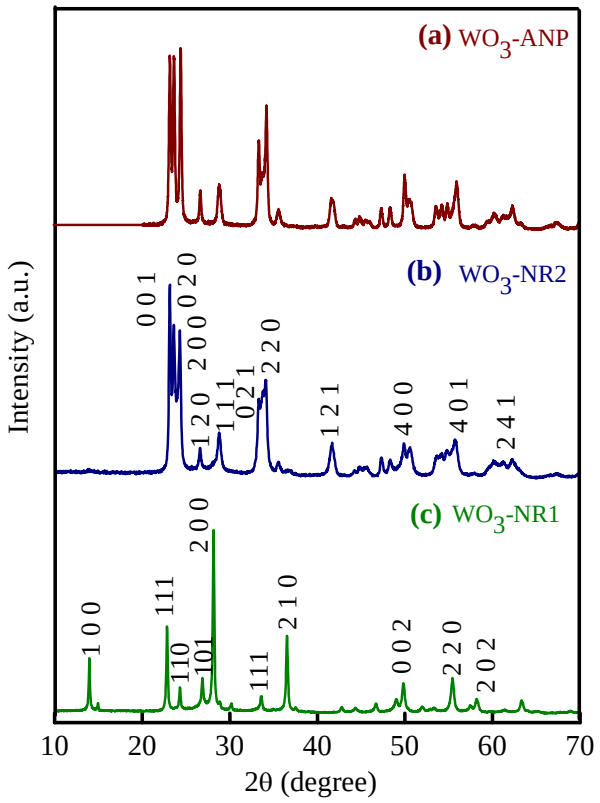

Figure 4.1: Powder X-ray diffraction patterns of as synthesized WO_3 **(a)** anisotropic nanoparticles **(b)** nanorods2 and **(c)** nanorods1.

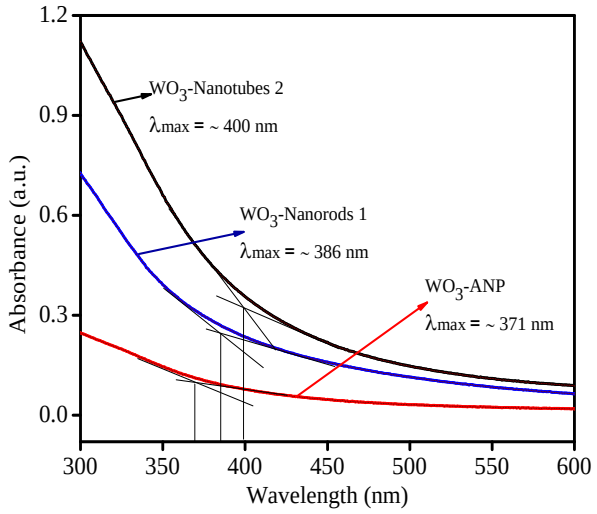

Figure 4.2: UV-visible absorption spectra of WO_3 nanospheres, nanorods1 and nanorods2.

the maximum exciton absorption (λ_{max}) decreases with the decrease in size of NPs. The TEM images in figure 4.3 (a-f) showed that some separate and aggregated WO_3 NPs having cubical, hexagonal or rectangular asymmetric shapes in the size range of 40-70 nm. Few aggregated and overlapped rod like (NRs) morphologies with average length 120-160 nm, width 20-25 nm. WO_3 nanorods having surface area 61 m^2g^{-1} displayed higher TC (10-12%) than WO_3 anisotropic nanoparticles (6-8%) possessing lower surface area 41 m^2g^{-1} due to the differences in their shape, surface exposed atoms and long phonon mean free path etc.

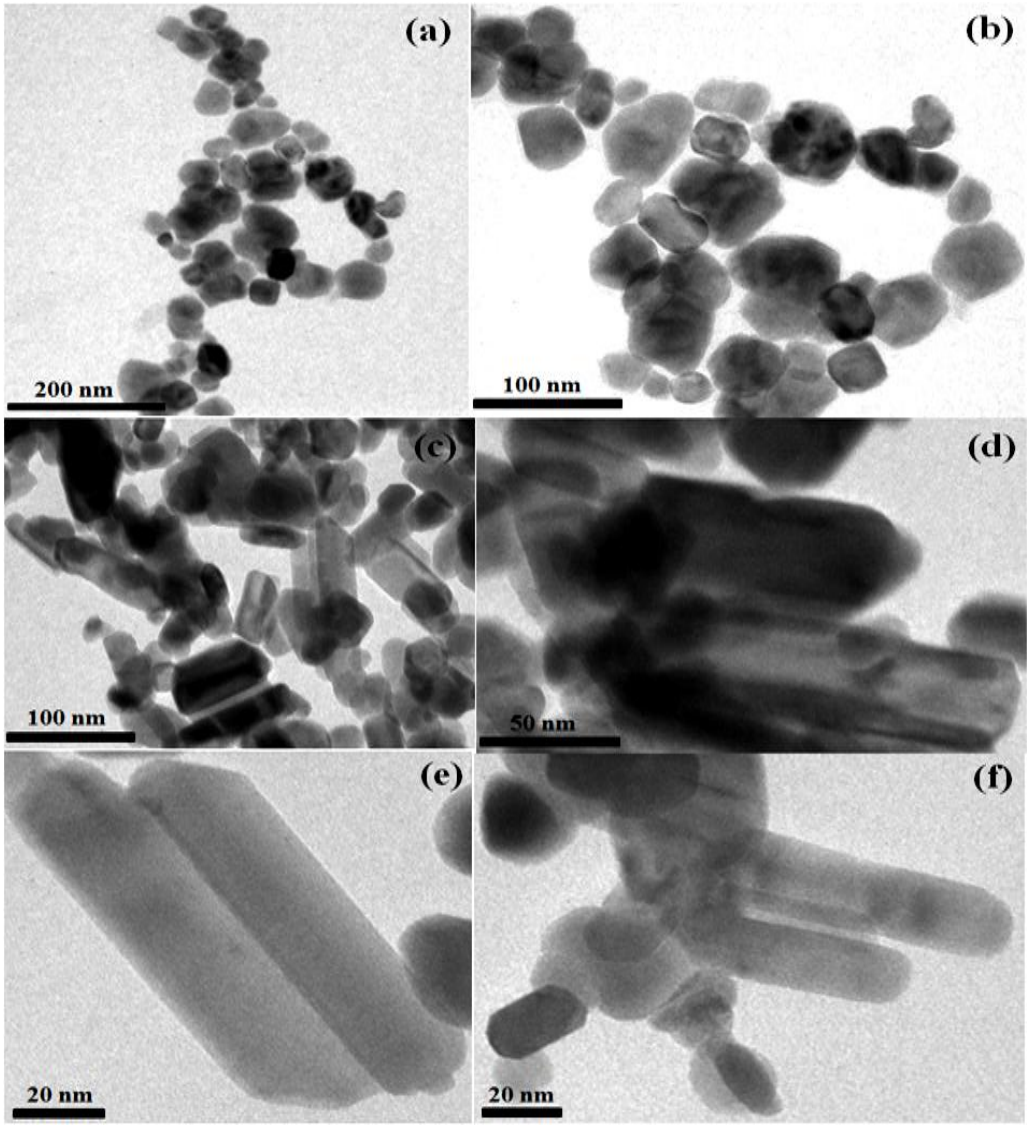

Figure 4.3: TEM images of WO_3 **(a-b)** anisotropic nanoparticles **(c-d)** Nanorods2 and **(e-f)** Nanorods1.

***4.3.2 Effect of volume fractions, shapes and solvents on thermal conductivity*:**

The TC of WO_3-DIW and EG suspension in figure 4.4 (a-b) revealed that TC increases with the increase in volume fraction (0.01 to 1%) after 30 min sonication at 23 °C. The enhancement in TC increases up to certain volume fraction (0.5%), but after that it slightly decreases (~2%). It was observed that WO_3 nanorods (NRs) dispersed both in DIW and EG showed higher

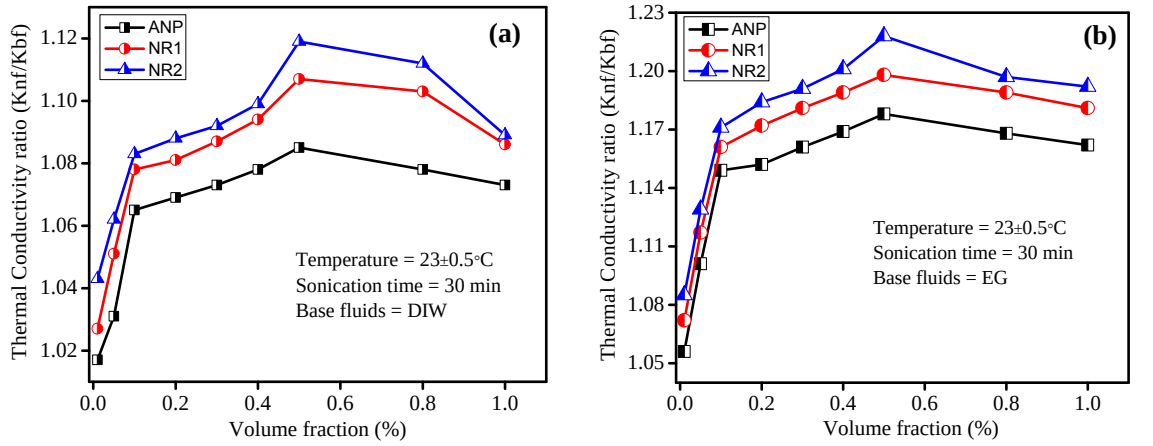

Figure 4.4: Variation in thermal conductivity as a function of volume fraction and shape of WO_3 nanoparticles dispersed in (a) de-ionized water and (b) ethylene glycol.

enhancement (10-12%) in TC than anisotropic NPs (ANPs) (7-8%) dispersion. The TC of DIW and EG mixture (1:1) was found to be 0.360 ±5 W/m.K at 23 ± 0.5 °C, which was significantly enhanced after addition of WO_3 NPs in it as displayed in figure 4.5 (a). It was observed that WO_3 NRs suspension again showed higher TC than WO_3 ANPs suspension. The enhancement in TC

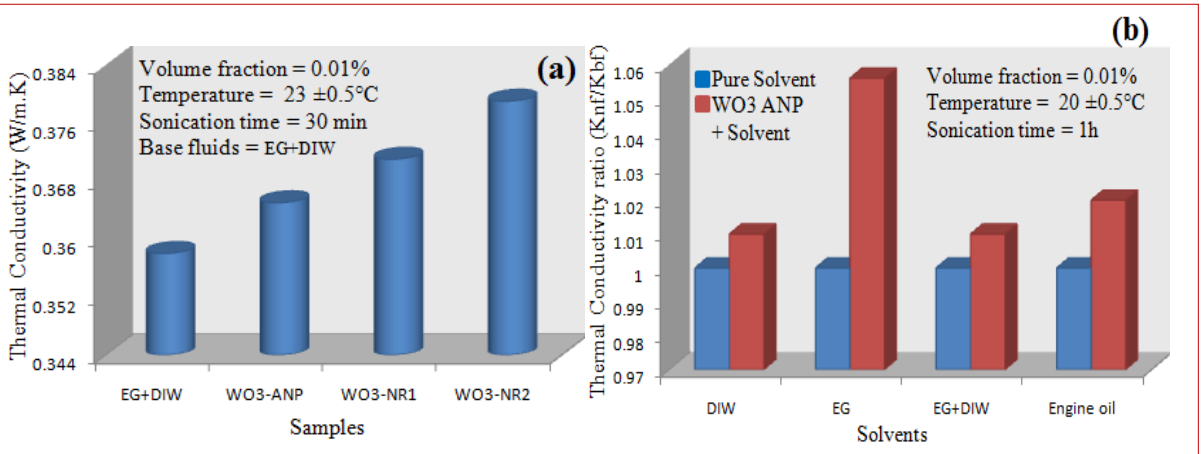

Figure 4.5 (a): Variation in thermal conductivity of WO_3 (anisotropic, nanorods1 and nanorods2) nanoparticles when dispersed in DIW+EG (50:50). **(b)** Comparative effect of solvents on enhancement in thermal conductivity.

of various solvents was also compared with each other by dispersing same volume fraction of NPs (0.01%) in it as shown in figure 4.5 (b). It was noticed that EG based dispersion showed more enhancement in TC ratio (3-4%) than other solvents (DIW, EG:DIW and Engine oil) based dispersion.

Thus, it is verified that WO_3 NRs based dispersion showed constantly higher TC than ANPs based dispersion because of the higher geometric surface area per particle, compactness in structure, less interparticles distance and large phonon mean free path in nanorods structure. Yang et al. [24] also reported that Brownian motion could be predominant for spherical NPs in suspension while the diffusive heat conduction mechanism will progressively take over the dominance as the aspect ratio increases and showed higher TC. As heat-transfer mostly takes place at surfaces, then it is obvious to use particles with larger surface area where a large percentage of atoms reside on their surface and making them available for the heat conduction. The main plausible explanation for above behavior is that the distance between NPs decreases as the particle concentration increases. Much of the enhancement in the TC can be ascribed to increased particle-to-particle interactions at higher concentrations but when concentration is too high particles easily agglomerate and increase the cluster sizes which easily settle down and drop the enhancement of TC. Therefore, optimization of particles concentration is important for maximum enhancement in TC. The higher TC enhancement in EG dispersion is due to its more viscosity which improves the dispersion rate and decrease the settling rate of NPs, but in case of DIW the NPs are not much suspended for longer time and they settle down easily.

4.3.3 Effect of density on thermal conductivity and volume fraction on refractive index

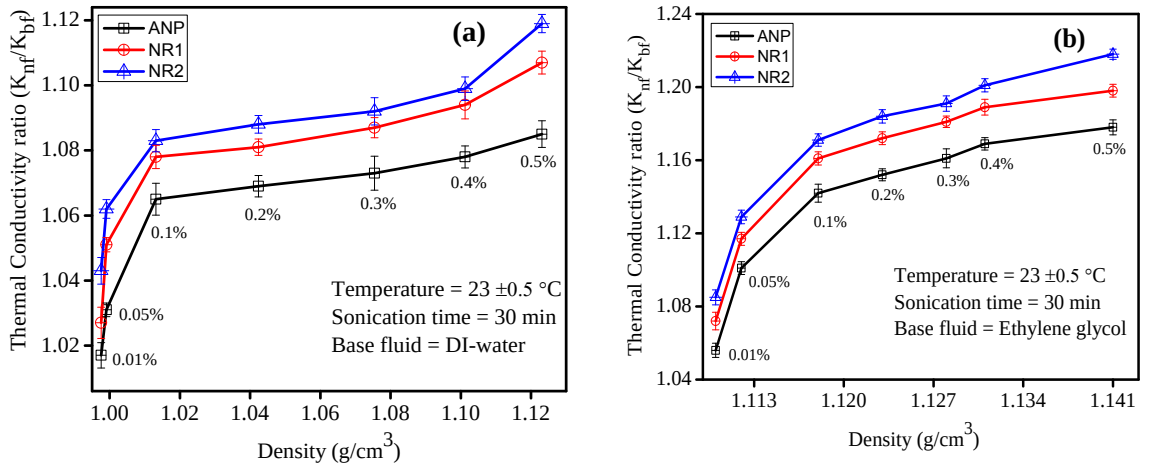

Figure 4.6: Variation in thermal conductivity as a function of density and volume fraction of WO_3 nanoparticles dispersed in **(a)** De-ionized water **(b)** Ethylene glycol.

Variation in TC as a function of density is displayed in figure 4.6 (a-b) at 23 ±5% °C. In DIW and EG dispersion of WO_3 NPs, the density increases with increase in concentration of NPs and TC also increases as shown in figure 4.6 (a-b). The refractive index of suspension also increases with increase in volume fraction (0.01-1%) in both DIW and EG suspension as shown in figure 4.7.

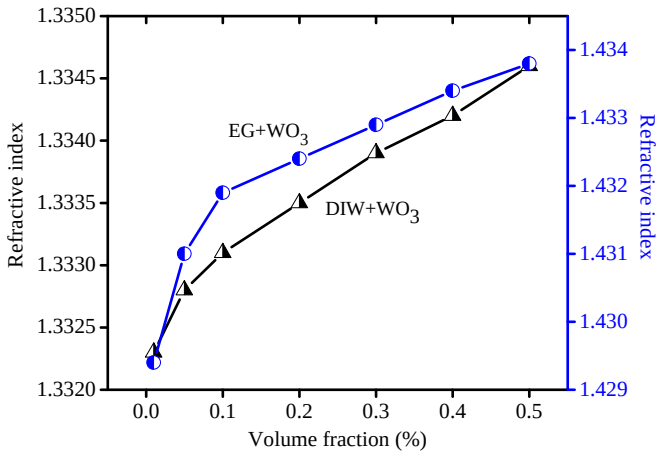

Figure 4.7: Change in refractive index of WO_3 nanoparticles when dispersed in **(a)** De-ionized water and **(b)** Ethylene glycol.

4.3.4 Effect of stabilizers on thermal conductivity

Nanoparticles have high surface energy so it is easy for NPs to aggregate and settle down easily in base fluid and finally lowering the TC of NFs [25,26]. Therefore, controlling the aggregation of

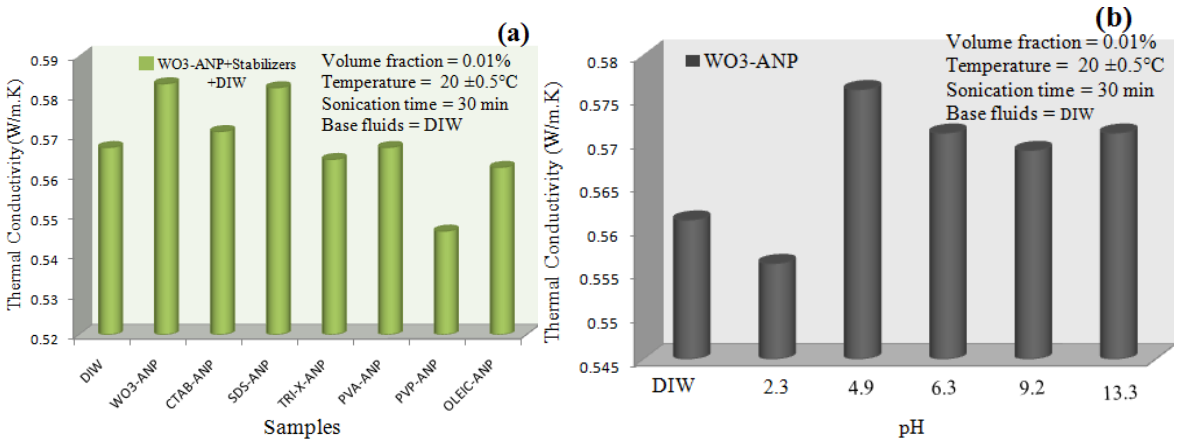

Figure 4.8: **(a)** Effect of stabilizers and **(b)** pH on thermal conductivity of WO_3-aqueous suspension.

NPs in the base fluid has become the most important issue for preliminary research of NFs. In many research articles, ultrasonication and surfactants [27,28] have been used to decrease the aggregation of NPs in base fluids, but optimization of surfactants for maximum TC and stability is not clear. In this context, cationic, anionic and neutral surfactants have been used for

maximum enhancement in TC and stability of NPs in base fluids. Figure 4.8 (a) presents the effect of stabilizers on the TC of WO_3-DIW based suspension. It was observed that SDS showed higher dispersion stability and TC as compare to other stabilizers (like CTAB, TritonX-100, PVP, PVA and oleic acid) due to its anionic surfactant which can partly ionize in water and provide anionic species, while WO_3 NPs carry positive charges in an aqueous medium and having a strong attraction for anionic groups. The negatively charged group alienated from SDS is adsorbed on the positively charged NPs surface and as a result the surface is negatively charged because of the ionization of SDS, therefore the effect of electrostatic stabilization is achieved. This leads to the reduced agglomeration and improved mobility, eventually resulting in the best dispersion system and increase the TC.

4.3.5 Electrokinetic studies

The pH values have significant role in dispersion stability of NPs which is correlated to an electrostatic charge on the particles surface and can be investigated as zeta potential. In this study, 0.01% WO_3-DIW suspension was prepared and the pH value (2-12) of samples was adjusted with HCl and NaOH as shown in figure 4.8 (b) and figure 4.9 (b). The obtained isoelectric point (IEP) of the WO_3-DIW suspension is at pH value of 1.5-2 (figure 4.9b) as measured by zeta potential, at this point TC of the suspension also decreases as shown in figure 4.8 (b). At the IEP, the precipitation and agglomeration of WO_3 NPs were observed. It was also observed that below pH 4, the zeta potential values (figure 4.9b) of the particle surface are at the minimum; therefore the force of electrostatic repulsion between particles is not enough to

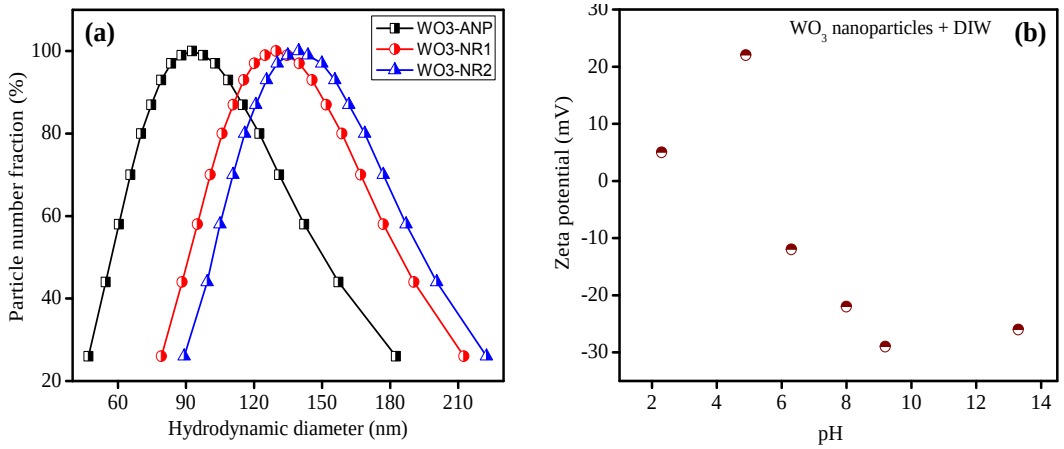

Figure 4.9 (a): Particle size distribution of WO_3 nanoparticles when dispersed in de-ionized water **(b)** zeta potential versus pH plot for WO_3 nanoparticles aqueous suspension.

overcome the attraction force between particles. As displayed in figure 4.8 (b) and 4.9 (b) with the change in pH from isoelectric point, the absolute value of the zeta potential of the particle surface increases and also improve the TC of the suspension. This is due to adequate prevention of attraction and collision between particles caused by Brownian motion. Figure 4.9 (a) showed the particle size distribution (hydrodynamic diameter) of NPs in base fluids, ANP showed smaller hydrodynamic diameter as compare to nanorods due to difference in their morphology.

4.3.6 Theoretical studies

The Maxwell model [29] is applicable to uniform and low volume fraction liquid-solid suspensions with randomly dispersed and uniformly sized spherical particles.

$$\frac{k_{eff}}{k_f} = \frac{k_p + 2k_f + 2\phi\left(k_p - k_f\right)}{k_p + 2k_f - \phi\left(k_p - k_f\right)} \qquad (1)$$

Where k_p and k_f are the conductivities of the particle and the base fluid and ϕ is concentration of NPs**.**

Hamilton and Crosser [30] tailored Maxwell's model to determine the effective TC of non-spherical particles by applying a shape factor.

$$\frac{k_{eff}}{k_0} = \frac{k_p + (n-1)k_0 + (n-1)\left(k_p - k_0\right)\phi}{k_p + (n-1)k_0 - \left(k_p - k_0\right)\phi} \qquad (2)$$

Where k_p and k_0 are the conductivities of the particle and the base fluid and ϕ is concentration of NPs. According to this model, suspensions of particles with high shape factor should have higher thermal conductivities.

As predicted by Maxwell model (figure 4.10a), the TC increases with increase in volume fraction, but experimental results showed more enhancement in TC than this model. The effect of non-spherical particles on TC was explained by Hamilton-Crosser model as shown in figure 4.10 (b), TC increases with the increase in volume fraction and elongated particle showed higher TC than spherical particle. Again, experimental results showed higher enhancement in TC than theoretical model.

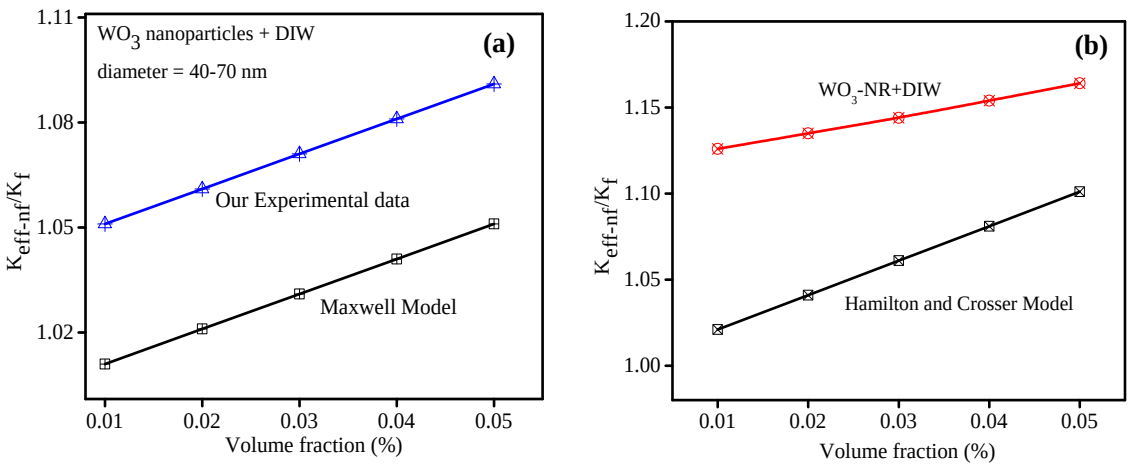

Figure 4.10 (a-b): Thermal conductivity ratio comparison between theoretic model's predictions and our experimental data of WO_3-de-ionized based nanofluids.

4.4. Conclusions

In this study, WO_3 nanoparticles were successfully prepared and dispersed in various solvents to investigate their relative thermal conductivity. It was found that cylindrical shaped nanoparticles showed more enhancements in TC than spherical shaped nanoparticles due higher surface exposed atoms, crystallinity and lengthy shape. TC increases with the increase in volume fraction up to certain level and EG based dispersion showed higher thermal conductivity ratio than other base fluids. Depending upon the stabilizer's nature and their interaction with NPs, the dispersion stability and TC can also be improved for longer time. Dispersion stability of NPs was also improved by varying the pH values. It was found that well dispersed NPs also help in long term stability could be well correlated with zeta potential values for displaying effective thermal conductivity. It was observed that experimental results showed higher thermal conductivity than theoretically predicated model, so there is need for optimized model which predict the TC accurately.

Section B:

A thin layer of SiO_2 coating for highly improved dispersion stability and thermal conductivity of WO_3-H_2O suspension

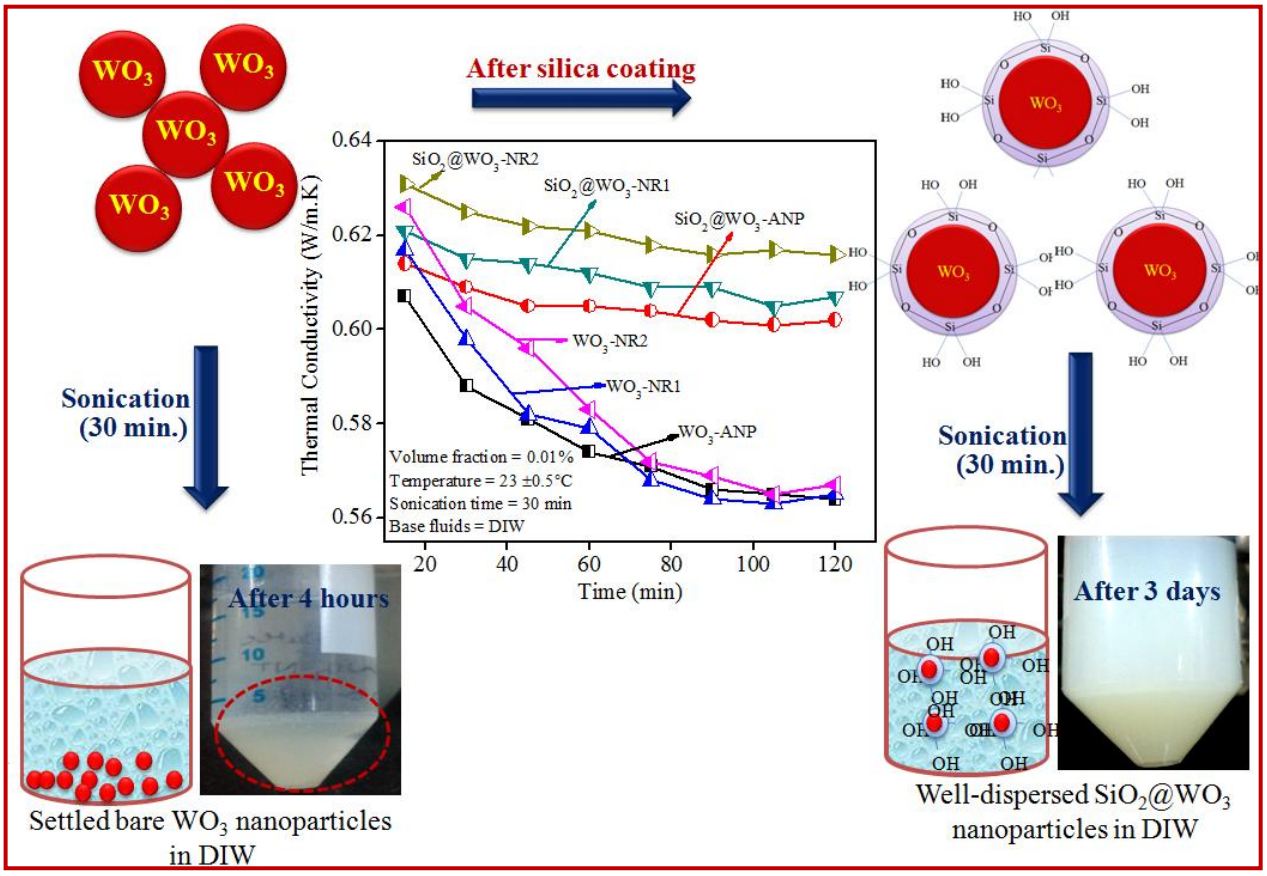

Abstract: Long term dispersion stability for an improved thermal conductivity is a challenging issue that needs to be solved for heat transfer applications**.** Hence, this research investigated that a thin layer of SiO_2 coating (2-5 nm) over WO_3 nanostructures (SiO_2@WO_3) of different shapes exhibited superior dispersion (0.01%) stability for longer duration as evident by steady zeta potential (-30 ↔ -60.70 mV), no significant change in particle-size (139↔147 nm) distribution, density (1.001↔0.988 g/cm^3) and refractive index (1.335↔1.332) etc. Thin Si-OH layer over WO_3 surface imparts superior hydrophilicity, larger surface area for effective solute-solvent (SiO_2@WO_3-H_2O) interaction for improved colloidal stability showing no sedimentation and color change of SiO_2@WO_3 dispersion (0.01%) even after 3 days due to repulsive interaction between negatively charged Si-O$^-$ particles. Thereby, thermal conductivity is found to be quite stable (0.631↔0.618 W/m.K) up to 3 days, whereas aqueous suspension of bare WO_3 particles quickly settle down and thermal conductivity rapidly decreased to a value of 0.584 W/m.K. Depending on the thickness of SiO_2 layer and volume fraction of SiO_2@WO_3, a maximum of 8-10% increment of thermal conductivity was achieved where anisotropic WO_3 displayed always higher enhancement in (~5%) thermal conductivity than typical spherical nanoparticles.

4.5 Introduction

Conventional heat transfer fluids (such as water, ethylene glycol or transformer oil) are usually used in heat transfer processes [31-35] in industrial heating/cooling purpose. These fluids display poor TC relative to solid metals [36,37] resulting in a drawback to use of these fluids for heat dissipation applications. To overcome this limitation, the TC of these fluids can be enhanced by dispersing suitable metal oxide nanoparticles (Al_2O_3, CuO, SiO_2 and TiO_2 etc) in it as reported [38-44] in many review articles. These nanosized particles having higher surface-to-volume ratio and surface active atoms which not only improves the heat transfer efficiency but also increased the dispersion stability. As heat transfer takes place generally through the surface atoms [45], anisotropic nanoparticles (NPs) having more surface exposed atoms in different edges or corners further can alter the material [46,47] properties significantly for improved heat conduction capacity. For example, Murshed *et al.* [48] dispersed spherical and cylindrical TiO_2 NPs (1-5%) in de-ionized water (DIW) and found 30-33% enhancement in TC. Pal *et al.* [16,17] reported 15 to 17% enhancement in TC for cylindrical shape of metal oxide (TiO_2 and CuO) NPs dispersed in DIW (0.1%) at 25°C. For a particle loading of 0.3%, WO_3 suspension showed 13.8%

enhancement in TC reported by Yoo *et al.* [49]. An enhancement of 28-31% in TC were reported [50,51] for aqueous CuO (1-5%) and Al_2O_3 suspension.

It is well-known that NPs aggregate and precipitate with passage of time unless it is effectively passivated with suitable surface active agents, and difficult to re-disperse in water due to their high surface [52] energy. The aggregation of NPs results not only the clogging of microchannels [53] but also decreasing the TC of heat transfer fluids. Therefore, preventing aggregation and sedimentation of NPs in making stable dispersion for improved heat transfer process has become the primary issue in nanofluids (NFs) research. Studies to date have shown that the amount and charge of NPs in base fluids, interaction between the particles and dispersant directly affect the stability of the suspension. For example, Jiang et al. [54] and Li et al. [55] showed that the most important factors affecting the stability of carbon nanotubes and Cu/H_2O suspensions were the NP's concentration, viscosity of base liquid, pH value and dispersant type etc. Saterlie et al. [56] studied the effect of different surfactants (SDBS, PVP, CTAB and oleic acid) on long term dispersion (0.55%) stability and TC of Cu/H_2O suspension. However, it suppressed the TC that deteriorate gradually due to chemical interaction and charge imbalance resulting into coagulation of NPs with passage of time.

Therefore, a chemically inert, transparent, hydrophilic Si-OH surface having larger surface area for better solute-solvent interaction and dispersion stability could be effective to show stable TC. Moreover, high thermal and chemical stability, electrical insulation of SiO_2 particles [57] could be beneficial for heat transfer systems like cooling for high voltage applications. Both *et al.* [58] tried to improve dispersion stability of SiO_2 supported Ag NPs (15-20 nm) in transformer oil up to one hour without using any surfactant. An enhancement in TC of 15% was observed when 0.60 wt% silver was supported on 0.07 wt% SiO_2. Many researchers [59-61] also demonstrated the potential advantages of SiO_2 coating over Au, Ag, Cu, CdSe and CdS quantum size particles for stabilizing them against instantaneous agglomeration for improved physicochemical properties. A thin layer of SiO_2 shell deposition also protects the core material such as CdS NPs [62] from its self-oxidation and photocorrosion under UV light irradiation. Tungsten trioxide (WO_3) being its stability and ease of preparation, moderate heat capacity and thermal properties, it is widely used for chemical/catalytic reactions, mechanical sensors and engineering applications. However, the research about the size and shape dependent thermal properties such as TC of WO_3 is rarely investigated in the literature. As SiO_2 has

comparable TC (1.32 W/m.K) to that of WO_3 (1.63 W/m.K), a layer of SiO_2 coating not only improves hydrophilicity for homogeneous dispersion but also does not hinder or suppress the resultant TC of SiO_2@WO_3 composites. After SiO_2 coating, an electrical double layer at the water/Si-OH interfaces may lead to increase the zeta potential, thereby increased the electrostatic repulsion forces, thus will reduced the precipitation rate of SiO_2@WO_3 NPs. Hence, an effect of a thin layer of SiO_2 coating over WO_3 NPs surface for better dispersion stability and thermal conductivity of SiO_2@WO_3 aqueous dispersion are studied in correlation with the DLS particle size distribution, zeta potential, density and refractive index data analysis.

4.6 Experimental section

4.6.1 Materials and methods

The various shapes of WO_3 NPs have been synthesized; the detail description is given in **Chapter 1**, **section 1.5.1.6.**

4.6.2 Characterizations

As synthesized NPs were characterized by various techniques, the details of the techniques are given in **Chapter 1**, **section 1.5.7.**

4.6.3 Preparation of Nanofluids

Nanofluids were prepared by two-step methods as mentioned in **Chapter 1, section 1.5.2**

4.6.4 Measurement of thermal conductivity, density and refractive index

The experimental details are given in **Chapter 1, section 1.5.3, 1.5.4.**

4.6.5 Measurement of particle size distribution and zeta potential

The experimental procedure is given in **Chapter 1, section 1.5.6.**

4.7 Results and discussion

4.7.1 Morphological characterizations

The TEM images (figure 4.11a-b) displayed some separate and aggregated WO_3 NPs (black) having hexagonal, polygonal and cubical shapes with average diameter in the range of 30-70 nm which are covered with a thin layer (2-5 nm) of SiO_2 shell (grey contrast). At higher resolution (figure 4.11c-d), some images shows few hexagonal SiO_2@WO_3 NCs possessing uniform layer of silica coating. Few overlapped nanorods (NR1 and NR2) like morphologies (average length 120-160 nm, width 10-15 nm) coated with a thin SiO_2 layer of 2-7 nm throughout their surface as

seen in figure 4.11e-f. The presence of SiO_2 coating was further confirmed by EDS elemental analysis (figure 4.12a-c) showing 0.61-1.04 weight% Si, 77-78 weight% W and 21.14-21.42 weight% O in all three SiO_2@WO_3 NCs. The HR-TEM image of SiO_2@WO_3 NCs in figure 4.12 (d) clearly represents the characteristic lattice fringes (0.287 nm corresponds to 1 0 0 planes) of thin SiO_2 layer and WO_3 core material (0.378 nm corresponds to 0 0 1 planes). The formation of a core (WO_3 nanorod)-shell (SiO_2) like lengthy nanorods having distinct lattice fringes of WO_3 indicating the good crystallinity of the as-prepared WO_3 NR1 shown in figure 4.12 (e). The lattice spacing of 0.345 nm represents the *d*-spacing of (2 0 0) planes of WO_3 NPs growth along the crystallographic *c*-axis [63]. The WO_3 NPs have typical wurtzite (hexagonal) and monoclinic crystal structure.

4.7.2 FTIR and Particle size distribution analysis

The FT-IR spectra (figure 4.13a) of SiO_2@WO_3 NPs showing the vibrational stretching peak at ~1080 cm^{-1} for Si-O-Si formation relative to no such band in bare WO_3 NPs. The DLS particles size distribution analysis (figure 4.13b) revealed the hydrodynamic diameter (94 nm) of bare WO_3 NPs increased (102 nm) after coating a thin layer of SiO_2 shell. Both these analysis indicate the presence of SiO_2 in the as prepared samples.

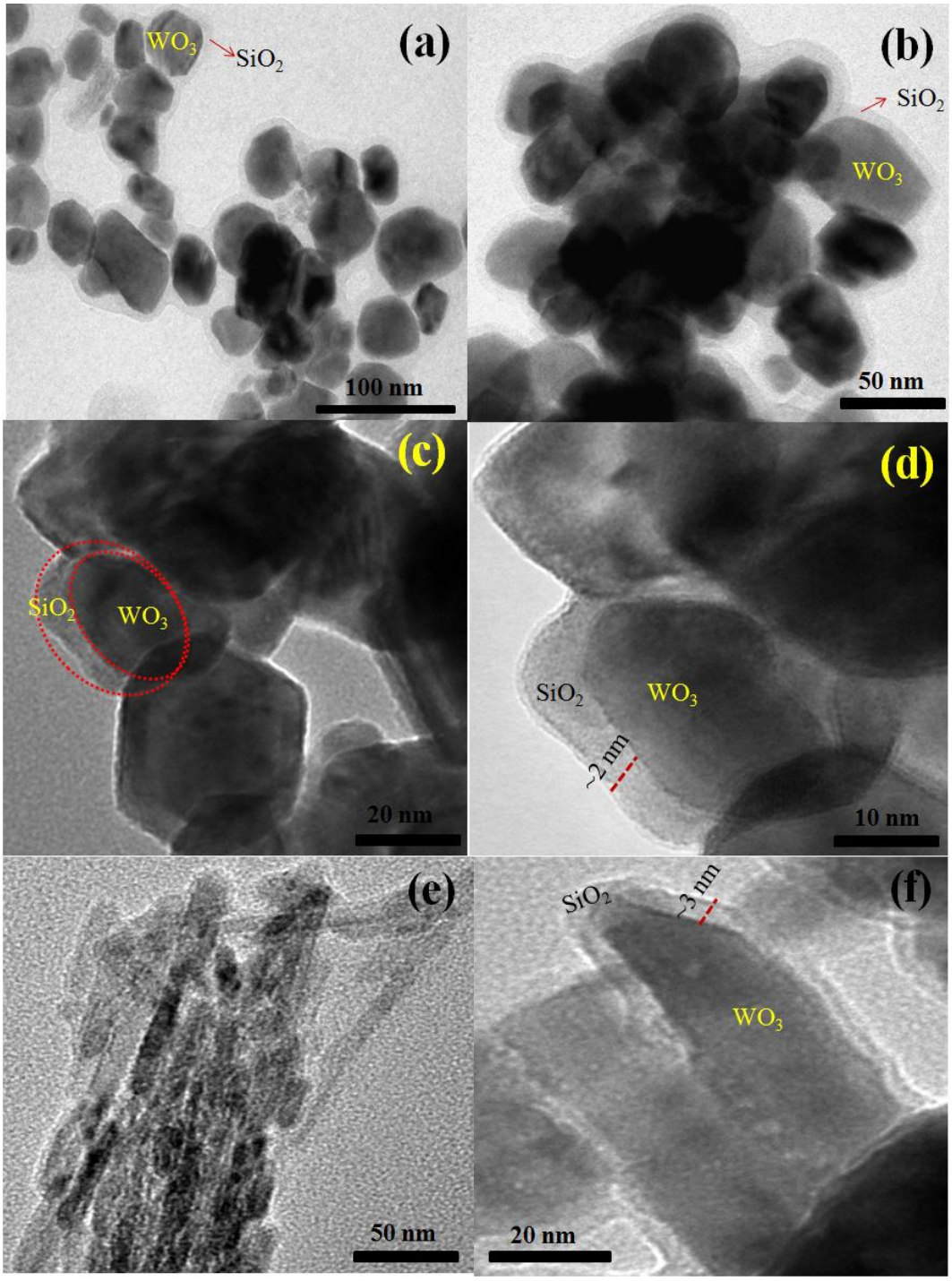

Figure 4.11: Transmission electron microscopy (TEM) images of SiO_2 coated WO_3 **(a-d)** anisotropic nanoparticles, **(e)** lengthy nanorods1 (NR1) and **(f)** nanorods2 (NR2).

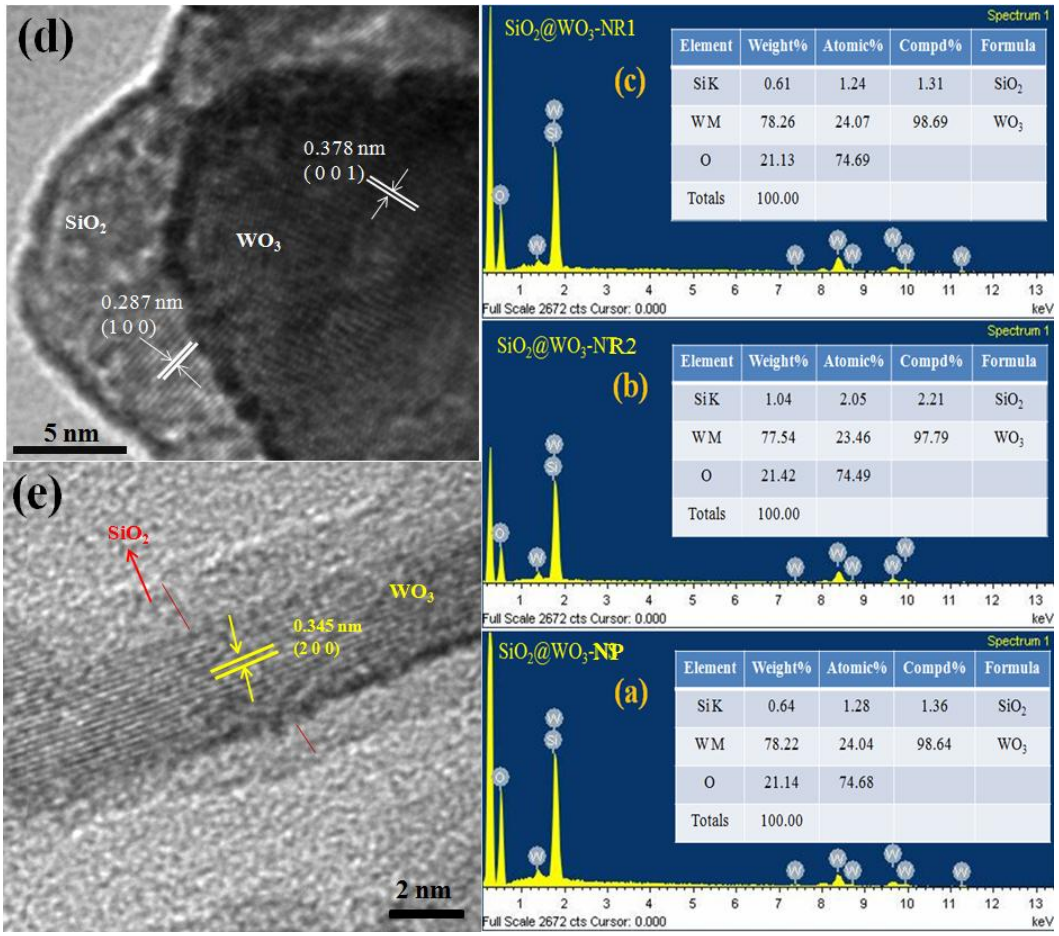

Figure 4.12: **(a-c)** Energy dispersive x-ray analysis (EDS) pattern of SiO_2 coated WO_3 nanoparticles and **(d-e)** HR-TEM images of SiO_2 coated WO_3 nanoparticles.

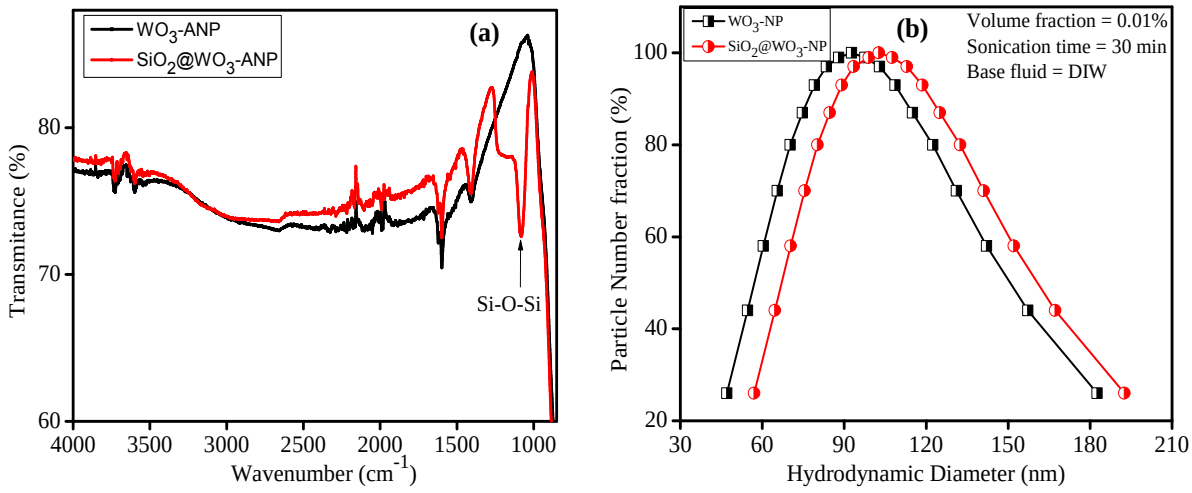

Figure 4.13 (a): FT-IR spectra and (b) particle size distribution (aqueous suspension) of bare and SiO_2 coated WO_3 nanoparticles.

4.7.3 Effect of silica coating and shape on thermal conductivity

Figure 4.14 (a) showed that the TC of pure DIW is increased after the dispersion (0.01%) of bulk WO_3, while as-prepared WO_3 NPs dispersion notably improved the TC as compared to these bulk powders. It was found that with the increase in SiO_2 layer deposition using different amount (80-160 µl) of TEOS hydrolysis, the TC gradually increased (~9%) with the increase in shell thickness of SiO_2 (80-120 µl), but then again decreases (~4%) beyond 120-160 µl of TEOS deposition. It was also observed in figure 4.14 (b) that lengthy SiO_2@WO_3 NR2 in DIW dispersion (0.01%) always exhibited higher (~8-10%) TC than bare WO_3 dispersion up to a certain amount (140 µl) of SiO_2 deposition onto WO_3 surface, and then it again decreased with increasing amount of SiO_2 layer thickness. The dispersion of lengthy WO_3 nanorods always showed higher (~5%) TC than conventional bare WO_3 NPs dispersion in DIW, and SiO_2 coating further increased the TC in certain extent because the variation in NPs size in NFs is influenced by the attraction and repulsion forces among the particles. In general, nanorods possessing higher per-particle surface area and more surface exposed atom may conduct more heat transfer relative to symmetric WO_3 NPs. Such disparity could also be attributed to the variation in surface morphology, crystallinity and grain boundaries etc.

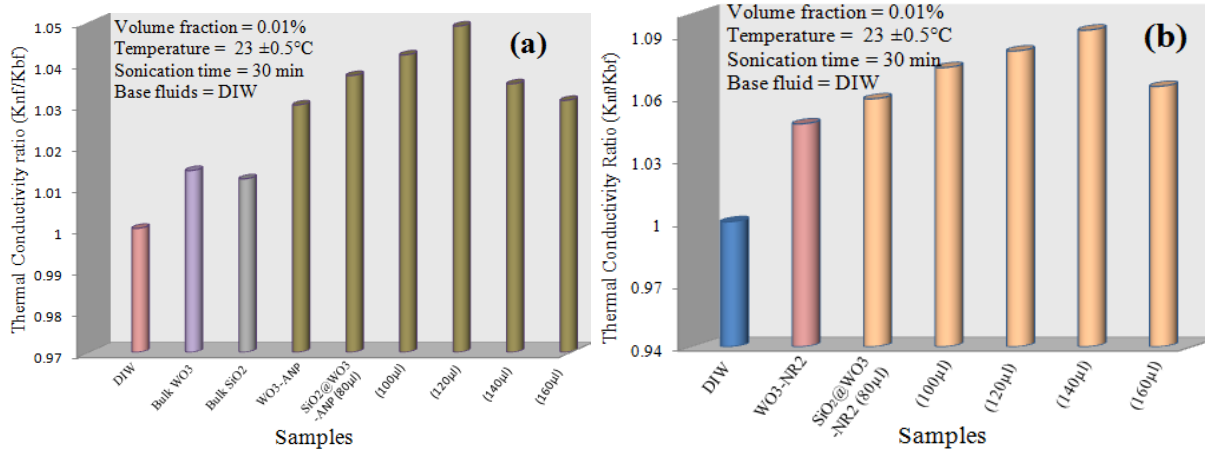

Figure 4.14: Influence of different amount of SiO_2 shell deposition over WO_3 **(a)** anisotropic nanoparticles and **(b)** nanorods2 for the optimum thermal conductivity.

This improved TC of SiO_2@WO_3 nanocomposites (NCs) relative to bulk WO_3 is not only due to SiO_2 layer deposition but participation of both WO_3 and SiO_2 NPs in heat conduction because of the beneficial surface properties of quantum size particles. The most importantly, a thin layer of SiO_2 coating induced hydrophilicity to SiO_2@WO_3 NCs for better wettability in DIW where Si-OH shell increased the repulsive interaction between the negatively charged Si-OH particles. The SiO_2 shell credited to increased hydrophilicity [64] of the WO_3 surface due to the generation of a hydroxyl group (-OH) that makes homogeneous colloidal suspension of the resultant SiO_2@WO_3 NCs showing no self-agglomeration and sedimentation, hence imparts superior dispersion stability as evident by almost no color changes of SiO_2@WO_3 suspension in falcon tube for longer duration (up to 3 days).

4.7.4 Evaluation of dispersion stability of aqueous suspension of SiO_2@WO_3 nanocomposites by measuring TC, density, refractive index, zeta potential, particle size distribution and their corresponding photographs

This long term dispersion is further verified by the zeta potential (an indicator of colloidal stability having a value [65] in the range of + 30 to -30 mV) measurement of aqueous suspension (pH = 6.32 - 7.45) of SiO_2@WO_3 NCs exhibiting considerably higher zeta potential value - 45 to -60 mV (table-1) after a thin layer of SiO_2 coating as compared to -16 to -27 mV of bare WO_3 NPs suspension that quickly settle down in the bottom of falcon tube within 30-60 min even after adequate ultrasonication (for 30 min) and therefore, TC decreased to a value equal to DIW. Thus, an optimum shell thickness of silica layer is required for maximum enhancement

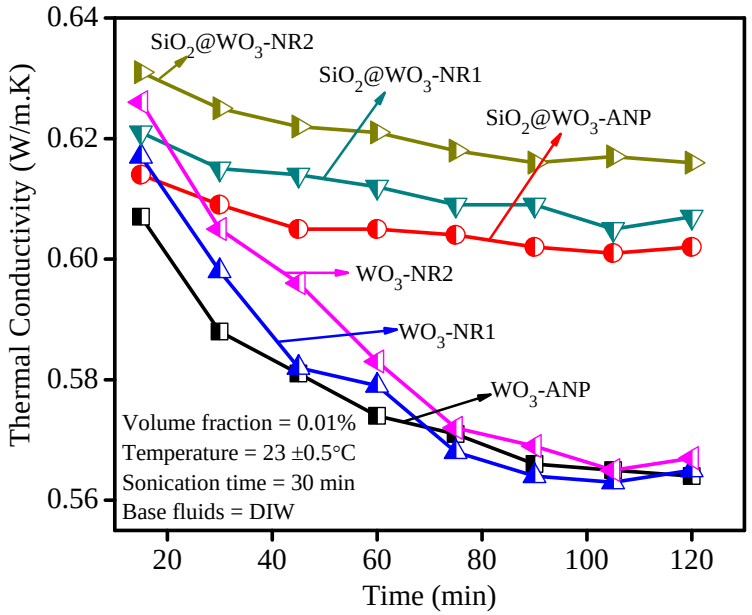

Figure 4.15: Decrease in thermal conductivity and dispersion stability of bare and SiO_2 coated WO_3 nanoparticles suspension in water.

in TC due to long network channel of Si-O-Si, and covalent bonding[37] between Si-O-W could improved the phonon transfer and thereby increased the heat transfer rate from one particle to other particle. A thick layer of SiO_2 deposition could probably suppress the intrinsic TC of WO_3 NPs that ultimately ends-up with the characteristic properties of large amount SiO_2 particles resides over WO_3 NPs. Both Van der Waals and electrostatic forces are important factors in the suspension stability of a NF controlling the repulsive forces between particles and thus, governs the NPs agglomeration. When NPs are affected by stronger attractive forces, they form cluster of larger size which precipitating down to the bottom of the falcon tube.

The potential advantages of a thin layer of silica coating for improved dispersion stability and stable TC is further verified as a function of analysis/settling time of the same sample without any mechanical disturbance. Figure 4.15 showed that irrespective of the size and shape of WO_3 NPs, each SiO_2@WO_3 NCs dispersion (0.01%) in DIW showing notable stability in TC (2-3% decrease) up to 120 min as compared to complete sedimentation of bare WO_3 NPs within 60 min, even after 30 min sonication each resulting into decrease in TC to a value of DIW. Again lengthy (NR2) SiO_2@WO_3 NCs dispersion always exhibited higher TC than typical NPs. This sample is undisturbed without further ultrasonication and TC was measured for 3 days in succession with a time interval of 2 h up to 8 h at a stretch as shown in figure 4.16. It was observed that all SiO_2 coated WO_3 suspension showed only 2-3% decrease in TC after 3 days (figure 4.16a) due to highly stable and uniform colloidal suspension as manifested by its white color sol without any

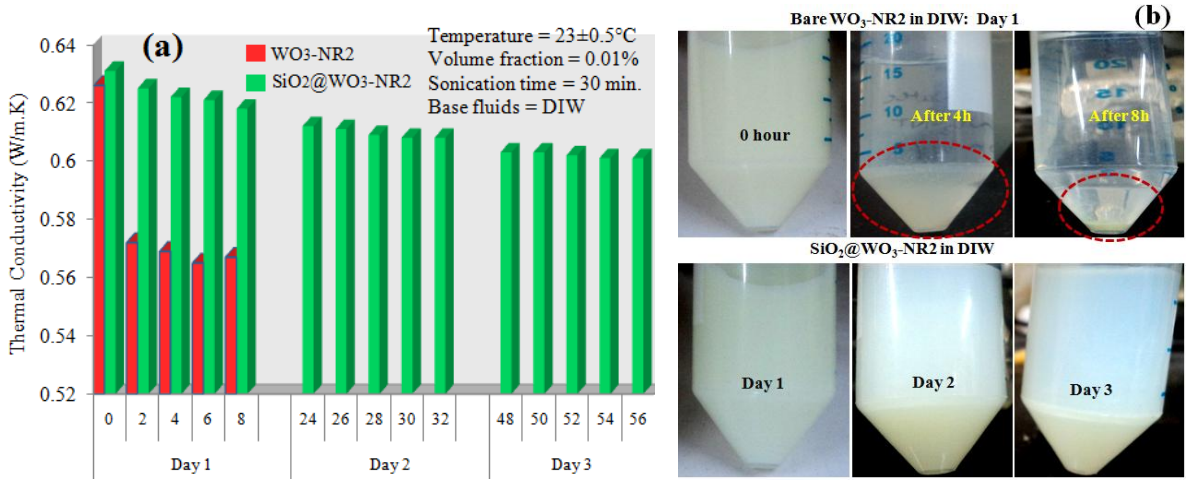

Figure 4.16 (a): Variation in thermal conductivity of bare and SiO_2 coated WO_3-NR2 aqueous suspension with passage to time (1-3 days after preparation of samples) and **(b)** Photographs of these bare and SiO_2 coated WO_3-NR2 aqueous suspension.

coagulation of the SiO_2@WO_3 NPs (figure 4.16b), whereas bare WO_3 NPs dispersion rapidly settles down, and TC reduced to a value of DIW within 2 h after 30 min sonication as revealed by

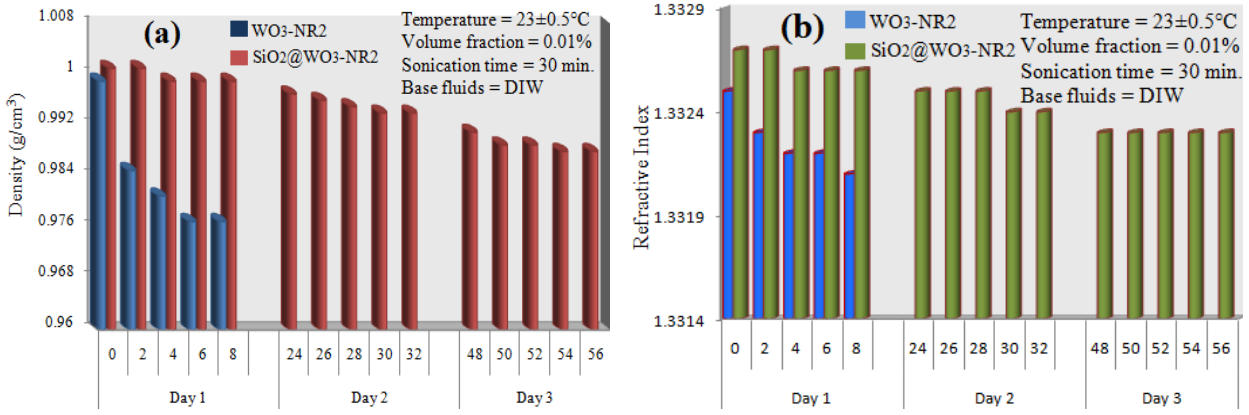

Figure 4.17 (a-b): Variation in density and refractive index of bare and SiO_2 coated WO_3-NR2 aqueous suspension with passage to time (1-3 days after preparation of samples).

its transparent color solution (figure 4.16b) where agglomerated bare WO_3 NPs are entirely precipitated in the bottom of the falcon tube.

The density and refractive index of all samples were measured after every 2 hours in a day for 3 days as shown in figure 4.17 (a-b). It was found that density of bare WO_3 NPs aqueous dispersion quickly decreased from 0.999 to 0.976 g/cm^3 during 8 h due to faster sedimentation of NPs as compared to very small changes from 1.001 to 0.998 for SiO_2@WO_3 NCs during 3 days of analysis indicating its better dispersion. Such small changes in density is occurred because relatively smaller particles slowly settling down relative to large sized particles as can be clearly seen in figure 4.17 (a). Similar

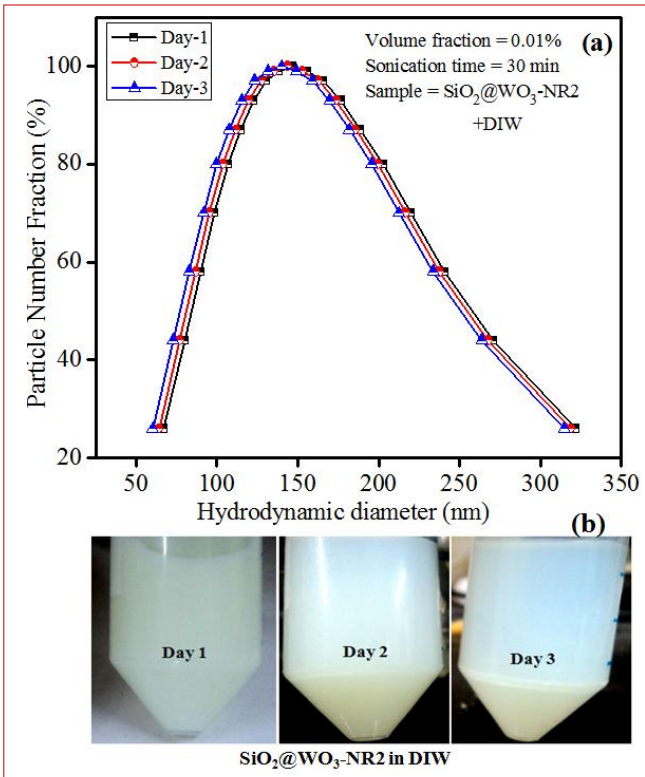

Figure 4.18 (a): Particle size distribution of SiO_2@WO_3-NR2 in aqueous suspension after 1-3 days of sample preparation and **(b)** photographs of same samples.

behavior is also observed (figure 4.17b) in the measured changes in the refractive index where a little decrease (0.5%) in refractive index was found for SiO_2@WO_3 NPs up to 3 days relative to more rapid decrease within 8 h in case of bare WO_3 suspension.

Due to repulsive interaction between the surface coated Si-OH groups, the agglomeration of NPs is highly retarded hence the particle size distribution and color of SiO_2@WO_3 NCs in DIW suspension did not change much due to superior colloidal stability for longer duration (2-3 days) as observed in figure 4.18. Thus, it revealed that due to uniform, homogenous and stable aqueous dispersion of SiO_2@WO_3 NCs, all the above physical properties did not altered appreciably relative to bare WO_3 NPs. As a result, improved and stable TC is obtained during longer duration due to repulsive interaction among the Si-OH coated WO_3 nanoparticles.

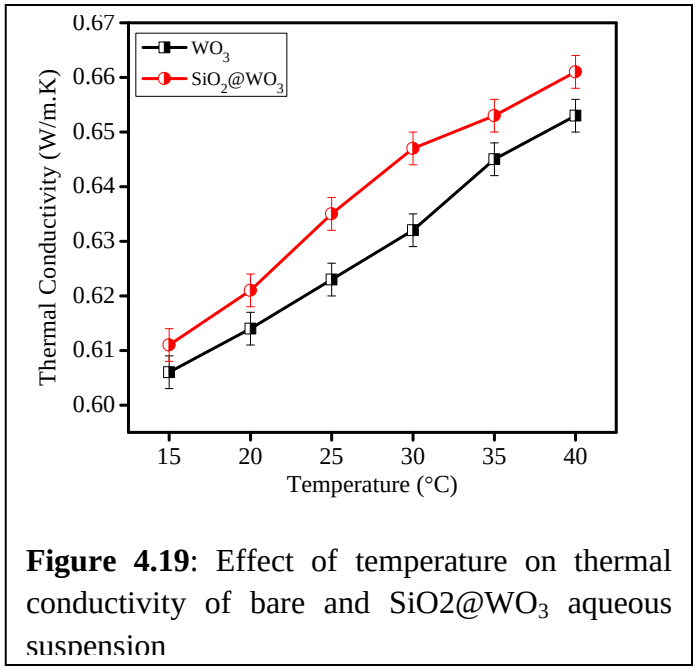

Figure 4.19: Effect of temperature on thermal conductivity of bare and SiO2@WO_3 aqueous suspension

4.7.5 Effect of temperature on thermal conductivity

The thermal conductivity increases with increase in temperature as shown in figure 4.19. With the increase in temperature the kinetic energy and Brownian motion of the particles increase which directly increase the thermal conductivity of the suspension. At loading of 0.01 vol.% of SiO_2@WO_3 in de-ionized water, an enhancement in thermal conductivity was increased from ~7-14% at 15-40°C. It was observed that SiO_2@WO_3

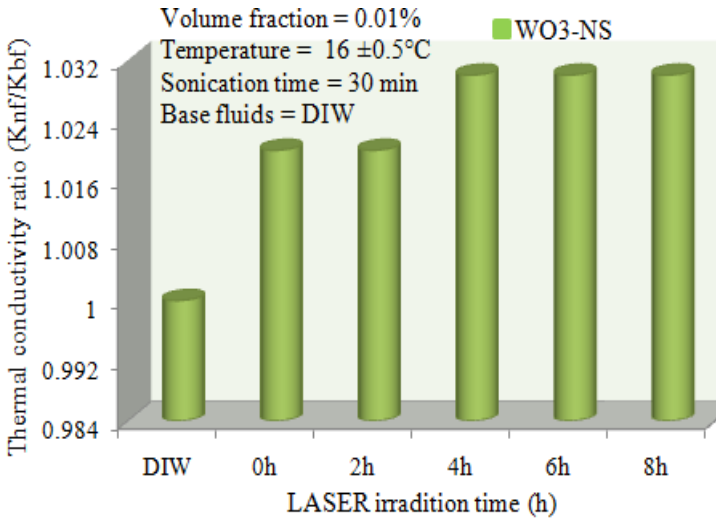

Figure 4.20: Effect of LASER irradiation on thermal conductivity of aqueous suspension of WO3 nanoparticles

suspension showed more enhancements in thermal conductivity than bare WO_3 aqueous suspension.

4.7.6 Effect of LASER irradiation on thermal conductivity

Figure 4.20 showed the effect of LASER irradiation on thermal conductivity of WO_3 NPs based aqueous suspension. It was found that thermal conductivity does not show any change after 2-8 h LASER irradiation, this might due to coagulation of particles by laser heat or insufficient energy to breakdown the particles into smaller size.

4.8 Conclusions

In summary, the beneficial effect of a thin layer of SiO_2 coating over WO_3 nanostructures for superior dispersion stability for long term due to hydrophilic and repulsive interaction between the WO_3-SiOH composites are investigated with the supportive evidences of particle size distribution, zeta potential, density and refractive index analysis as indicator parameter for stable suspension. As a result, SiO_2 coated WO_3 composite particles always exhibited higher TC than bare WO_3 NPs dispersion which generally undergoes quick agglomeration and precipitation. Further optimization of silica shell layer is needed for exhibiting long term dispersion stability and maximum thermal conductivity. It also found that lengthy cylindrical shapes exhibit more enhancements in TC than conventional NPs.

References

[1] J. Wang, E. Khoo, P.S. Lee and J. Ma, *J. Phys. Chem. C.* 2009, **113**, 9655-9658.

[2] C.C. Liao, F.R. Chen and J.J. Kai, *Sol. Energy Mater.Sol. Cells*.2007, **91**, 1282-1288.

[3] U. Cvelbar, K. Ostrikov, A. Drenik and M. Mozetic, *Appl. Phys. Lett.*2008, **92**, 133505-3.

[4] G. Xi and J. Ye, *Inorg. Chem.*2010, **49**, 2302-2309.

[5] Y. Yu, J.C. Yu, C.Y. Chan, Y.K. Che, J.C. Zhao, L. Ding, W.K. Ge and P.K. Wong, *Appl. Catal.,B.* 2005, **61,** 1-11.

[6] B. Y. Xia, B. Wang, H.B. Wu, Z. Liu, X. Wang and X. W. Lou**,** *J. Mater. Chem.* 2012, **22**, 16499-16505.

[7] R. Ostermann, D. Li, Y. Yin, J.T. McCann and Y. Xia, *Nano Lett.* 2006, **6**, 1297-1302.

[8] X.Y. Zhang, H.P. Li, X.L. Cui and Y.H. Lin, *J. Mater. Chem.*2010, **20**, 2801-2806.

[9] A. Mukherji, B. Seger, G.Q. Lu and L.Z. Wang, *ACS Nano.* 2011, **5**, 3483-3492.

[10] Y. Li, J. Zhou, S. Tung, E. Schneider and S. Xi, *Powder Technol.* 2009, **196**, 89-101.

[11] R. Saidura, K.Y. Leongb and H.A. Mohammad, *Renew. Sust. Energy Rev.* 2011, **15**, 1646-1668.

[12] M.S. Liu, M.C.C. Lin, I.T. Huang and C.C. Wang, *Chem. Eng. Technol.* 2006, **29**, 72-7.

[13] C.T. Nguyen, G. Roy. C. Gauthier and N. Galanis, *Appl. Therm. Eng.* 2007, **27**, 1501–6.

[14] W. Duangthongsuk and S. Wongwises, *Int. J. Heat Mass Transfer.*2010, **53**, 334–44.

[15] S.M.S. Murshed, K.C. Leong and C. Yang, *Int. J. Therm. Sci.*2005, **44**, 367-73.

[16] B. Pal, S.S. Mallick and B. Pal, *Colloids Surf., A.*2014, **459**, 282-289.

[17] B. Pal, S.S. Mallick and B. Pal, *J. Nanosci. Nanotechnol.*2015, **15**, 3670-3676.

[18] D.H. Yoo, K.S. Hong and H.S. Yang, *Thermochim. Acta.* 2007, **455**, 66-9.

[19] H.T. Zhu, C.Y. Zhang, Y.M. Tang, and J.X. Wang, *J. Phys. Chem. C.* 2007, **111**, 1646-50.

[20] J.W. Gao, R.T. Zheng, H. Ohtani, D.S. Zhu, and G. Chen, *Nano. Lett.* 2009, **9**, 4128-32.

[21] X. Zhang, H. Gu and M. Fujii, *Exp. Therm. Fluid Sci.* 2007, **31**, 593-599.

[22] P.D. Shima, J. Philip and B. Raj, *J. Phys. Chem. C.*2010, **114**, 18825-18833.

[23] R. Singh and B. Pal, *J. Mol. Catal. A: Chem.* 2013, **371**, 77–85.

[24] B. Yang and Z.H. Han, *Appl. Phys. Lett.* 2006, 89, 083111-3.

[25] D. Lee, J.W. Kim and B.G. Kim, *J. Phys. Chem. B.* 2006, **110**, 4323-4328.

[26] P. Keblinski and J. Thomin, *Phys. Rev. E.* 2006, **73**, 010502-4.

[27] E. Illes and E. Tombacz, *J. Colloid Interface Sci.* 2006, **295**, 115-123.

[28] A.B. Jodar-Reyes, A. Martin-Rodriguez and J.L. Ortega-Vinuesa, *J. Colloid Interface Sci.* 2006, **298**, 248-257.

[29] J.C. Maxwell, A Treatise on Electricity and Magnetism, 2nd ed.; Clarendon: Oxford, U.K., 1881; Vol. 1.

[30] R.L. Hamilton, O.K. Crosser, *Ind. Eng. Chem. Fundam.*1962, **1**, 187-191.

[31] S.U.S. Choi, *J. Heat Transfer.* 2009, **131**, 033106-9.

[32] Y. Li, J. Zhou, S. Tung, E. Schneider and S. Xi, *Powder Technol.* 2009, **196**, 89−101.

[33] D. Wen, G. Lin, S. Vafaei and K. Zhang, *Particuology*, 2009, **7**, 141-150.

[34] S.M.S. Murshed, K.C. Leong and C.Yang, *Appl. Therm. Eng.* 2008, **28**, 2109-2125.

[35] X.Q. Wang and A.S. Mujumdar, *Int. J. Therm. Sci.* 2007, **46,** 1-19.

[36] S.K. Das, S.U.S. Choi and H.E. Patel, *Heat Transfer Eng.* 2006, **27**, 3−19.

[37] J.A. Eastman, S.U.S. Choi, S. Li, W. Yu and L.J. Thompson, *Appl. Phys. Lett.* 2001, **78,** 718-720.

[38] S.K. Das, S.U.S. Choi, W. Yu and T. Pradeep, *John Wiley & Sons: Hoboken*, NJ, 2008.

[39] W.Yu, D.M. France, J.L. Routbort and S.U.S. Choi, *Heat Transfer Eng*. 2008, **29,** 432.

[40] P. Keblinski, J.A. Eastman and D.G. Cahill, *Mater. Today*. 2005, **8,** 36-44.

[41] L.S. Sundar and K.V. Sharma, *Int. J. Nanoparticles*. 2008, **1,** 66-77.

[42] R.S. Vajjha and D.K. Das, *Int. J. Heat Mass Transfer.* 2009, **52 ,** 4675-82.

[43] D. Zhu, X. Li, N. Wang, X. Wang, J. Gao and H. Li, *Curr. Appl Phys*. 2009, **9,** 131–139.

[44] Y. Hwang, J.K. Lee, C.H. Lee, Y.M. Jung, S.I. Cheong, C.G. Lee, B.C. Ku and S.P. Jang, *Thermochim. Acta*. 2007, **455,** 70-74.

[45] P.D. Shima, J. Philip and B. Raj**,** *J. Phys. Chem. C* 2010,**114,**18825–18833.

[46] M. Haruta, *Chem. Rec.* 2003, **3**, 75-78.

[47] S.M.S. Murshed, K.C. Leong and C. Yang, *Int. J. Therm. Sci.* 2005, **44,** 367-73.

[48] D.H. Yoo, K.S. Hong and H.S. Yang, *Thermochim. Acta.* 2007, **455,** 66-69.

[49] H.T. Zhu, C.Y. Zhang, Y.M. Tang and J.X. Wang, *J. Phys. Chem. C*. 2007, **111,** 1646-50.

[50] J.W. Gao, R.T. Zheng, H. Ohtani, D.S. Zhu and G. Chen, *Nano. Lett.* 2009, **9,** 4128-32.

[51] D. Lee, J.W. Kim and B.G. Kim, *J. Phys. Chem. B.* 2006, **110,** 4323-4328.

[52] A. Ghadimi, R. Saidur and H.S.C. Metselaar, *Int. J. Heat Mass Transfer*. 2011, **54,** 4051–4068.

[53] W. Jiang, G. Ding and H. Peng, *Int J. Therm. Sci*. 2009, **48,** 1108-15.

[54] X.F. Li, D.S. Zhu, X.J. Wang, N. Wang, J.W. Gao and H. Li, *ThermochimActa*. 2008, **103,** 469-98.

[55] S.M. Saterlie, H. Sahin, B. Kavlicoglu, Y. Liu and A.O. Graeve, *Chem. Mater*. 2012, **24,** 3299-3306.

[56] R.G. Chaudhuri and S. Paria, *Chem. Rev.*2012, **112**, 2373-2433.

[57] S.S. Botha, P. Ndungu and B.J. Bladergroen, *Ind. Eng. Chem. Res.* 2011, **50**, 3071–3077.

[58] T. Liu, D. Li, Y. Zou, D. Yang, H. Li, Y. Wu and M. Jiang, *J. Colloid Interface Sci*. 2010, **350,** 58-62.

[59] T. Li, J. Moon, A.A. Morrone, J.J .Mecholsky, D.R. Talham and J.H. Adair, *Langmuir.* 1999, **15,** 4328.

[60] A.L. Rogach, D. Nagesha, J.W. Ostrander, M. Giersig and N.A. Kotov, *Chem. Mater.* 2000, **12**, 2676.

[61] N. Gupta and B. Pal, *J. Nanosci. Nanotechnol*.2013, **13,** 5069-5079.

[62] Z. G. Zhao and M. Miyauchi, *J. Phys. Chem. C.* 2009, **113,** 6539-6546.

[63] J. Wang, E. Khoo, S.P. Lee and J. Ma, *J. Phys. Chem. C*. 2009, **113,** 9655–9658.

[64] H.J. Cha, Y.H. Kim, H.G. Cha and Y.S. Kang, *Surf. Rev. Lett.* 2007, **14**, 693-704.

[65] D. Lee, J.W. Kim and B.G. Kim, *J. Phys. Chem. B.* 2006, **110,** 4323-4328.

Phase-dependent Thermophysical Properties of α-and γ-Al_2O_3 in Aqueous Suspension

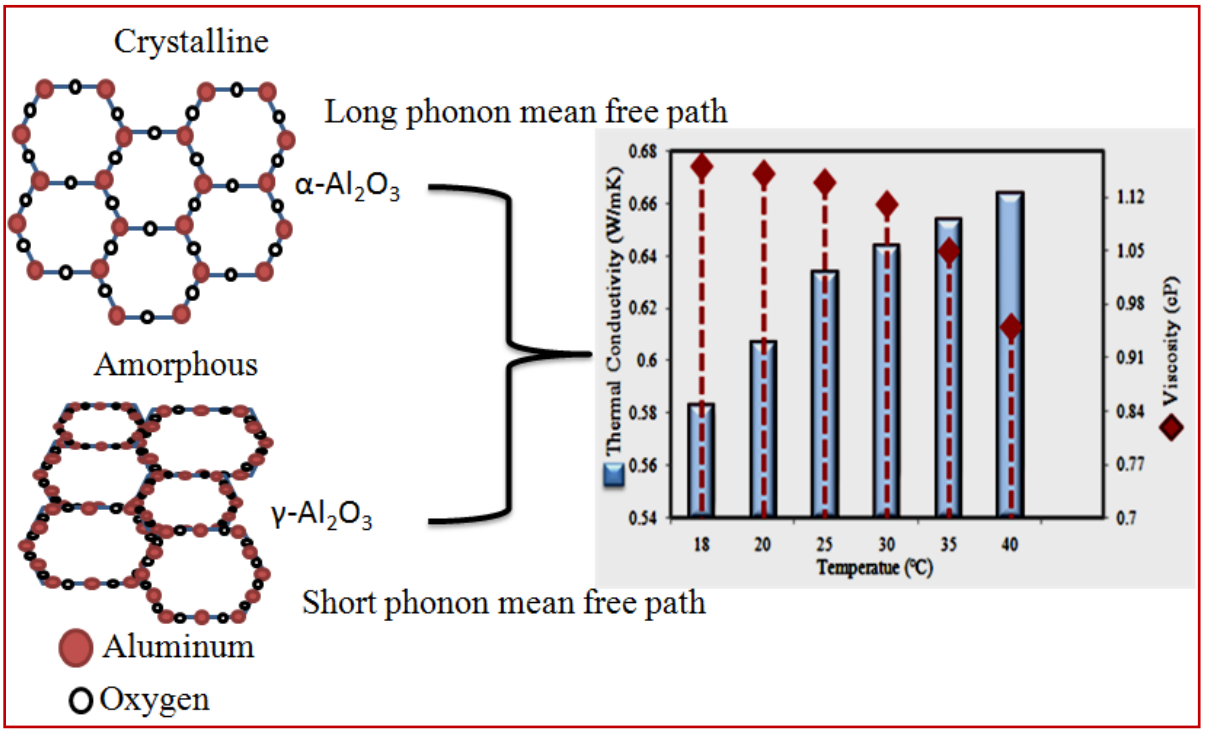

Abstract: This study demonstrates the thermal conductivity and viscosity of as prepared crystalline α-Al_2O_3 and amorphous γ-Al_2O_3 nanoparticles, having size in the range of 30-50 nm. The α-Al_2O_3 and γ-Al_2O_3 aqueous suspension exhibited ~10% and 6% enhancement in thermal conductivity of de-ionized water, but α-Al_2O_3 showed (~4-6%) higher thermal conductivity than γ-Al_2O_3 aqueous suspension. This is ascribed to better crystallinity of α-Al_2O_3 phase having regular and long order arrangement of atoms which favours in rapid transfer of phonon vibration from one atom to another than amorphous γ-Al_2O_3 phase with irregular atomic arrays, and thereby decreases the heat transfer rate. Ultra-sonication helps in the breakdown of large clusters with an increase the dispersion stability and thermal conductivity as verified by particle size distribution and zeta potential measurements. The viscosity of both (α, γ-Al_2O_3 phase**)** aqueous suspension is higher than de-ionized water. Viscosity is inversely proportional to thermal conductivity, which increased with increase in concentration and decrease with increase in temperature. The Al_2O_3 aqueous suspension showed Newtonian characteristics at lower concentration (0.05 vol.%).

5.1 Introduction

A nanofluid is a dispersion of NPs in base liquids. It has been reported that NFs provide significant heat-transfer enhancement compared to conventional heat transfer fluids. The suspension of crystalline NPs showed fluids higher thermal conductivity than base fluids [1-4]. Cooling has now become a vital characteristic for thermal management due to continuous development in technology and forthcoming more powerful tools in lasers, communication, optics and electronics having miniaturized size [5,6]. The aqueous or non-aqueous suspension of Al_2O_3 NPs is recently studied for cooling applications due to high TC of solid NPs than liquid [7-9]. Particles with a nanoscale dimension provide a higher surface area, which not only increases the heat transfer rate but also improves the particles dispersion stability in the conventional heat transfer fluids [10,11]. Researchers have been trying to enhance the heat transfer performance of conventional coolants by suspending tiny metallic, non-metallic and metal oxide particles in de-ionized water and ethylene glycol depending upon their volume fraction (VF), particle size, shape, pH and temperature [12-15]. Some research groups [16-19] found 4 to 30% enhancement in TC by varying particle size (10 to 200 nm) and volume fraction (0.05 to 4 vol.%) of γ-Al_2O_3 in DI water and EG. Beck et [20] al. showed decrease in TC of alumina nanoparticles dispersion

having size lower than 50 nm and TC was increased with increasing particle sizes (100-282 nm). Teng et al. [21] presented the influence of concentration, particle size and temperature on increased TC of aqueous suspension of Al_2O_3 particles. In some other reports [22-24] found that by increasing the temperature from 31-51°C, the enhancement in TC was found to be 2 to 32.4% for Al_2O_3 dispersed in DI water and EG. Kole et al. [25] suspended less than 50 nm Al_2O_3 (3.5 vol.%) using oleic acid as stabilizer in a car engine coolant and found 10.41% TC enhancement and verified the stability of such fluids for more than 80 days. Engineering applications of NPs dispersion that make use of fluid flow not only involve information on their thermal properties, but the suitable rheological properties of the aqueous suspension are also very important [26]. In the Al_2O_3-water mixture viscosity increases between 20% and 30% for 3 vol.% Al_2O_3 solution as compared to water alone [27]. Das et al. [28] verified an increase of viscosity (VS) with increased particle concentrations and Kole et al. [25] demonstrated a transition from Newtonian characteristics to non-Newtonian behavior with increasing content of Al_2O_3 in the engine coolant. Recently, Beck et al. [29] suggested the temperature dependence TC and viscosity of EG-based suspension in the range of 296 to 400 K. Chandrasekar et al. [30] reported 15.91% and 21.53% increase in Nusselt numbers when Al_2O_3-water NFs was used with wire coil inserts WC2 and WC3, respectively. Teng et al. [31] also studied the effect of phase transition of Al_2O_3 on thermal conductivity.

Alumina exists in a variety of metastable structures, such as χ, κ, γ, η, δ, θ, and ρ, as well as its stable α-Al_2O_3 phase and each has a unique crystal structure and propertie [32,33]. This polymorphism can be categorized in terms of the oxygen sublattice structure and the distribution into this sublattice of aluminium ions in octahedral and tetrahedral interstitial sites [34]. Thus, in α-Al_2O_3, the oxygen sublattice is hexagonal-close-packed (hcp) structured with 2/3 of octahedral sites occupied with cations, while γ, η, θ have a face-centred cubic (fcc) array of oxygen atoms and cations present in a variety of proportions in both octahedral and tetrahedral sites [35,36]. This different atomic arrangement in various phases of Al_2O_3 directly affects the surface properties of materials such as heat transfer rate, mean free path of phonon vibrations etc. From the literature, it is not well understood that how phase transition of Al_2O_3 NPs influence its thermo-physical properties like TC, specific heat and VS etc. So this study focuses on the preparation of most stable (α, γ) phase of Al_2O_3 and compares their influences on TC and VS as a function of NPs concentration, temperature, sonication and settling time.

5.2 Experimental Section

5.2.1 Preparation and characterization of α-Al_2O_3 and γ-Al_2O_3 particles

Aluminium sulphate hydrate ($Al_2(SO_4)_3 \cdot xH_2O$) and propanol ($CH_3CH_2CH_2OH$) were purchased from Loba Chemicals, India and used without further purification. De-ionized water was obtained using an ultra filtration system (Milli-Q, Milipore) with a measured conductivity 35 mho cm^{-1} at 25 °C. A 1 M $Al_2(SO_4)_3 \cdot xH_2O$ solution was prepared by dissolving it in 20 ml distilled water and then added it slowly into 40 ml propanol and obtained white precipitate of $Al(OH)_3$ was dried in an oven at 70-80 °C for 6 to 8 h and calcined at 700 to 1100 °C in a muffle furnace for 3 to 4 h [37]. The formation of γ-phase takes place at 700 °C and formation of α-phase takes place at 1100 °C. Their crystal structure and grain size were investigated by powder X-ray diffraction study with PANalytical's X'Pert Pro with Cu Kα (λ = 1.5406 Å) radiation. Size and shape analysis was done by Transmission Electron Microscope (Hitachi 7500 model) with Al_2O_3 powder samples dispersed in methanol.

5.2.2 Thermal conductivity, viscosity and electro-kinetic parameter analysis

Al_2O_3 particles were dispersed into DI-water with different VF in the range of 0.01% to 1%. Ultrasonication (frequency ± 42 KHz ± 6%, Bransonic-3510 E-DTH) has been carried out for several hours (2 to 10 h) to prevent particle's agglomeration. The TC of all samples was measured by using KD2 Pro Thermal Property Analyzer (Decagon Devices, Inc., USA) after calibrating with glycerin (provided by Decagon Company) and DI-water. The VS of the aqueous suspension was measured by a Brookfield Programmable Rheometer (Model: DV-III ULTRA) appropriately connected to Temperature Controlled Bath to vary the fluid temperature between 5 and 80 °C. Particle size distribution and surface charge was measured by (DLS) Dynamic Light Scattering (Brook haven 7610 instrument) and Zeta potential analyzer. Aqueous suspension of 20 ml (0.05 VF) of Al_2O_3 was sonicated for 4 to 8 h and used (1.5 ml) for DLS and zeta potential measurement.

5.3 Results and discussion

5.3.1 Structural and morphological characterization

The XRD patterns in figure 5.1 (a) shows the strongly intense sharp peaks characteristic to rhombohedral structure of α-Al_2O_3 with R3c (167) symmetry as per JCPDS Card No: 46-1212. The sharp diffraction peaks indicative of high crystallinity of α phase whose average crystallite size was determined by the Scherrer formula [38] and found in the range of 30-40 nm for α-phase and 4-10 nm for γ-phase. No any other characteristic peaks of impurities have been observed, indicating the high purity of as-prepared sample. Figure 5.1 (b) shows relatively broad and weak peaks (111), (311), (400) and (440) for cubic structure of amorphous γ-Al_2O_3 phase (JCPDS Card No. 10-0425). Alteration of all pure alumina into the single α-phase was observed starting from 1050 °C, as indicated by figure 5.1 (a). The sharp peaks of the α-phase specify the relatively large grain sizes and well-defined long-range order, which indicate the collapse of the porous structure characteristic of the low-temperature phases (χ, κ, γ, η, δ, θ, and ρ) and the consequent diminishment of the powder surface area [39]. The formation of γ-Al_2O_3 is due to progressive dehydration and desorption of surface hydroxyl groups that led to its amorphous nature. The peaks display broad and diffuse profiles, demonstrating the presence of small crystalline grains and compositional fluctuations. This is consistent with the location of the Al^{3+} ions either by the tetrahedral or octahedral sites within the spinel structure [40].

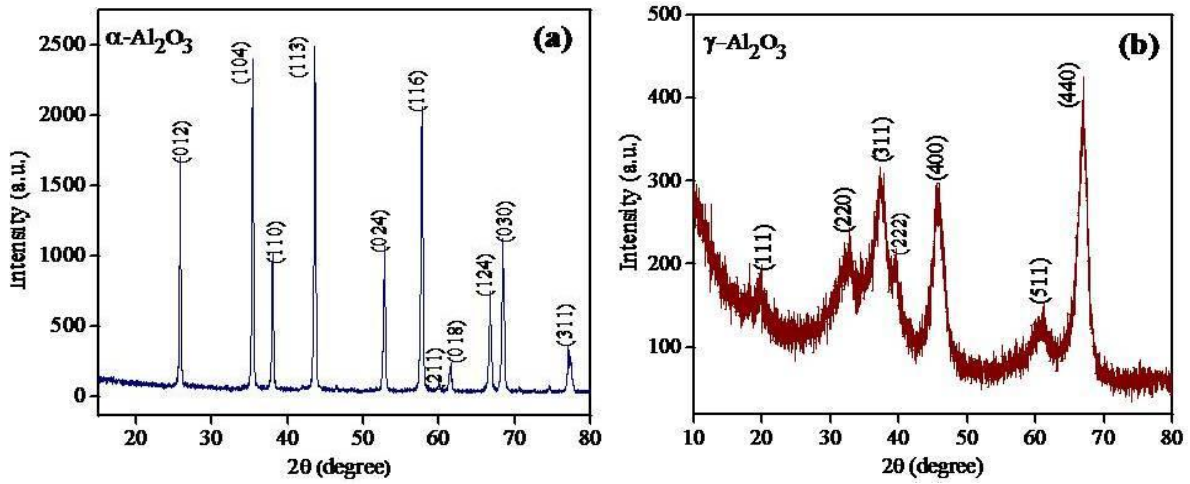

Figure 5.1: XRD patterns of (a) α-Al_2O_3 and (b) γ-Al_2O_3 particles.

The Transmission Electron Microscopy (TEM) images in figure 5.2 (a-b) showed well crystalline α-Al_2O_3 NPs, which are overlapped with each other. An individual particle shows size range between 40-50 nm but due to overlapping of large number of particles, size increases up 0.10 μm and could not be reduced even with significant ultra-sonication. Figure 5.2 (c-d) displayed TEM images of amorphous γ-Al_2O_3 NPs which are also agglomerated and form large

cluster. The actual size or individual size of NPs is in 30-40 nm range but it tends to agglomerate and resulted in large cluster with size up to 0.15 µm. The reason for overlapping of NPs and consequence in large cluster is the more interaction between hydroxyl groups present on the surface, trapping of small particles into large cluster, high surface-to-volume ratio, high surface charge or van der Waals interaction between them [41]. The NPs size distribution in aqueous was also verified by Dynamic light scattering and zeta potential analyzer, which also shows µm size of particles.

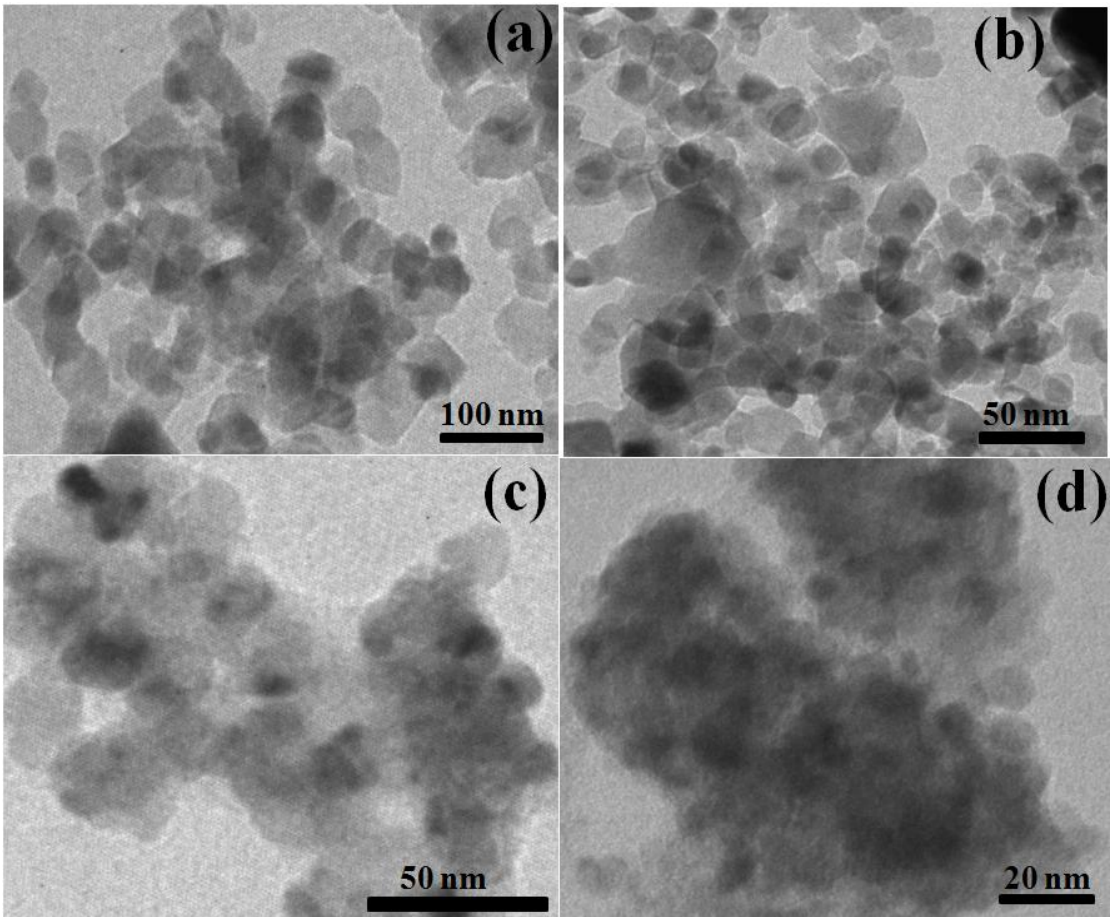

Figure 5.2: TEM images of: **(a-b)** α-Al_2O_3 and **(c-d)** γ-Al_2O_3 particles.

5.3.2 Thermal Conductivity of Al_2O_3-DI water suspensions

figure 5.3 (a) shows that with an increase in sonication time, TC increases for α-Al_2O_3 and γ-Al_2O_3 suspension in comparison to DI water having TC = 0.597 W/m.K at 26 °C. During 2 to 4 h

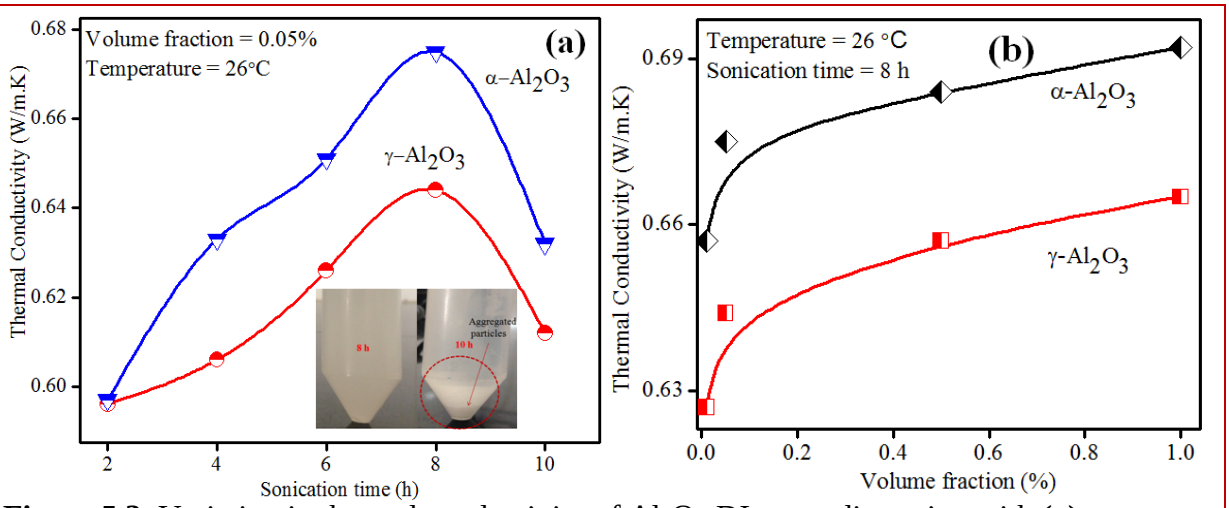

Figure 5.3: Variation in thermal conductivity of Al_2O_3-DI water dispersion with **(a)** sonication time and **(b)** volume fraction.

sonication, the TC increases slightly, but after 6-8 h it increases sharply and decreases thereafter 10 h of sonication. The α-Al_2O_3 aqueous suspension always displayed higher TC (4-6%) than γ-Al_2O_3 aqueous suspension. It was also found that TC increases with increase in volume fraction from 0.01 to 1 vol% for both phases, but again α-phase always shows more enhancement in TC than γ-phase as shown in figure 5.3 (b). The reason for higher TC in α-Al_2O_3 aqueous suspension is its high crystallinity than amorphous γ-phase. In γ-phase some void spaces are present in its crystal structure which becomes obstacle in the path of phonon vibration and thereby decreases heat transfer rate. It is evident that there is an optimum sonication time (8 h) at which the Al_2O_3 aqueous suspension found to be more stable. This is due to supersonic waves travel longitudinally within the liquid medium and cause alternate positive and negative pressure waves in the liquid, which results in the homogeneous distribution of particles in the continuous liquid phase and Brownian motion of particles increases and helps in rapid heat transfer rate [42]. The decrease in stability and TC after 10 h sonication is probably due to the formation of some defects/disorder in Al_2O_3 structure as reported by some research groups [43,44,41]. The most probable explanation for increased volume fraction is that the distance between NPs decreases as the particle concentration increases and enhancement in the TC can be attributed to increased particle-to-particle interactions at higher concentrations [45], but optimization of volume fraction

is also important here for commercialization of these aqueous suspension for cooling applications.

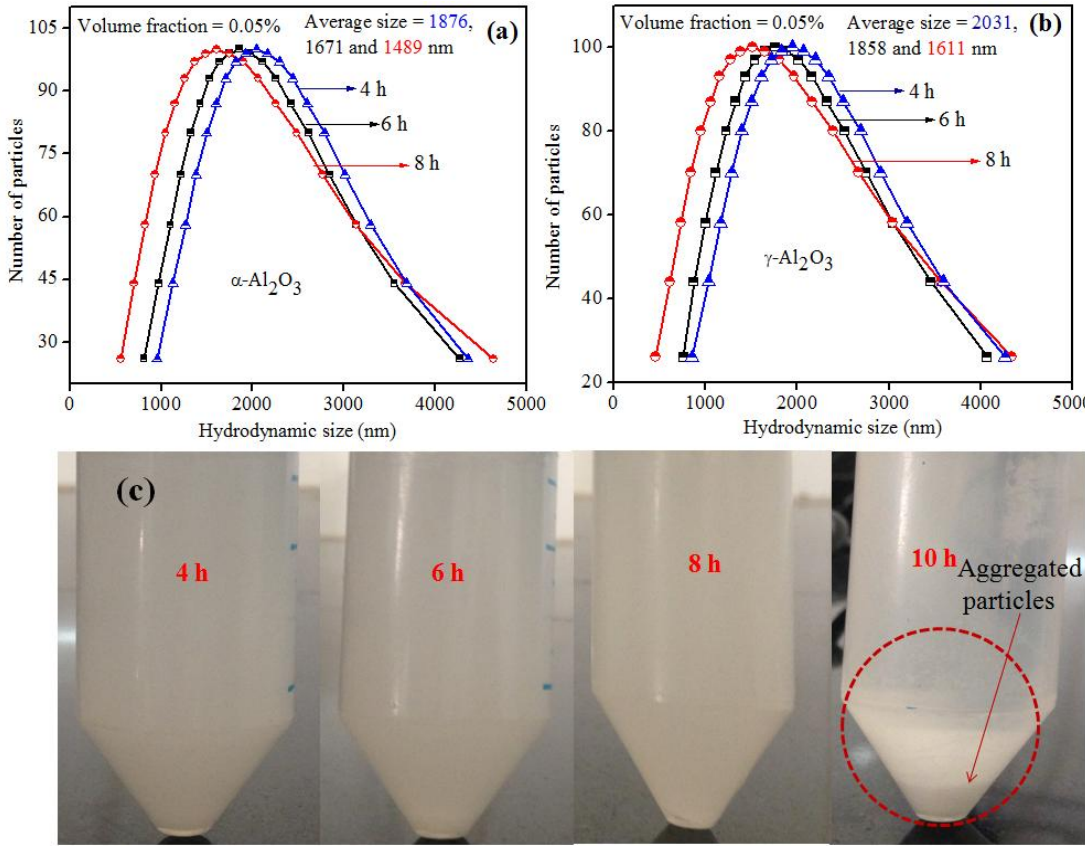

Figure 5.4: Particle size distribution of **(a)** α-Al_2O_3, **(b)** γ-Al_2O_3 dispersed in de-ionized water after 4 to 8 h sonication and **(c)** Photographs of Al_2O_3 suspension after sonication for 4-10 h.

The effect of sonication time on dispersion stability was further verified by DLS particle size distribution and Zeta potential measurements. The decrease in cluster size (1.8 to 1.4 µm) with increasing the sonication time from 4 to 8 h was due to strong sonic waves which break down large cluster into smaller one as presented in figure 5.4. However, after 10 h sonication, the particle's surface charge density might be increased [41] which leads to aggregation due to higher force of attraction between them. As a result, the particles settled down as shown in figure 5.4 (c), hence DLS particle size distribution do not give any conclusive result that might be beyond the upper limit of instrument's measurement (2 nm-5 µm). The improved dispersion stability was also verified by zeta potential measurement. For α-Al_2O_3 and γ-Al_2O_3 suspension (0.05%) sonicated for 4 to 8 hours, the zeta potential values varies from -33 to -38 mV and -31 to

-35 mV (characteristic value for stable suspension), respectively, indicating better dispersion stability than 10 h sonicated sample showing notably lower zeta potential -12 mV probably due to particles agglomeration which quickly settles down as evident in the comparative images (figure 5.4c) of Al_2O_3 suspension.

The heat-transfer rate depends on the temperature gradient and TC of the material. Change of temperature affects the Brownian motion of particles and clustering of particles, which results in dramatic changes of TC. The variation in TC for both aqueous suspensions with temperature (figure 5.5a) from 18 to 30 °C revealed that TC increases with increase in temperature, where α-Al_2O_3 showed more enhancements in TC than γ-Al_2O_3 due to more crystallinity of α-phase. The Brownian motion intensifies with an increase in temperature as per the kinetic theory of

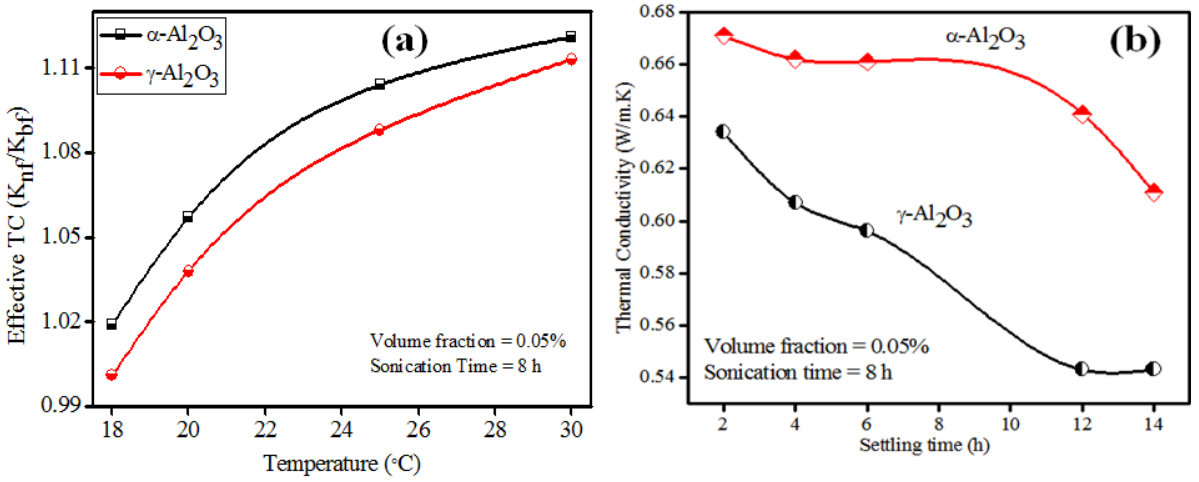

Figure 5.5: Variation in thermal conductivity of Al_2O_3-DI water dispersion as a function of **(a)** temperature and **(b)** settling time.

particles. With the increase in temperature, the Brownian motion and phonon vibration become stronger and this assists the rapid heat transfer rate from one particle to another.

Another aspect of aqueous suspension research that has received relatively low attention is the effect of settling time on the TC. In this paper, settling time indicates the time after the completion of sonication. Even though nano-size dispersion is expected to remain stable, this is generally not the case in reality (especially when the powders are added in solvents in a two step process). The NPs tend to agglomerate, form clusters and settle down; this reduction in the stability could decrease the TC of suspension with time (Yoo et al., 2007) [46]. Contrary to this theory, however, is another theory according to which aggregation is a more likely cause for the enhanced TC of suspension. Thus, there is no agreement between the various research groups

about the relation of particle agglomeration, stability and the various thermo-physical properties of suspension. This is without doubt that the time dependent properties of suspensions are to be examined for commercial use, where long-term stability is essential factor. In the present experimental program, suspensions were prepared after 8 hours of sonication and then left undisturbed for several hours. One reading was tested for TC just after the end of sonication (i.e. a freshly prepared sample). Afterwards, in every 2 hours, the samples were tested for TC, i.e. the different settling timings achieved were: 0, 2, 4, 6, 12 and 14 hours. It is clearly shown that during initial hours (2 to 6 h) of settling time, α-Al_2O_3 aqueous suspension showed slight decrease in TC and thereafter a sharp decrease in TC was observed (figure 5.5b) after 12 to 14 h settling, whereas γ-Al_2O_3 aqueous suspension shows sharp decrease in TC in initial hours and then become almost constant beyond 8 h settling. The reason for this is stronger attractive forces by which large size cluster formation takes place and prone to precipitating down to the bottom of the liquid. Smaller particles, in contrast, are more easily dispersed and suspended in liquid when they are affected by repulsive forces. Both van der Waals and electrostatic forces are important factors in the dispersion stability of solids in liquid.

5.3.3 Viscosity of Al_2O_3-DI water suspensions

Viscosity describes the internal resistance of a fluid to flow and it is an important property for all thermal applications involving fluid, the pumping power is related with the viscosity of a fluid.

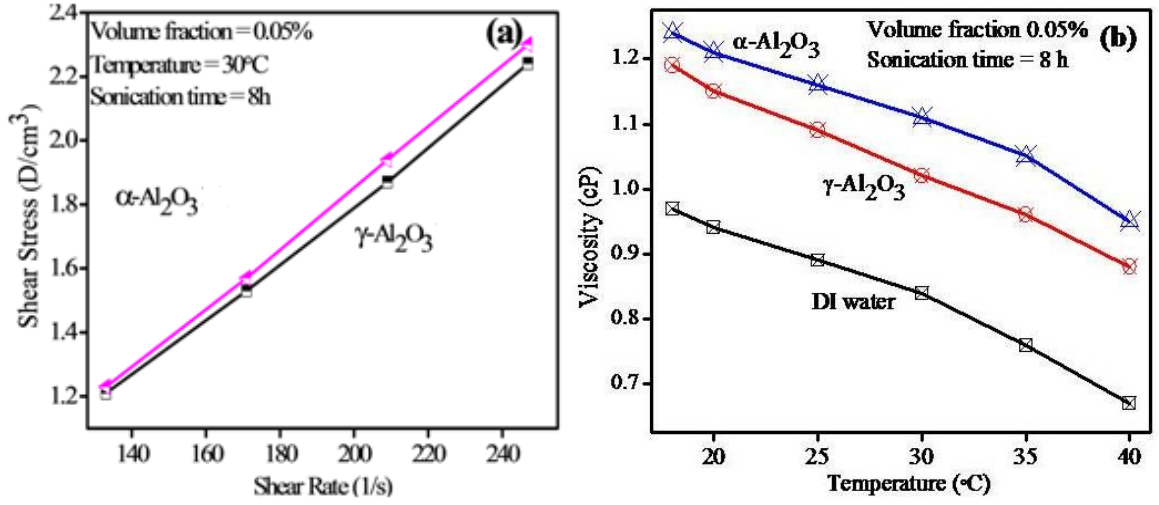

Figure 5.6: **(a)** Shear stress as a function of shear rate and **(b)** viscosity of Al_2O_3-water dispersion at different temperature.

The VS of Al_2O_3 aqueous suspension is affected by many factors, such as volume fraction, particle size, particle aspect ratio and aggregate size [47]. In this case we address two other factors, shear-rate dependence and temperature dependence VS, which are very important for the fundamental understanding of their heat transfer applications. The shear stress increases linearly with the shear rate for low loading (0.05%) of Al_2O_3 in DI-water at 30°C indicating the Newtonian behavior of Al_2O_3 DI-water suspension (figure 5.6a). The study of the temperature dependence of viscosity of suspension is also very important because it influences the hydrodynamics that affects the heat transfer of cooling system. Figure 5.6(b) shows that viscosity reduces with an increase in temperature, indicates that with an increase in temperature the intra and intermolecular interactions between the molecules become weak and increase the surface tension which automatically becomes less viscous. The correlation between TC, VS and temperature is shown in figure 5.7 and it was found that with increase in temperature TC increases but VS decreases, so they are inversely proportional to each other. As the temperature increases, the time of interaction between neighbouring molecules of a liquid decreases because of the increased velocities of individual molecules and increases the average kinetic energy of the molecules in a liquid. The greater average kinetic energy of the molecules more easily overcomes the attractive forces that tend to hold the molecules together.

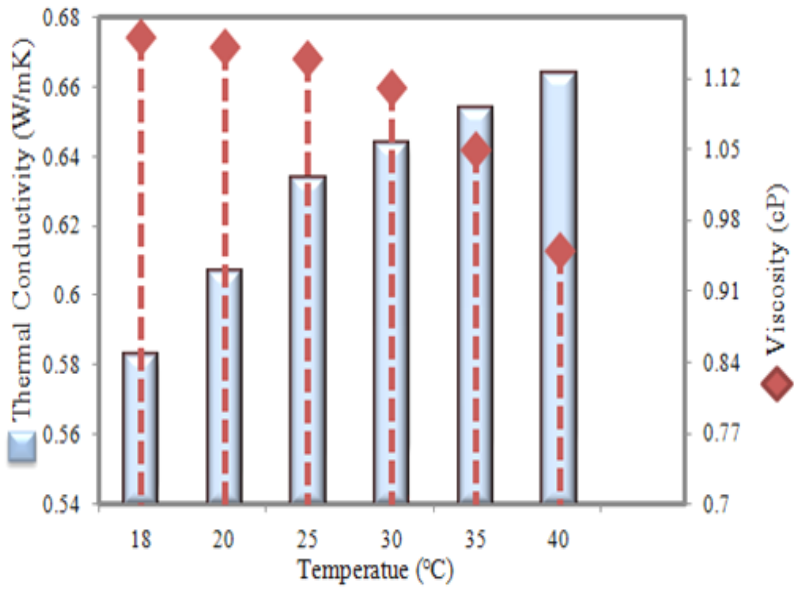

Figure 5.7: Comparative graph of thermal conductivity and viscosity of α-Al_2O_3 aqueous suspension as a function of temperature.

5.4. Conclusions

In summary, an experimental investigation of the TC and VS for α and γ-Al_2O_3 aqueous suspension was studied. It was found that α-phase is best for thermal conduction as compare to γ-phase due to its effective crystalline nature. The α-Al_2O_3 dispersion is more stable than γ-Al_2O_3 dispersion for longer time which directly affects the TC of suspension. The TC remarkably increases with temperature, concentration, sonication time, crystallinity and stability of NPs in aqueous suspension. The correlation between TC and VS as a function of temperature is inversely proportional to each other. From viscosity data it was found that loading of lower particle concentration, the Al_2O_3 aqueous suspension showed Newtonian behavior for both phases. So it is concluded here that optimization of experimental conditions for higher TC and long term stability of NPs in conventional heat transfer fluids is very importance to their commercial availability in cooling applications.

References:

[1] S.U.S. Choi, Z.G. Zhang, W. Yu, F.E. Lockwood and E.A. Grulke, *Appl. Phys. Lett*. 2001, **79,** 2252-2254.

[2] B. Wang, H. Li, and X. Peng, *Int. J. Therm. Sci*.2002, **11,** 193–288.

[3] J.A. Eastman, S.U.S. Choi, S. Li, W. Yu and L.J. Thompson, *Appl. Phys. Lett.*2001, **78,** 718–720.

[4] S. Lee, S.U.S. Choi, S. Li and J.A. Eastman, *J. Heat Transfer*1999, **121,** 280-288.

[5] M. Corcione, M. Cianfrini and A. Quintino, *Int. J. Therm. Sci.*2012, **56,** 58-69.

[6] C.T. Nguyen, G. Roy, C. Gauthier and N. Galanis, *Appl. Therm. Eng.*2007, **27,** 1501-1506.

[7] N. Putra, W. Roetzel and S.K. Das, *Heat Mass Transf*. 2003, **39,** 775-784.

[8] S.Z. Heris, S.G. Etemad and M.N. Esfahan, *Int. Commun. Heat Mass Trans*. 2006, **33,** 529-535.

[9] S.Z. Heris, M.N. Esfahan and S.G. Etemad, *Int. J. Heat Fluid Fl*.2007, **28,** 203-210.

[10] S.K. Das, S.U.S. Choi, W. Yu and T. Pradeep, Nanofluids: Science and Technology New York: Wiley; 2008.

[11] X.Q. Wang and A.S. Mujumdar, *Int. J. Therm. Sci.*2007, **46,** 1-19.

[12] C. Choi, H.S. Yoo and J.M. Oh, *Curr. Appl. Phys.* 2008, **8,**710-712.

[13] C.H. Li and G.P. Peterson, *J. Appl. Phys.* 2006, **99,** 084314-8.

[14] E.V. Timofeeva, A.N. Gavrilov, J.M. McCloskey and Y.V. Tolmachev, *Phys. Rev. E*. 2007, **76,** 061203-948-951.

[15] S.K. Das, N. Putra, P. Thiesen and W. Roetzel, *ASME J. Heat Transfer.* 2003, **125,** 567-574.

[16] H. Xie, J. Wang, T. Xi, Y. Liu and F. Ai, *J. Appl. Phys.*2002, **91,** 4568-4572.

[17] J.H. Lee, K.S. Hwang, S.P. Jang, B.H. Lee, J.H. Kim, S.U.S. Choi and C.J. Choi, *Int. J. Heat Mass Trans.* 2008, **51,** 2651-656.

[18] D.W. Oh, A. Jain, J.K. Eaton, K.E. Goodson and J.S. Lee, *Int. J. Heat Fluid Fl.*2008, **29,** 1456-1461.

[19] Y. Xuan and Q. Li, *Int. J. Heat Fluid Fl.*2000, **21,** 58-64.

[20] M.P. Beck, Y. Yuan, P. Warrier and A.S. Teja, J. Nanopart. Res. 2009, 11, 1129-1136.

[21] T.P. Teng, Y.H. Hung, T.C. Teng, H.E. Mo and H.G. Hsu, Appl. Therm. Eng. 2010, 30, 2213-2218.

[22] H. Masuda, A. Ebata, K. Teramae and N. Hishinuma, *NetsuBussei*, 1993, **7 ,** 227-233.

[23] C.H. Chon, K.D. Kihm, S.P. Lee and S.U.S. Choi, *Appl. Phys. Lett.*2005, **87,** 153107.

[24] S.K. Das, N. Putta, P. Thiesen and W. Roetzel, *J. Heat Transfer*.2003, **125,** 567–574.

[25] M. Kole and T.K. Dey, *J. Phys. D Appl. Phys*.2010, **43,** 315501.

[26] H. Chen, Y. Ding and A. Lapkin, *Powder Technol.*2009, **194,** 132-141.

[27] C.T. Nguyen, F. Desgranges, G. Roy, N. Galanis, T. Mare, S. Boucher and H.A. Mintsa, *Int. J. Heat Fluid Flow.* 2007, **28,** 1492-1506.

[28] S.K. Das, N. Putra and W. Roetzel, *Int. J. Heat Mass Trans.* 2003, **46,** 851-862.

[29] M.P. Beck, Y. Yuan, P. Warrier and A.S. Teja, *J. Nanopart. Res.* 2010, **12,** 1469-1477.

[30] M. Chandrasekar, S. Suresh and A. Chandra Bose, *Exp. Therm Fluid Sci.* 2010, **34**, 122-130.

[31] T.P. Teng, *Energy Convers. Manage.* 2013, **67**, 369-375.

[32] B.E. Yoldas, *J. Am. Ceram. Soc*.1982, **65,** 387-393.

[33] B.C. Lippens and J.H. De Boer, *ActaCryst.* 1964, **17,**1312.

[34] A. Boumaza, L. Favaro, J. Le´dion, G. Sattonnay, J.B. Brubach, P. Berthet, A.M. Huntz, P. Royc and R. Tetot, *J. Solid State Chem.*2009, **182,** 1171-1176.

[35] S.J. Wilson and J.D.C.M. Connell, *Solid State Chem.* 1980, **34,** 315-322.

[36] T.C. Chou and T.G. Nieh, *J. Am. Ceram. Soc*.1991, **74,** 2270-2279.

[37] M.S. MeorYusoff and M. Muslimin, *Malaysian Journal of Analytical Sciences***.**2007, **11,** 262-268.

[38] Y.X. Pang and X. Bao, *J. Mater. Chem.*2002, **12,** 3699–3704.

[39] S. Cava, S.M. Tebcherani, I.A. Souza, S.A. Pianaro, C.A. Paskocimas, E. Longo and J.A. Varela, *Mater. Chem. Phys*. 2007, **103,** 394–399.

[40] G.Gutirrez, A. Taga and B. Johansson, *Phys. Rev. B.* 2001, **65,** 1–4.

[41] X. Wang, X. Li and S. Yang, *Energy Fuels.* 2009, **23**, 2684–2689.

[42] S.P. Jang and S.U.S. Choi, *Appl. Phys. Lett.* 2004, **84,** 4316–4318.

[43] W. Rashmi, A.F. Ismail, I. Sopyan, A.T. Jameel, F. Yusof, M. Khalid and N.M. Mubarak, *J. Exp. Nanosci.* 2011, 6, 567–579.

[44] M.J. O'Connell, S.M. Bachilo, C.B. Huffman, V.C. Moore, M.S. Strano, E.H. Haroz, K.L. Rialon, P.J. Boul, W.H. Noon, C. Kittrell, J. Ma, R.H. Hauge, R. B. Weisman, R.E. Smalley, O'Connell et al., *Science.* 2002, **297**, 593-596.

[45] D. Kwek, A. Crivoi and F. Duan, *J. Chem. Eng. Data*. 2010, **55,**5690–5695.

[46] D.H. Yoo, K.S. Hong and H.S. Yang, *J. Thermochim. Acta*. 2007, **455,** 66-69.

[47] I.M. Mahbubul, R. Saidur and M.A. Amalina, *Int. J. Heat Mass Trans.* 2012, **55,** 874–885.

Conclusions

Chapter 2: **Section A**: In summary, the anisotropic shapes of TiO_2 NPs influence the TC of NFs as a function of their morphological difference. Anisotropic shapes showed 20-27% enhancement in thermal conductivity only at lower volume fraction (0.05 to 1 vol.%), but in literature same enhancement is shown at higher volume fraction (3 to 8 vol.%). Due to small interparticles distance, high compactness, high surface atom exposure and much greater mean free path of longitudinal phonons of TiO_2 nanorods, it shows always higher thermal conductivity than porous TiO_2 nanotube and TiO_2 P-25. EG always shows higher dispersion stability than DI water because of higher viscosity of EG. So it is concluded here that optimization of experimental conditions, anisotropic shape, appropriate theoretical models and long term dispersion stability of NPs is very essential for cooling applications.

Section B: In summary, the beneficial effect of a thin layer of SiO_2 coating over TiO_2 nanostructures for superior dispersion stability and thermal conductivity are investigated with the supportive evidences of particle size distribution, zeta potential, density and refractive index analysis as indicator parameter for stable suspension. As a result, SiO_2 coated composite particles always exhibited higher TC than bare NPs dispersion which generally undergoes quick agglomeration and precipitation. Further optimization of SiO_2 shell thickness is important for exhibiting long term dispersion stability and maximum enhancement in thermal conductivity. It was also found that lengthy nanorods based suspension exhibit more enhancements in TC than spherical NPs.

Chapter 3: **Section A**: In the present study, anisotropic shapes (nanowires and nanorods) of CuO nanostructures based dispersion showed higher enhancement in thermal conductivity than spherical shaped CuO based dispersion as expected by Hamilton-Crosser model. The experimental results displayed higher thermal conductivity than theoretically predicated models. It is concluded here that with the increase in volume fraction, the thermal conductivity and density also increased. The effective thermal conductivity is also well correlated with zeta potential values and particle size distribution data. The extended sonication time helps in breakdown of large clusters into smaller sized particles which enhances the thermal conductivity.

Section B: In this study, the beneficial effect of a thin layer of SiO_2 coating over CuO nanostructures for superior dispersion stability and thermal conductivity are investigated with the supportive evidences of particle size distribution, zeta potential, density and refractive index analysis as indicator parameter for stable suspension. As a result, SiO_2 coated composite particles always exhibited higher TC than bare NPs dispersion which generally undergoes quick agglomeration and precipitation. Further optimization of SiO_2 shell thickness is important for exhibiting long term dispersion stability and maximum enhancement in thermal conductivity. It was also found that lengthy nanorods based suspension exhibit more enhancements in TC than spherical NPs. Thermal conductivity enhancement can be further increased by increasing the volume fraction of SiO_2@CuO nanocomposites.

Chapter 4: **Section A**: In this study, WO_3 nanoparticles were successfully prepared and dispersed in various solvents to investigate their relative thermal conductivity. It was found that cylindrical shaped nanoparticles showed more enhancements in TC than spherical shaped. TC increases with the increase in volume fraction up to certain level and EG based dispersion showed higher thermal conductivity ratio than other base fluids. Depending upon the stabilizer's nature and their interaction with NPs, the dispersion stability and TC can also be improved for longer time. Dispersion stability of NPs was also improved by varying the pH values. It was found that well dispersed NPs also help in long term stability could be well correlated with zeta potential values for displaying effective thermal conductivity. It was observed that experimental results showed higher thermal conductivity than theoretically predicated model, so there is need for optimized model which predict the TC accurately.

Section B: In summary, the beneficial effect of a thin layer of SiO_2 coating over WO_3 nanostructures for superior dispersion stability for long term due to hydrophilic and repulsive interaction between the WO_3-SiOH composites are investigated with the supportive evidences of particle size distribution, zeta potential, density and refractive index analysis as indicator parameter for stable suspension. As a result, SiO_2 coated WO_3 composite particles always exhibited higher TC than bare WO_3 NPs dispersion which generally undergoes quick agglomeration and precipitation. Further optimization of silica shell layer is needed for exhibiting long term dispersion stability and maximum thermal conductivity. It also found that lengthy cylindrical shapes exhibit more enhancements in TC than conventional NPs.

Chapter 5: In summary, an experimental investigation of the TC and VS for α and γ-Al_2O_3 aqueous suspension was studied. It was found that α-phase is best for thermal conduction as compare to γ-phase due to its effective crystalline nature. The α-Al_2O_3 dispersion is more stable than γ-Al_2O_3 dispersion for longer time which directly affects the TC of suspension. The TC remarkably increases with temperature, concentration, sonication time, crystallinity and stability of NPs in aqueous suspension. The correlation between TC and VS as a function of temperature is inversely proportional to each other. From viscosity data it was found that loading of lower particle concentration, the Al_2O_3 aqueous suspension showed Newtonian behavior for both phases. So it is concluded here that optimization of experimental conditions for higher TC and long term stability of NPs in conventional heat transfer fluids is very importance to their commercial availability in cooling applications.

1. **Bhupender Pal,** Soumya Suddha Mallick and Bonamali Pal, "Shape dependent thermal conductivity of TiO_2-De-ionized water and ethylene glycol dispersion," published in Journal of Nanoscience and Nanotechnology,15 (2015) 3670-3676.

2. **Bhupender Pal,** Soumya Suddha Mallick and Bonamali Pal, "Anisotropic CuO nanostructures of different size and shape exhibit thermal conductivity superior than typical bulk powder," published in Journal of Colloids and Surfaces A: Physicochemical and Engineering Aspects, 459 (2014) 282–289.

3. **Bhupender Pal,** Soumya Suddha Mallick and Bonamali Pal, "Phase-dependent thermophysical properties of α-and γ-Al_2O_3 in aqueous suspension, Journal of Industrial & Engineering Chemistry, 25 (2015) 99-104.

4. **Bhupender Pal** and Bonamali Pal, **"**Influence of CuO Nanostructures on the Thermal Conductivity of DI Water and Ethylene Glycol Based Nanofluids," Particulate Science and Technology, 33 (2015) 224–228.

5. **Bhupender Pal,** Soumya Suddha Mallick and Bonamali Pal, "WO_3 nanostructures of different size and shape for improved thermal conductivity and dispersion stability in aqueous suspension," submitted in Thermochimica Acta.

6. **Bhupender Pal,** Soumya Suddha Mallick and Bonamali Pal, "A thin layer of SiO_2 coating for highly improved dispersion stability and thermal conductivity of WO_3-H_2O suspension," submitted in International Journal of Heat and Mass Transfer.

7. **Bhupender Pal,** Soumya Suddha Mallick and Bonamali Pal, SiO_2@TiO_2 nanocomposites for enhanced thermal conductivity and dispersion stability in de-ionized water, under preparation.

8. **Bhupender Pal,** Soumya Suddha Mallick and Bonamali Pal, SiO_2@CuO nanocomposites for enhanced thermal conductivity and dispersion stability in de-ionized water, under preparation.

Other publications:

1. **Bhupender Pal and Bonamali Pal**, Tuning the Optical and Photocatalytic Properties of Anisotropic ZnS Nanostructures for the Selective Reduction of Nitroaromatics*,"* Chemical Engineering Journal, 263 (2015) 200–208.

Paper presented in Conferences

1. **Bhupender Pal and Bonamali Pal, "**Influence of CuO Nanostructures on the Thermal Conductivity of DI water and Ethylene glycol based," presented in International conference on powder, granule and bulk solids: innovations and application-2013, Thapar University, Patiala.

2. **Bhupender Pal and Bonamali Pal**, "Surfactant Effects on Dispersion Stability and Thermal conductivity of Titania-Based Nanofluids," presented in International conference on Nanotechnology in the Service of Health, Environment & Society, NanoSciTech-2014*,"* on 13-15th February, 2014 held in Punjab University, Chandigarh.

3. **Bhupender Pal and Bonamali Pal**, "Phase transition-influenced thermal conductivity and viscosity of Al_2O_3 based nanofluids," presented in National conference on Innovative Molecules for Sustainable Future (NCIMSF-2013) on 24-26th October, 2013 held in SCBC Thapar University, Patiala.

4. **Bhupender Pal and Bonamali Pal**, "Synthesis of Alumina, Titania, and Copper Oxide Nanoparticles and Its Application in Nanofluids" presented in NanoSciTech-2012, on 16-18th February, 2012 held in Punjab University, Chandigarh.

5. **Bhupender Pal and Bonamali Pal**, "Effects of Volume Fraction, Temperature, and Sonication time on the Thermophysical Properties of Al_2O_3-Water Nanofluids," presented in National Symposium on New Frontiers in Chemistry on 15-16th February, 2013 held in Punjabi University Patiala, Punjab.

6. **Bhupender Pal and Bonamali Pal**, "Investigation of Thermal Conductivity of CuO-Water and Ethylene glycol Based Nanofluids," presented in Emerging Technologies-Micro to Nano-2013, on 23-24th February, 2013 held in BITS Pilani, Goa Campus.

7. **Bhupender Pal and Bonamali Pal**, Effect of Silica coating on Dispersion Stability and Thermal conductivity of CuO-based nanofluids," oral presentation in New Frontiers in Chemical Sciences NFCS-01 on 15th November, 2014 held in Kalsa College, Patiala, Punjab.

Article

Journal of
Nanoscience and Nanotechnology
Vol. 14, 1–7, 2014
www.aspbs.com/jnn

Shape Dependent Thermal Conductivity of TiO_2-Deionized Water and Ethylene Glycol Dispersion

Bhupender Pal[1], Soumya Suddha Mallick[2], and Bonamali Pal[1,*]

[1] School of Chemistry and Biochemistry, Thapar University, Patiala 147004, Punjab, India
[2] Department of Mechanical Engineering, Thapar University, Patiala 147004, Punjab, India

This paper presents the importance of different shapes and crystal phases of TiO_2 nanostructures such as TiO_2 P-25 (70:30 anatase and rutile), as-prepared nanorods (pure anatase) and sodium titanate nanotubes (orthorhombic $Na_2Ti_2O_5 \cdot H_2O$ crystal) on the thermal conductivity of de-ionized water and ethylene glycol. It revealed that TiO_2 nanorods ($L \times W$ = 81–134 nm × 8–13 nm and surface area = 79 m^2 g^{-1}) showed always higher thermal conductivity than porous nanotubes ($L \times W$ = 85–115 nm × 9–12 nm and surface area = 176 m^2 g^{-1}) and commercial TiO_2 P-25 (30–55 nm surface area = 56 m^2 g^{-1}), which was explained by their differences in crystallinity, crystal phases, compactness, surface exposed atoms, surface area and much greater mean free path of longitudinal phonon vibrations along its lateral dimensions. The subsequent effect of sonication time from 5–10 h results into the breakdown of TiO_2 nanorods cluster (42 to 28 nm) with the instantaneous increase in negative zeta potential values from −31 to −45 mV, respectively, seems to be an additional cause for enhancement in its thermal conductivity.

Keywords: Titania Nanoparticles, Dispersion Stability, Thermal Conductivity, Zeta Potential, Nanoparticle Shape, pH Effect.

1. INTRODUCTION

Nanofluid (NF) is a two-phase mixture in which the continuous phase is usually a liquid (de-ionized water, ethylene glycol or oils) and the dispersed phase is extremely fine nanoparticles (NPs).[1–5] Nanofluids are considered as a good candidate for heat transfer applications due to their superior thermophysical properties (*thermal conductivity, specific heat and viscosity*, etc.) than conventional heat-transfer fluids and can be used for cooling applications in nuclear reactors, transportation industry, electronics and biomedical.[6–9] A variety of factors such as volume fraction, size, shape, nature of NPs, pH, temperature, Brownian motion and aggregation of NPs have been proposed to play the vital roles in thermal conductivity[10–13] of nanofluids. Thermal conductivity and viscosity of nanofluids are also dependent on the physicochemical and structural features of nanomaterials and solvents.[14–17]

Over the last several decades, scientists and engineers have been attempting to develop fluids which offer better cooling or heating performance for thermal systems as compared to conventional heat-transfer fluids.[18, 19] The solid particles with sizes ranging from μm to mm have shown improved thermal properties, but such suspensions are unstable and prone to clogging systems with small channels.[16] Nanoparticles due to their extremely small size, higher surface atom exposure, high surface to volume ratio and larger surface area may increase the heat transfer efficiency, improves the long-term stability and reduces the clogging of microchannels. High thermal conductive materials such as CNTs, Cu, Ag, Au, CuO, TiO_2 and Al_2O_3 spherical particles have been extensively studied.[20–25] Choi et al.[1] found 20% increase in heat transfer rate of CuO NPs in de-ionized water (DI water) and Eastman et al. showed 40% increment in thermal conductivity by using CuO NPs in ethylene glycol (EG).[5] Das et al.[26] reported the four-fold increase in thermal conductivity over a temperature range of 21–51 °C of Al_2O_3 (38.4 nm) and CuO (28.6 nm) NPs dispersion in DI water. In recent years, TiO_2 is considered as a suitable NF's material due to its light weight, hydrophilicity, non-toxicity, stability and reasonable thermal conductivity, etc. For example, Masuda et al.[20] studied the thermophysical properties of the metallic oxides (TiO_2 and Al_2O_3) dispersed in DI water and found thermal conductivity of TiO_2-water NFs at a 4.3 vol% were

*Author to whom correspondence should be addressed.

Colloids and Surfaces A: Physicochem. Eng. Aspects 459 (2014) 282–289

Contents lists available at ScienceDirect

Colloids and Surfaces A: Physicochemical and Engineering Aspects

journal homepage: www.elsevier.com/locate/colsurfa

Anisotropic CuO nanostructures of different size and shape exhibit thermal conductivity superior than typical bulk powder

Bhupender Pal[a], Soumya Suddha Mallick[b], Bonamali Pal[c,*]

[a] Thapar University, Patiala 147004, Punjab, India
[b] Department of Mechanical Engineering, Thapar University, Patiala, Punjab, India
[c] School of Chemistry and Biochemistry, Thapar University, Patiala 147004, Punjab, India

HIGHLIGHTS

- Various shapes of CuO nanoparticles such as nanospheres, nanorods and nanowires.
- CuO nanowires showed higher thermal conductivity than nanorods and nanospheres.
- Experimental results showed higher thermal conductivity than theoretical models.
- As the volume fraction and density increased, thermal conductivity also increased.

GRAPHICAL ABSTRACT

Variation in dimensions of CuO nanoparticles directly influences the thermal conductivity of conventional heat transfer fluids (such as ethylene glycol and water). It was observed here that CuO nanowires show higher thermal conductivity than nanorods and nanospheres dispersion, this may be due to long mean-free-path of phonon vibration which helps in enhancing the heat transfer rate per particles.

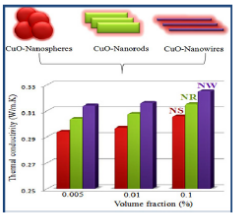

ARTICLE INFO

Article history:
Received 28 March 2014
Received in revised form 11 July 2014
Accepted 15 July 2014
Available online 23 July 2014

Keywords:
CuO nanostructures
Thermal conductivity
Density
Zeta potential
Dispersion stability

ABSTRACT

This work demonstrates the preparation of monoclinic crystalline CuO nanospheres (5–10 nm), nanorods ($L \times W$ = 100–140 nm × 30–40 nm) and nanowires (200–210 nm × 2–5 nm) for the study of thermal conductivities when dispersed in de-ionized water and ethylene glycol (0.005–0.1 vol%). It has been observed that CuO nanorods and nanowires having surface area 53 and 61 $m^2\ g^{-1}$, respectively, always displayed higher thermal conductivity than CuO nanospheres possessing lower surface area (41 $m^2\ g^{-1}$), which attributed to the differences in their per-particle surface area, percentage of surface exposed atoms, anisotropic lengthy shape, large phonon-mean-free paths. The experimental results revealed higher thermal conductivities than obtained from theoretical models due to particle shape effect as expected from Hamilton–Crosser equation. It has also been found that density is directly proportionally to thermal conductivity and increases with the increase in volume fraction. The decrease in aggregated particle size (130–104 nm) and an increase in zeta potential value (−32 to −37 mV) of CuO nanospheres causes more stability of CuO dispersion with 3–6 h of sonication.

1. Introduction

Nanocrystalline semiconductor particles have drawn considerable interest in recent years because of their special properties such as a large surface-to-volume ratio, higher activity, and special electronic and optical properties as compared to [1–3] bulk

* Corresponding author. Tel.: +91 175 2393443; fax: +91 175 2364498.
E-mail address: bpal@thapar.edu (B. Pal).

http://dx.doi.org/10.1016/j.colsurfa.2014.07.017
0927-7757/

G Model
JIEC-2259; No. of Pages 6
ARTICLE IN PRESS

Journal of Industrial and Engineering Chemistry xxx (2014) xxx–xxx

Contents lists available at ScienceDirect

Journal of Industrial and Engineering Chemistry

journal homepage: www.elsevier.com/locate/jiec

Phase-dependent thermophysical properties of α-and γ-Al_2O_3 in aqueous suspension

Bhupender Pal [b], Soumya Suddha Mallick [c], Bonamali Pal [a,*]

[a] School of Chemistry and Biochemistry Thapar University, Patiala 147 004, Punjab, India
[b] Thapar University, Patiala 147004 Punjab, India
[c] Department of Mechanical Engineering, Thapar University, Patiala, Punjab, India

ARTICLE INFO

Article history:
Received 17 May 2014
Received in revised form 7 October 2014
Accepted 18 October 2014
Available online xxx

Keywords:
Alumina phase transition
Zeta potential of Al_2O_3 suspension
Thermal conductivity
Viscosity of water–Al_2O_3 dispersion

ABSTRACT

This study demonstrates the thermal conductivity (TC) and viscosity of as prepared crystalline α-Al_2O_3 and amorphous γ-Al_2O_3 particles, having size in the range of 30–50 nm. The α and γ-Al_2O_3 aqueous suspension exhibited ~10% and 6% enhancement in TC than de-ionized water, but α-Al_2O_3 showed (~4–6%) higher TC than γ-Al_2O_3 aqueous suspension due to more crystallinity of α phase than γ phase. Ultrasonication helps in the breakdown of large clusters which further improves the dispersion stability and TC as verified by dynamic light scattering and zeta potential measurements. The Al_2O_3 aqueous suspension showed Newtonian characteristics at lower concentration.

Introduction

Nanofluid (NF), a suspension of nanoparticles in a base liquid, has been found to provide a considerable heat-transfer enhancement compared to "conventional" fluids such as water and ethylene glycol, the suspended crystalline nanoparticles have three orders of thermal conductivities (TC) larger than that of the base liquid [1–4]. Due to continuous growth in technology and upcoming more powerful tools in optics, lasers, communication, and electronics having miniaturized size, cooling has become an important aspect for thermal [5,6] management. The aqueous or non-aqueous suspension of Al_2O_3 nanoparticles (NPs) is recently studied for cooling applications due to high TC of solid NPs than liquid [7–9]. Particles with a nanoscale dimension provide a more surface area, which not only enhances the heat transfer rate but also increases the particles suspension stability in the conventional heat transfer fluids [10,11]. Researchers have been trying to enhance the heat transfer performance of conventional coolants by suspending tiny metallic, non-metallic and metal oxide particles in DI water and ethylene glycol (EG) depending upon their volume fraction (VF), particle size, shape, pH and temperature [12–15]. Some research groups [16–19] found 4 to 30% enhancement in TC by varying particle size (10 to 200 nm) and volume fraction (0.05 to 4 vol.%) of γ-Al_2O_3 in DI water and EG. Beck et al. [20] showed decrease in TC of alumina nanoparticles dispersion having size lower than 50 nm and TC was increased with increasing particle sizes (100–282 nm). Teng et al. [21] presented the effect of particle size, concentration and temperature on increased TC of aqueous suspension of Al_2O_3 particles. In some other reports [22–24] found that by increasing the temperature from 31 to 51 °C, the enhancement in TC was found to be 2 to 32.4% for Al_2O_3 dispersed in DI water and EG. Kole et al. [25] dispersed <50-nm Al_2O_3 (3.5 vol.%) using oleic acid as surfactant in a car engine coolant and observed 10.41% TC enhancement and demonstrated the stability of such fluids for more than 80 days. It may be mentioned here that engineering applications of NPs suspension that employ fluid flow not only require information on their thermal properties, but the appropriate rheological properties of the aqueous suspension is also very significant [26]. In the Al_2O_3–water mixture viscosity (VS) increases between 20% and 30% for 3 vol.% Al_2O_3 solution as compared to water alone [27]. Das et al. [28] demonstrated an increase of VS with increased particle concentrations and Kole et al. [25] demonstrated a transition from Newtonian characteristics to non-Newtonian behavior with increasing content of Al_2O_3 in the engine coolant. Recently, Beck et al. [29] suggested the temperature dependence TC and VS of EG-based suspension in the range of 296 to 400 K. Chandrasekar et al. [30] observed Nusselt numbers were increased by 15.91% and 21.53% when Al_2O_3/water nanofluid is used with wire coil inserts WC2 and WC3, respectively, at Re = 2275 compared to those of

* Corresponding author Tel.: +91 175 2393443; fax: +91 175 2364498.
E-mail address: bpal@thapar.edu (B. Pal).

http://dx.doi.org/10.1016/j.jiec.2014.10.018
1226-086X/

Please cite this article in press as: B. Pal, et al., J. Ind. Eng. Chem. (2014), http://dx.doi.org/10.1016/j.jiec.2014.10.018

Particulate Science and Technology, 33: 224–228

ISSN: 0272-6351 print/1548-0046 online
DOI: 10.1080/02726351.2014.953647

Taylor & Francis
Taylor & Francis Group

Influence of CuO Nanostructures on the Thermal Conductivity of DI Water and Ethylene Glycol Based Nanofluids

BHUPENDER PAL and BONAMALI PAL

School of Chemistry and Biochemistry, Thapar University, Patiala, Punjab, India

The influence of cupric oxide (CuO) nanostructures on the thermal conductivity of deionized (DI)water and ethylene glycol (EG) was investigated here. CuO nanospheres (average diameter 7 nm) and nanorods (L × W = ~120 nm × 4 nm) have been synthesized; their structural and morphological characterizations have been done by powder x-ray diffraction (XRD), UV-visible spectrophotometer, and transmission electron microcopy (TEM). The CuO nanospheres and nanorods have been dispersed separately in DI water and EG with four different volume fractions (0.005–0.1%). The results showed that an enhancement in thermal conductivity for CuO nanospheres and CuO nanorods was found to be 15% and 17% with respect to DI water, 19% and 21% with respect to EG. The enhancement in thermal conductivity in case of CuO nanorods is due to large surface area, crystallinity, and network formation of nanorods in base fluids which directly help in the transfer of phonon vibrations rapidly from one atom to another atom and increase the heat-transfer rate. Thus, the CuO–EG based-nanofluids exhibited 4–5% higher thermal conductivity than CuO–DI water based nanofluids, nanorods always showed higher thermal conductivity (2–3%) than nanospheres in both base fluids.

Keywords: Base fluids, CuO nanostructures, sonication time, thermal conductivity, volume fraction

1. Introduction

Colloidal nanomaterials exhibit unique physical properties that have led them to become key ingredients in many applications including paints, coatings, ceramics, drug delivery, and food processing (Gibbs et al. 1999; Davis et al. 2008). A particular class of suspensions, that is, nanofluids (Eastman et al. 2004) composed of ultrafine nanoparticles at low concentration (~100 nm or smaller, ~1 vol % or less), currently has gained considerable attention owing to reports of unusual physical phenomena, most notably dramatically increased thermal conductivity and critical heat flux relative to the particle-free fluid (Xie et al. 2003; Keblinski et al. 2005; Wang et al. 2007). These characteristics are highly desirable for thermal management applications where there is a need for innovative coolants, and numerous studies have been directed toward understanding how these effects depend on parameters associated with the particles (material, shape, size, volume fraction) and the bulk fluid (composition, pH, stabilizing additives) (Eastman et al. 2001; Xie et al. 2002; Das et al. 2003; Murshed et al. 2005).

Address correspondence to: Bonamali Pal, School of Chemistry and Biochemistry, Thapar University, Patiala 147 004, Punjab, India. E-mail: bpal@thapar.edu

Color versions of one or more of the figures in the article can be found online at www.tandfonline.com/upst.

In the past decades, many research groups (Pak et al. 1998; Lee et al. 1999) have used metal oxide nanoparticles dispersion (in ethylene glycol (EG) and DI water) for heat transfer applications and got 40% to 60% increment in thermal conductivity. Most of the studies have been done on Al_2O_3, TiO_2, and CuO (Liu et al. 2006; Murshed et al. 2005) nanoparticle based dispersion in EG and DI water. Some research groups (Eastman et al. 2001) conducted heat transfer tests to assess the thermal performance of copper oxide and metallic nanofluids under turbulent flow conditions, and their results showed that the heat transfer coefficient of water containing 0.9 vol. % of CuO nanoparticles was improved by more than 15% when compared with pure water. The thermal conductivities of the CuO–water (Lee et al. 1999) nanofluids were measured by the transient hot-wire method, and a 12% improvement was reported with the CuO content being 3.4 vol.%. The experimental results of CuO nanofluids exhibited higher thermal conductivity as compared with those calculated by the Hamilton and Crosser (1962) model, which neglected the size effect.

It is widely accepted that these properties are closely related to not only their sizes but also their shapes. Therefore, controlling the morphologies of nanomaterials is one of the most important issues and effective ways to obtain desirable properties (Kong et al. 2003). The preparation of metal nanostructures has received much attention because